7.09 Hot Spots and Melting Anomalies

G. Ito, University of Hawaii, Honolulu, HI, USA

P. E. van Keken, University of Michigan, Ann Arbor, MI, USA

Nomenclature

g	acceleration of gravity ($m\,s^{-2}$)
$\bar{h}$	average swell height (m)
q_p	plume heat flux associated with swell buoyancy flux
s	hot-spot swell volume flux
t	time (s)
x	horizontal dimension (m)
x_r	distance between plume source and ridge axis (m)
B	buoyancy flux ($kg\,s^{-1}$)
C	composition
C_1, C_2, C_3	constants used in scaling of swell width
E	equation of an ellipse
F	fraction partial melting
H	thickness of fluid
L_0	characteristic length scale (m)
M	volumetric rate of melt generation ($m^3\,s^{-1}$)
P	pressure (Pa)
Q	volume flux of buoyant material ($m^3\,s^{-1}$)
Ra	thermal Rayleigh number
Ra_c	critical Rayleigh number
T	temperature (K)
U_p, U	plate speed, seafloor spreading rate ($m\,s^{-1}$)
V	volume (m^3)
$\bar{W}$	average intraplate swell width (m), or steady-state ridge-axis swell depth (m)
W	swell width (m)
W_0	characteristic width scale (m)
α	thermal expansivity (K^{-1})
δ	thickness of boundary layer (m)
κ	thermal diffusivity ($m^2\,s^{-1}$)
τ	characteristic growth time (s)
η, μ	viscosity (Pa s)
ρ	density ($kg\,m^{-3}$)
ρ_c	crustal density ($kg\,m^{-3}$)
ρ_m	mantle density ($kg\,m^{-3}$)
ρ_w	density of sea water ($kg\,m^{-3}$)
ΔT	Temperature (contrast (K))
$\Delta\rho$	density difference between buoyant and normal mantle ($kg\,m^{-3}$)

7.09.1 Introduction

The original work by Wilson (1963, 1973), Morgan (1971, 1972), and Crough (1978) established the concept of 'hot spot' as a broad swelling of topography capped by volcanism, which, combined with plate motion, generates volcanoes aligned in a chain and with ages that progress monotonically. In some cases, these chains project back to massive volcanic plateaus, or large igneous provinces (LIPs), suggesting that hot-spot activity began with some of the largest magmatic outbursts evident in the geologic record (Morgan, 1972; Richards *et al.*, 1989; Duncan and Richards, 1991). Hot-spot volcanism is dominantly basaltic and therefore largely involves melting of mantle peridotite, a process that also produces mid-oceanic ridge volcanism. Yet mid-ocean ridge basalts (MORBs) and hot-spot basalts typically have distinct radiogenic isotope characteristics (Hart *et al.*, 1973; Schilling, 1973). These differences indicate that the two forms of magmatism come from mantle materials that have preserved distinct chemical identities for hundreds of millions of years.

The above characteristics suggest that hot-spot volcanism has an origin that is at least partly decoupled from plate processes. A straightforward explanation is that hot spots are generated by convective upwellings, or plumes of unusually hot, buoyant mantle, which rise from the lower mantle (Wilson, 1963, 1973; Morgan, 1971, 1972; Whitehead and Luther, 1975) possibly through a chemically stratified mantle (e.g., Richter and McKenzie, 1981). The large mushroom-shaped head of an initiating mantle plume and the trailing, more narrow plume stem has become a popular explanation for the formation of a LIP followed by a hot-spot track (e.g., Richards *et al.*, 1989; Campbell and Griffiths, 1990).

Studies of hot spots have flourished over the past few decades. Recent articles and textbooks have reviewed some of the classic connections between hot spots and mantle plumes (e.g., Jackson, 1998; Davies, 1999; Condie, 2001; Schubert *et al.*, 2001), the role of mantle plumes in deep-mantle convection and chemical transport (Jellinek and Manga, 2004), and oceanic hot spots (e.g., Ito *et al.*, 2003; Hekinian *et al.*, 2004). Alternative mechanisms, which emphasize processes in the asthenosphere and lithosphere, are being re-evaluated and some new ones proposed (Foulger *et al.*, 2005). It has become clear that few hot spots confidently show all of the above characteristics of the classic description. The term hot spot itself implies a

localized region of anomalously high mantle temperature, but some features that were originally called hot spots may involve mantle with little or no excess heat, volcanoes spanning large distances of a chain with similar ages, or both. Thus, the terms 'magmatic anomaly' or 'melting anomaly' may be more general and appropriate to describe the topic of this chapter.

Progress made in the last decade on studies of hot spots and melting anomalies is emphasized here. We summarize the recent observations and discuss the major dynamical processes that have been explored and evaluate their ability to explain the main characteristics. Mechanisms involving hot mantle plumes have seen the most extensive quantitative testing, but the recent observations compel the exploration and rigorous testing of other mechanisms. We summarize the main observations, outline mechanisms that have been proposed, and pose questions that need quantitative answers.

7.09.2 Characteristics

Guided by the classical description of hot spots, we examine four main characteristics: (1) geographic age progression along volcano chains, (2) initiation by massive flood basalt volcanism, (3) anomalously shallow topography surrounding volcanoes (i.e., a hot-spot swell), and (4) basaltic volcanism with geochemical distinction from MORBs. Given the marked progress in seismic methods over the past decade, we also summarize the findings of mantle seismic structure beneath hot spots and surface melt anomalies. **Table 1** summarizes what we have compiled about the above characteristics for 69 hot spots and melting anomalies. **Figure 1** shows a global map of their locations with abbreviations and the main large igneous provinces that we will discuss.

7.09.2.1 Volcano Chains and Age Progression

7.09.2.1.1 Long-lived age-progressive volcanism

At least 13 hot-spot chains record volcanism lasting >50 My (**Table 1**). The Hawaiian–Emperor and the Louisville chains, for example, span thousands of kilometers across the Pacific basin (~6000 and >4000 km, respectively), record volcanism for >75 My (Duncan and Clague, 1985; Watts *et al.*, 1988; Duncan and Keller, 2004; Koppers *et al.*, 2004), and were among the first chains that led to the establishment of the hot-spot concept. As both chains terminate at subduction zones, the existing volcanoes likely record only part of the activities of these hot spots. The Galápagos is the other Pacific hot spot with a similar duration. Its interaction with the Galápagos Spreading Center has produced two chains: the Galápagos Archipelago–Carnegie Ridge on the Nazca Plate (Sinton *et al.*, 1996) and the Cocos Ridge on the Cocos Plate. The Cocos Ridge records oceanic volcanism for ~14.5 My (Werner *et al.*, 1999) and projects toward the Caribbean LIP (Duncan and Hargraves, 1984), which has $^{40}Ar/^{39}Ar$ dates of 69–139 Ma (e.g., Sinton *et al.*, 1997; Hoernle *et al.*, 2004). The geochemical similarity of these lavas with the Galápagos Archipelago is compelling evidence for a ~139 My life span for the Galápagos hot spot (Hoernle *et al.*, 2002, 2004).

In the Indian Ocean, Müller *et al.*'s (1993b) compilation of ages associates the Réunion hot spot with volcanism on the Mascarene Plateau at 45 Ma (Duncan *et al.*, 1990), the Cocos–Laccadive Plateau ~60 Ma (Duncan, 1978, 1991), and finally the Deccan flood basalts in India, which are dated at 65–66 Ma (see also Sheth (2005)). The Comoros hot spot can be linked to volcanism around the Seychelles islands dated at 63 Ma (Emerick and Duncan, 1982; Müller *et al.*, 1993b). Volcanism associated with the Marion hot-spot projects from Marion island (<0.5 Ma (McDougall *et al.*, 2001)) along a volcanic ridge to Madagascar. While geologic dating is sparse, Storey *et al.* (1997) infer an age progression along this track back to ~88 Ma. The Kerguelen hot spot is linked to Broken Ridge and Ninetyeast Ridge on the Australian Plate, as well as multiple stages of volcanism on the Kerguelen Plateau dating to 114 Ma (Frey *et al.*, 2000; Nicolaysen *et al.*, 2000) (**Figure 2**).

In the Atlantic Ocean, the Tristan–Gough and St. Helena chains record volcanism on the African Plate for ~80 My (O'Connor and Roex, 1992; O'Connor and Duncan, 1990; O'Connor *et al.*, 1999). The connection of Tristan–Gough to the Paraná flood basalts in South America and the Etendeka basalts in Namibia suggests a duration for Tristan–Gough of ~130 My (see Peate (1997) and references therein). The Trindade–Martin Vaz chain (Fodor and Hanan, 2000) extends eastward from Brazil to where the Alto Paraniba and Poxoreu volcanic provinces erupted ~85 Ma (Gibson *et al.*, 1997). In the North Atlantic, the Madiera and Canaries chains have recorded age-progressive volcanism for nearly 70 My (Guillou *et al.*, 2004; Geldmacher *et al.*, 2005). The Canaries are unusual in that single volcanoes often remain active for tens of millions of years (**Figure 3**) (Geldmacher *et al.*, 2005).

Table 1 Global compilation of hot spots with their geophysical and geochemical characteristics

Name (abbreviation)	Hot spot E. Long., N. Lat.	Age progression?	Age range	Swell?/width (km)	Connection to LIP?	Geoch. distinct from MORB
Pacific						
Austral (AU)	−140.0, −29.37	No	0–58.1 Ma	Yes/600	No	$^{206}Pb/^{204}Pb$
Baja (BAJ)	−113, 27	—	—	No	No	—
Bowie-Kodiak (BOW)	−130, 49.5	Ok	0.1–23.8 Ma	Yes/250	No	May be $^{206}Pb/^{204}Pb$
Caroline (CAR)	−197, 5.3	Weak	1.4 Ma (east) to 4.7–13.9 Ma (west)	—	No	No
Cobb (COB)	−128.7, 43.6	Good	1.5–29.2 Ma	Yes/370	No	No
Cook (CK)	−149.5, −23.5	No	0.2–19.4 Ma	Yes/500	No	$^{206}Pb/^{204}Pb$
Easter (EAS)	−109, −27	Good	0–25.6 Ma	Yes/580	May be Tuamotu and Mid-Pacs	$^{206}Pb/^{204}Pb$
Foundation (FOU)	−111, −39	Good	2.1–21 Ma	Yes/250	No	$^{206}Pb/^{204}Pb$
Galápagos (GAL)	−91.6, −0.4	Yes	0–14.5 Ma offshore; 69–139 Ma, Caribbean LIP	Yes/300	Caribbean LIP	$^{206}Pb/^{204}Pb$
Geologist (GEO)	−157, 19	No	82.7–84.6 Ma	—	No	—
Guadalupe (GUA)	−118, 29	—	<3.4 to ~20.3 Ma	May be/?	No	—
Hawaiian-Emperor (HAW)	−155.3 18.9	Good	0–75.8 Ma	Yes/920	No	$^{3}He/4He$ and $^{87}Sr/^{86}Sr$ for Islands but not Emperors
Japanese-Wake (JWK)	—	No	78.6–119.7 Ma	No	No	$^{206}Pb/^{204}Pb$
Juan Fernandez (JFE)	−79, −34	Weak	1–4 Ma (2 volcanoes dated)	Yes/?	No	$^{3}He/4He$ and $^{87}Sr/^{86}Sr$
Line Islands (LIN)	—	No	35.5–91.2 My	Partially/?	May be Mid-Pacs	—
Louisville (LOU)	−141.2, −53.55	Good	1.1–77.3 Ma	Yes/540	Doubtfully OJP	$^{206}Pb/^{204}Pb$, may be $^{87}Sr/^{86}Sr$
Magellan Seamounts (MAG)	—	No	87–18.6 Ma	No	No	$^{87}Sr/^{86}Sr$ and $^{206}Pb/^{204}Pb$
Marquesas (MQS)	−138.5, −11	Ok	0.8–5.5 Ma	Yes/850	May be Shatsky or Hess	$^{87}Sr/^{86}Sr$, may be $^{206}Pb/^{204}Pb$
Marshal Islands (MI)	−153.5, −21.0	No	68–138 Ma	May be/?	No	$^{206}Pb/^{204}Pb$
Mid-Pacific	—	No	73.5–128 Ma	No	It could be a LIP	—

Mountains (MPM)						
Musician (MUS)	—	Ok	65.5–95.8 Ma	No	No	—
Pitcairn (PIT)	−129.4, −25.2	Good	0–11.1 Ma	Yes/570	No	$^{87}Sr/^{86}Sr$
Puka–Puka (PUK)	−165.5, −10.5	Ok	5.6–27.5 Ma	Yes/?	No	$^{206}Pb/^{204}Pb$
Samoa (SAM)	−169, −14.3	Weak	0–23 Ma	Yes/396	No	$^{87}Sr/^{86}Sr$, $^{3}He/^{4}He$, and $^{206}Pb/^{204}Pb$
San Felix (SF)	−80, −26	—	—	Yes/?	No	—
Shatsky (SHA)	—	Yes	128–145 Ma	No	It is a LIP	no
Society (SOC)	−148, −18	Good	0.01–4.2 Ma	Yes/?	No	$^{87}Sr/^{86}Sr$ and $^{206}Pb/^{204}Pb$
Socorro (SCR)	−111, 19	—	—	Yes/?	No	—
Tarava (TAR)	173, 3	Weak	35.9 Ma and 43.5 Ma	Yes/?	No	—
Tuamotu (TUA)	—	—	?	Yes/?	It could be a LIP	—
North America						
Yellowstone (YEL)	−111, 44.8	Yes	16–17 Ma	Yes/600	May be Columbia River Basalts	—
Australia						
Balleny (BAL)	164.7, −67.4	Weak	—	—	May be Lord Howe rise	$^{206}Pb/^{204}Pb$ (2 analyses)
East Australia (AUS)	143, −38	—	—	—	—	—
Lord Howe (LHO)	159, −31	—	—	—	It could be LIP	—
Tasmantid (TAS)	153, −41.2	Yes	—	Yes/290	May be Lord Howe rise	—
Atlantic						
Ascension/ Circe (ASC)	−14, −8	—	<1 Ma (Ascension) and 6 Ma (Circe)	820	No	$^{206}Pb/^{204}Pb$
Azores (AZO)	−28, 38	Seafloor spreading	0–20 Ma, possibly ~85 Ma	Yes/2300	No	$^{87}Sr/^{86}Sr$ and $^{206}Pb/^{204}Pb$
Bermuda (BER)	−65, 32	—	—	Yes/500 × 700 (parallel × perp to plate motion)	No	—
Bouvet (BOU)	3.4, −54.4	—	?	Yes/900	—	$^{206}Pb/^{204}Pb$, may be $^{87}Sr/^{86}Sr$ and $^{3}He/^{4}He$

(*Continued*)

Table 1 (Continued)

Name (abbreviation)	Hot spot E. Long., N. Lat.	Age progression?	Age range	Swell?/width (km)	Connection to LIP?	Geoch. distinct from MORB
Cameroon (CAM)	6, −1	No	1–32 Ma	Yes/500–600	No	$^{206}Pb/^{204}Pb$
Canaries (CAN)	−17, 28	Ok	0–68 Ma	No	No	$^{206}Pb/^{204}Pb$
Cape Verde (CAP)	−24, 15	No	Neogene	Yes/800	No	$^{87}Sr/^{86}Sr$ and $^{206}Pb/^{204}Pb$
Discovery (DIS)	−6.45, −44.45	—	25 Ma	Yes/600	No	—
Fernando Do Norona (FER)	−32, −4	—	—	Yes/200–300	—	$^{87}Sr/^{86}Sr$ and $^{206}Pb/^{204}Pb$
Great Meteor (GM)	−28.5, 31	—	—	Yes/800	—	—
Iceland (ICE)	−17.58, 64.64	Yes	0–62 Ma	Yes/2700	N. Atlantic LIP	$^{3}He/^{4}He$
Jan Mayen (JM)	−8, 71.17	—	—	Yes	N. Atlantic LIP?	$^{87}Sr/^{86}Sr$
Madeira (MAD)	−17.5, 32.7	Yes	0–67 Ma	No	No	$^{206}Pb/^{204}Pb$
New England (NEW)	−57.5, 35	Yes	81–103, 122–124 Ma	No	No	$^{206}Pb/^{204}Pb$, may be $^{87}Sr/^{86}Sr$
Shona (SHO)	−4, −52	—	not dated	Yes/∼900	—	—
Sierra Leone (SL)	−29, 1	—	not dated	—	It could be a LIP	—
St. Helena (SHE)	−10, −17	Yes	3–81 Ma	Yes/720	No	$^{206}Pb/^{204}Pb$
Trindade-Martin Vaz (TRN)	−12.2, −37.5	Probably	<1 Ma to ∼85 Ma	Yes/1330	Small eruptions north of Parana flood basalts and onto Brazilian margin	$^{87}Sr/^{86}Sr$ and $^{206}Pb/^{204}Pb$
Tristan-Gough (TRI)	−9.9, −40.4 (Gough); −12.2, −37.5 (Tristan)	Yes	0.5–80 Ma and 130 Ma	Yes/850	Rio Grande-Walvis and Parana-Entendeka	$^{87}Sr/^{86}Sr$
Vema (VEM)	16, −32	—	>11 Ma	Yes/200–300		—
Indian						
Amsterdam-St. Paul (AMS)	77, −37	No	—	Yes/300–500	May be Kerguelen	may be $^{87}Sr/^{86}Sr$

Comores (COM)	44, −12	Yes	0–5.4 Ma on island chain and ∼50 Ma (Seychilles)	Yes/700–800	—	$^{87}Sr/^{86}Sr$ and $^{206}Pb/^{204}Pb$
Conrad (CON)	48, −54	—	Not dated	Half-width 400 south of seamounts	It could be a LIP	—
Crozet (CRO)	50, −46	—	Not dated	Yes/1120	May be Madagascar	$^{206}Pb/^{204}Pb$, may be $^{87}Sr/^{86}Sr$ (but few samples)
Kerguelen (KER)	63, −49	Yes	0.1–114 Ma (Kerg) and 38–82 Ma (Ninety east-Broken Ridge)	Yes/1310	It is a LIP	$^{87}Sr/^{86}Sr$
Marion (MAR)	37.75, −46.75	Weak	<0.5 Ma (Marion) and 88 Ma (Madagascar)	Half-width 500 or Along-axis >1700	Madagascar Plateau and Madagascar Island flood basalts	may be $^{87}Sr/^{86}Sr$
Réunion (REU)	55.5, −21	Yes	0–66 Ma	Yes/1380	Mascarene, Chagos-Lacc. and Deccan 30–70 My	$^{3}He/^{4}He$ and $^{87}Sr/^{86}Sr$
Africa						
Afar (AF)	42, 12	No	—	—	—	—
East Africa/ Lake Victoria (EAF)	34, 6	No	—	—	—	—
Darfur (DAR)	24, 13	No	—	—	—	—
Ahaggar (AHA)	6, 23	No	—	—	—	—
Tibesti (TIB)	17, 21	No	—	—	—	—
Eurasia						
Eifel (EIF)	7, 50	No	—	—	—	—

Horizontal bars indicate that there are no data, where we did not find any data, or where available data are inconclusive.

This is significantly longer than, for example, the activity of Hawaiian volcanoes which have a main stage lasting ~1 My (e.g., Clague and Dalrymple, 1987; Ozawa *et al.*, 2005). The long life span of some of the Canary volcanoes has contributed to uncertainty in defining a geographic age progression, but is consistent with a slow propagation rate of age-progressive volcanism (**Figure 3**).

Iceland is often cited as a classic hot spot (**Figure 4**). The thickest magmatic crust occurs along the Greenland– and Faeroe–Iceland volcanic ridges extending NW and SE from Iceland. Anomalously thick oceanic crust immediately adjacent to these ridges shows datable magnetic lineations (Macnab *et al.*, 1995; White, 1997; Jones *et al.*, 2002b). Extrapolating the ages of these lineations onto the Greenland– and Faeroe–Iceland Ridges reveals age-progressive volcanism with seafloor spreading, which is most easily explained by the Iceland hot spot causing excess magmatism very near to or at the Mid-Atlantic Ridge (MAR) since the time of continental breakup (Wilson, 1973; White, 1988, 1997). Earlier volcanism occurs as flood basalts along the continental margins of Greenland, the British Isles, and Norway ~56 Ma, and even further away from Iceland in Baffin Island, West and East Greenland, and the British Islands beginning ~62 Ma (e.g., Lawver and Mueller, 1994; Saunders *et al.*, 1997). The latter date provides a minimum estimate for the age of the Icelandic hot spot.

A few volcano chains fail to record volcanism for longer than a few tens of millions of years but the initiation of volcanism or the connection to older

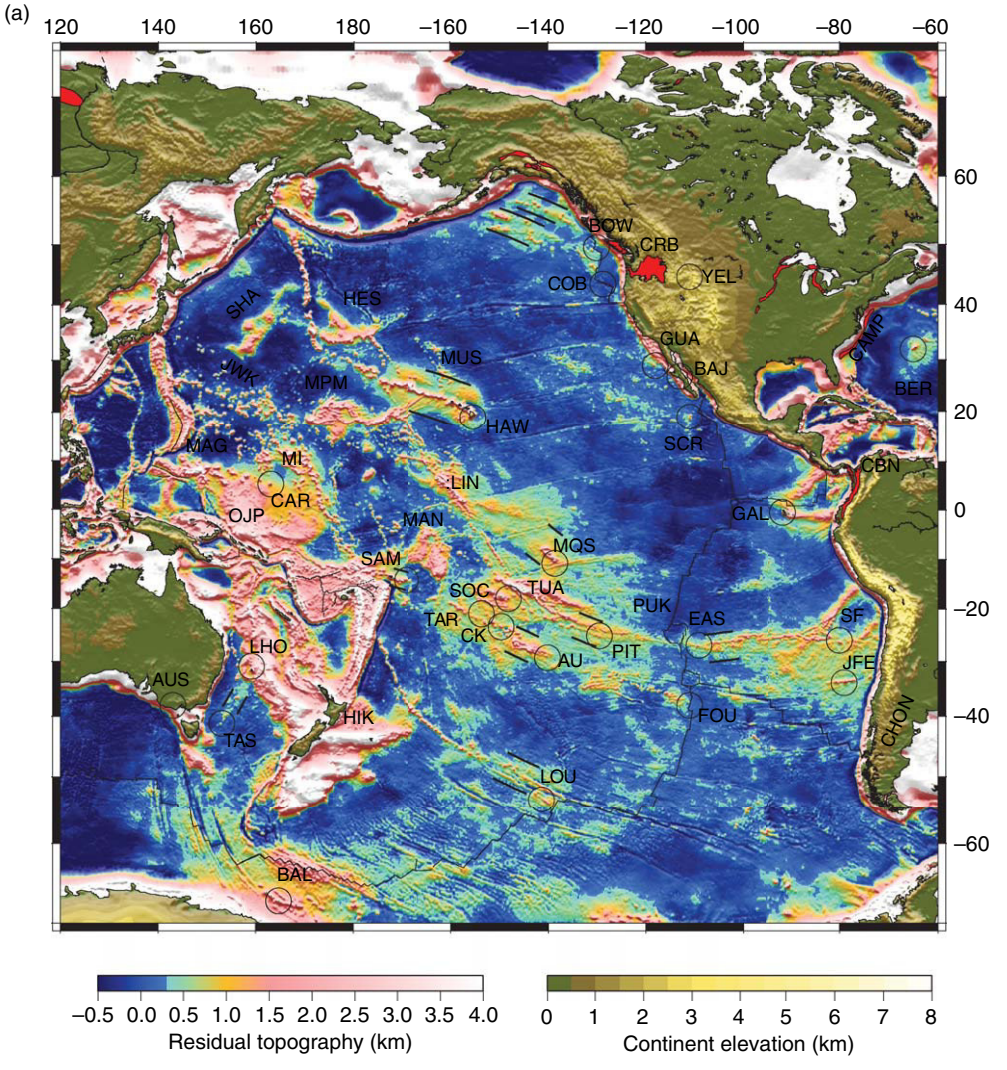

Figure 1 *(Continued)*

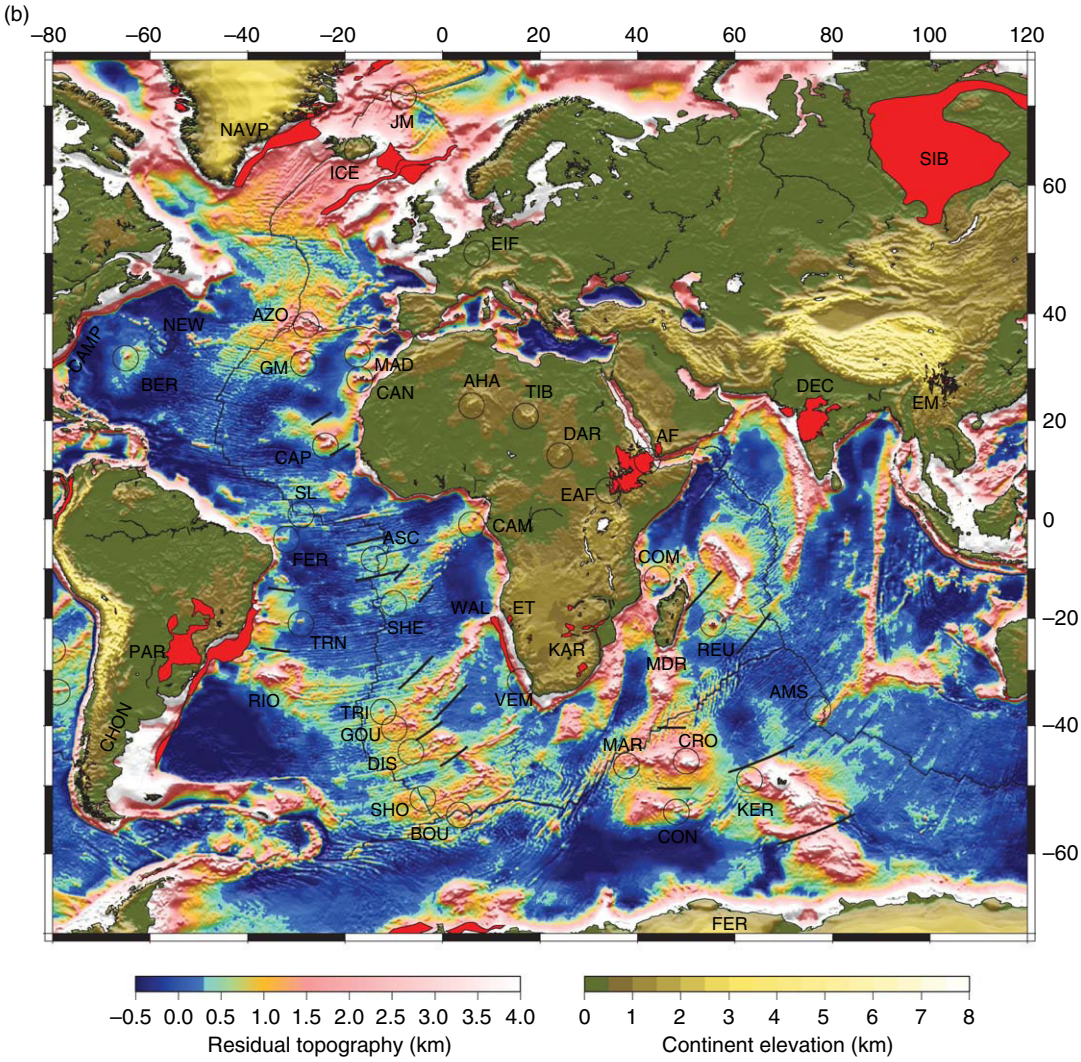

Figure 1 (a) Pacific region. Elevation on the continents and residual topography in the oceans. Residual topography is the predicted bathymetry grid of Smith and Sandwell (1997) corrected for sediment loading and thicknesses (Laske and Masters, 1997), and for seafloor subsidence with age (Stein and Stein, 1992) using seafloor ages, updated from Müller *et al*. (1993a) (areas without ages are interpolated using cubic splines). Grid processing and display was done using GMT (Wessel and Smith, 1995). Color change from blue to turquoise is at 300 m and delineates the approximate boundaries of anomalously shallow seafloor. Circles mark estimated locations of most recent (hot spot) volcanism. Pairs of lines are used to measure the widths of some of the hot-spot swells (**Table 1**). Flood basalt provinces on the continents and continental margins are red; abbreviations are identified in Section 7.09.2.3.2. Axes are in degrees latitude and east longitude. (b). Atlantic and Indian oceans.

volcanic provinces is somewhat unclear. For example, the New England seamount chain records ~20 My of oceanic volcanism (Duncan, 1984), but an extrapolation to the volcanic provinces in New England could extend the duration another 20 My (see O'Neill *et al.* (2005)). The duration of activity at the Azores hot spot is not clear. Gente *et al.* (2003) hypothesize that the Azores hot spot formed the Great Meteor and Corner seamounts as conjugate features ~85 Ma. Yet, age constraints of these edifices are poor and a geochemical association with the Azores group is yet to be tested. The most robust feature of this hot spot is its sudden influence on the MAR starting ~20 Ma as seen in geophysical surveys and dated using interpolations of seafloor isochrons (Cannat *et al*., 1999; Gente *et al*., 2003).

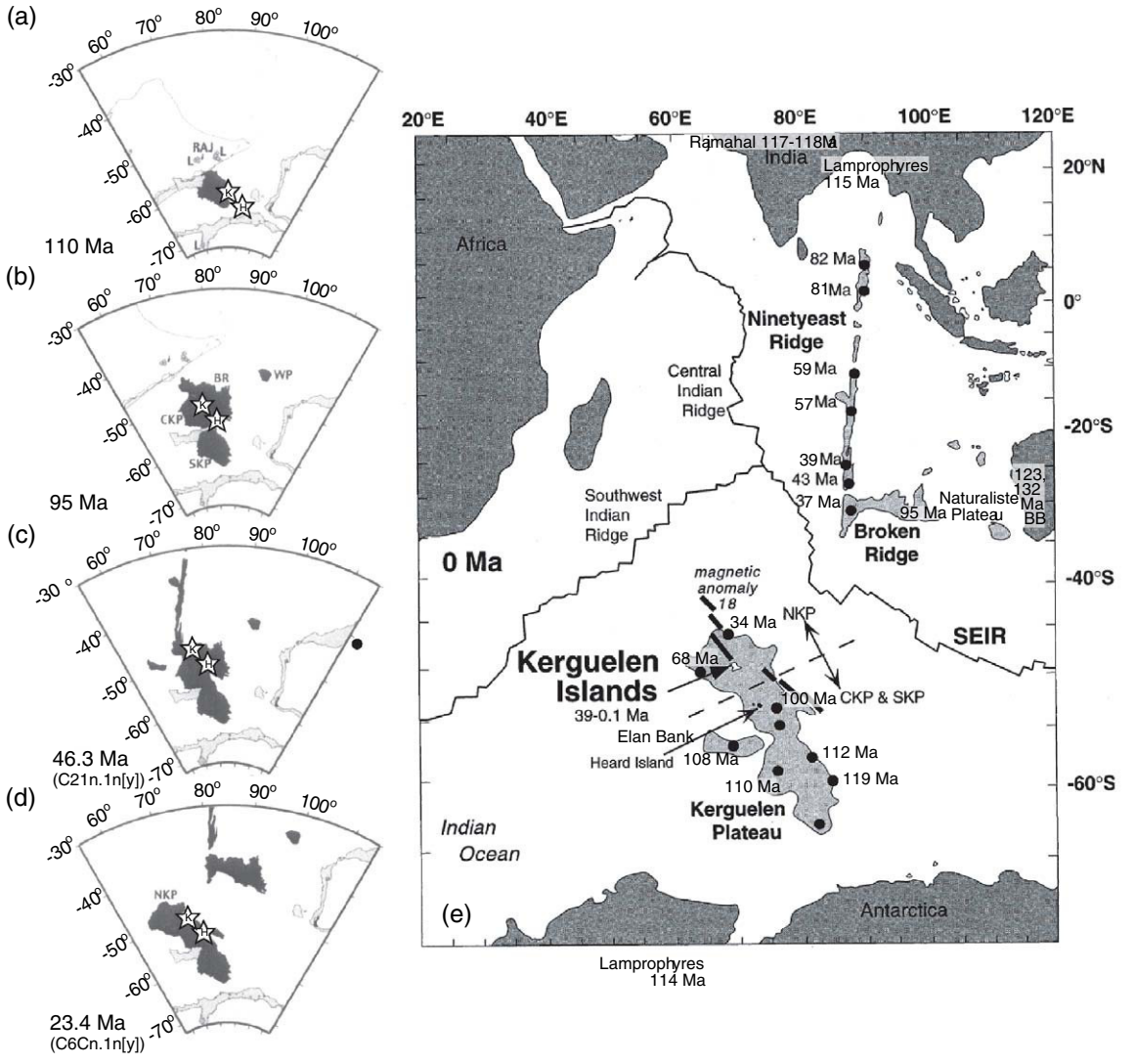

Figure 2 Evolution of the Kerguelen Plateau and hot-spot track. (a) The initial pulse of volcanism formed the Rajmahal Traps (RAJ), Lamprophreys (L) and the Southern Kerguelen Plateau (SKP) from ~120 to ~110 Ma. Stars mark reconstructed positions of the hot spot (Müller *et al*., 1993b) assuming a location at Kerguelen Archiplago (K) and Heard Island (H). By 110 Ma, seafloor spreading between India, Antarctica, and Australia is well underway. Formation of the Rajmahal Traps by the Kerguelen hot spot requires the hot spot to have moved by ~10° relative to the Earth's spin-axis (Kent *et al*., 2002) as consistent with a model of a mantle plume rising through a convecting mantle (Steinberger and O'Connell, 1998) (see also Section 7.09.3.5). (b) By 95 Ma, Central Kerguelen Plateau (CKP) and Broken Ridge (BR) have formed. (c) At 46.3 Ma, northward migration of the Indian plate forms the Ninetyeast Ridge along a transform fault in the mid-ocean ridge system. (d) The Southeast Indian Ridge has propagated northwestward to separate CKP and BR ~42 Ma, which continue drifting apart at 23.4 Ma. (e) Current configuration as shown by Nicolaysen *et al*. (2000), but with ages from Coffin *et al*. (2002). Bold line along NE margin of the plateau marks magnetic anomaly 18 (41.3–42.7 Ma). Reproduced from Coffin MF, Pringle MS, Duncan RA, *et al*. (2002) Kerguelen hotspot magma output since 130 Ma. *Journal of Petrology* 43: 1121–1139, by permission of Oxford University Press.

On the Pacific Plate (e.g., see Clouard and Bonneville (2005) and references therein), the Cobb (1.5–29.2 Ma (Turner *et al*., 1980; Desonie and Duncan, 1990) and Bowie–Kodiak chains (0.2–23.8 Ma (Turner *et al*., 1980)) terminate at the subduction zone south of Alaska. The Easter chain on the Nazca Plate extends to 25.6 Ma (Clouard and Bonneville, 2005) but the record on the Pacific Plate may extend further into the past, perhaps to the Tuamotu Plateau (Ito *et al*., 1995; Clouard and Bonneville, 2001). This tentative connection certainly warrants more age dating.

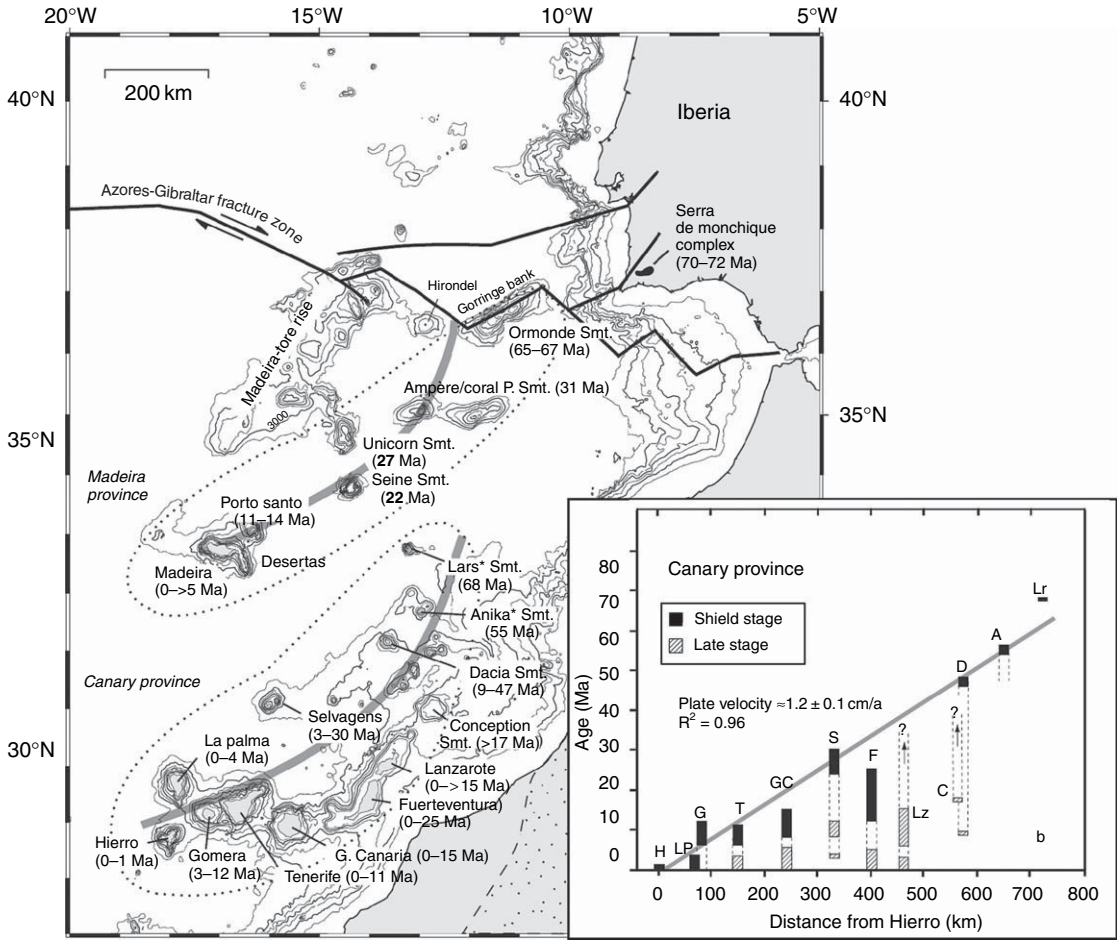

Figure 3 Map showing bathymetry around the Madeira and Canary group (only contours above 3500 m are shown). Stippled areas separate the two provinces based on geochemical distinctions. Thick gray lines mark possible hot-spot tracks. Lower-right plot shows the age range of the labeled volcanoes vs distance from Hierro. The oldest dates follow a trend of increasing age with distance at an average rate of ~12 km My^{-1}. Reproduced from Geldmacher J, Hoernle K, Van der Bogaard P, Duggen S, and Werner R (2005) New Ar-40/Ar-39 age and geochemical data from seamounts in the Canary and Madeira volcanic provinces: Support for the mantle plume hypothesis. *Earth And Planetary Science Letters* 237: 85–101.

7.09.2.1.2 Short-lived age-progressive volcanism

At least eight volcanic provinces show age-progressive volcanism lasting <22 My (e.g., Clouard and Bonneville, 2005). The Society and Marquesas (Caroff *et al.*, 1999) islands represent voluminous volcanism but for geologically brief durations of 4.2 and 5.5 My, respectively. Clouard and Bonneville (2001) use geometrical considerations to argue that the Marquesas hot spot could have formed the Line Islands and Hess Rise. If this interpretation is correct, the large gap in volcanism between the three provinces suggests a strongly time-varying mechanism. Durations of 10–20 My occur along the Pitcairn (0–11 Ma), Caroline (1.4–13.9 Ma), Foundation (2.1–21 Ma), Tarava (35.9–43.5 Ma), and Pukapuka (5.6–27.5 Ma) chains in the Pacific, as well as the Tasmandid chain (7–24.3 Ma) (McDougall and Duncan, 1988; Müller *et al.*, 1993b) near Australia.

An intriguing, yet enigmatic form of age-progressive volcanism is represented by the Pukapuka and Sojourn Ridges, which extend NW away from the East Pacific Rise. With respect to its geographic trend and duration, the Pukapuka Ridge resembles some of the other volcano chains in the region, such as the Foundation chain (**Figure 5**) (O'Connor *et al.*, 2002, 2004). The Pukapuka Ridge, however, stands out because of its smaller volcano volumes and the more rapid and variable rate of age progression (Janney *et al.*, 2000). It is thus unclear at this point whether these

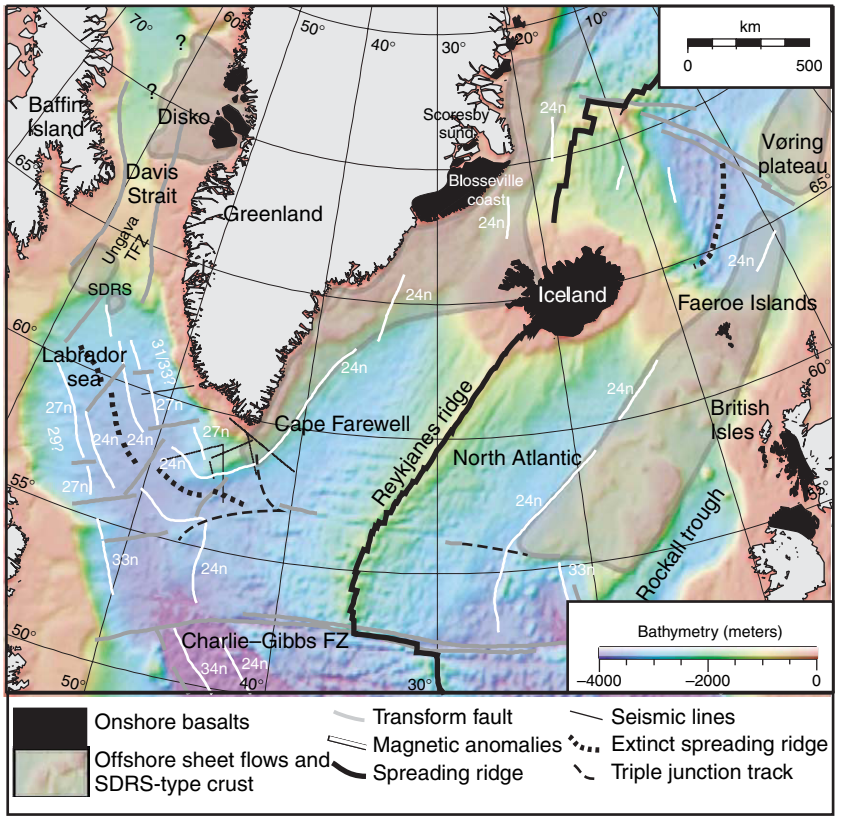

Figure 4 Distribution of Paleogene flood basalts in the North Atlantic Volcanic Province. Selective seafloor magnetic lineations, major transform faults, active and extinct spreading ridges, and seismic lines are marked as labeled. From Nielsen TK, Larsen HC, and Hopper JR (2002) Contrasting rifted margin styles south of Greenland; implications for mantle plume dynamics. *Earth and Planetary Science Letters* 200: 271–286.

differences indicate deviant behaviors of a common mechanism or a distinct mechanism entirely. Batiza (1982) proposed a distinction between hot-spot volcanoes and smaller (and more numerous) 'non-hot-spot' volcanoes. The association of such seamounts with near-axis, mid-ocean ridge volcanism is good reason to consider a volcano group non-hot-spot, but such a characterization is less straightforward for Pukapuka. While it projects to the region of the young Rano–Rani seamounts near the East Pacific Rise, most of Pukapuka formed on older seafloor (**Figure 5**). The above ambiguities blur the distinction between hot-spot and non-hot-spot volcanism.

7.09.2.1.3 No age-progressive volcanism

An important form of oceanic volcanism does not involve simple geographic age progressions. Amsterdam–St. Paul and Cape Verde are two examples that represent opposite extremes in terms of size and duration. Amsterdam–St. Paul is on the Southeast Indian Ridge, just NE of Kerguelen. Geochemical distinctions between lavas at Amsterdam–St. Paul and on Kerguelen suggest that they come from separate sources in the mantle (Doucet *et al.*, 2004; Graham *et al.*, 1999). With this interpretation, the Amsterdam–St. Paul hot spot represents a relatively small and short-lived ($\leq$5 My) melting anomaly. Its small size and duration, as well as its location on a mid-ocean ridge likely contribute to the lack of an identifiable age progression. The Cape Verde volcanoes, on the other hand, are larger and likely to have existed since early Neogene (e.g., McNutt, 1988). The islands do not show a monotonic age progression, but this is reasonably well explained with a hot spot occurring very close to the Euler pole that describes the motion of the African Plate relative to a hot-spot reference frame (McNutt, 1988).

Other examples of volcanoes with complex age-space relations are not well explained within the hot-spot framework. These include older provinces in the Pacific such as the Geologist seamounts, the Japanese and Markus–Wake seamounts, the Marshal Islands,

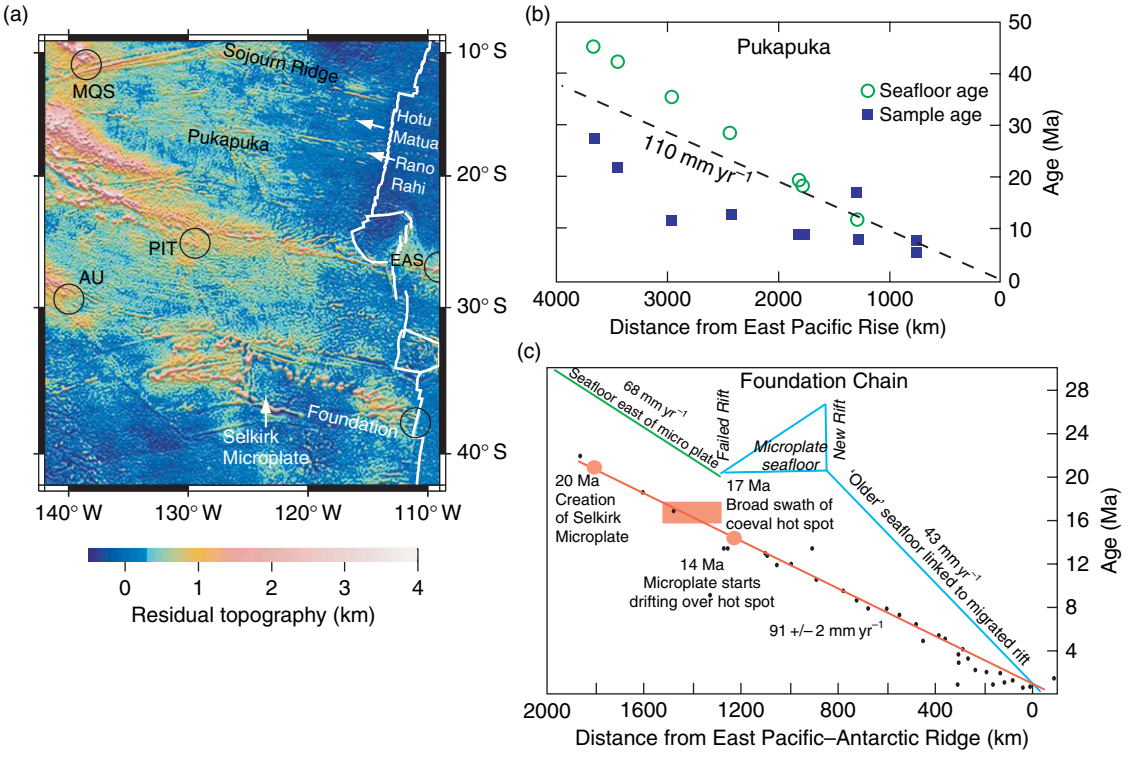

Figure 5 (a) Residual topography just east of the South Pacific Superswell. (b) Ages of samples seamounts along the Pukapuka Ridge and adjacent seafloor. (c) Figure showing ages along the Foundation Chain between 110° and 131° W. (b) Reproduced from Janney PE, Macdougall JD, Natland JH, and Lynch Ma (2000) Geochemical evidence from the Pukapuka volcanic ridge system for a shallow enriched mantle domain beneath the South Pacific Superswell. *Earth and Planetary Science Letters* 181: 47–60. (c) From O'Connor JM, Stoffers P, and Wijbrans JR (2004) The Foundation Chain: inferring hot-spot-plate interaction from a weak seamount trail. In: Hekinian R, Stoffers P, and Cheminee J-L (eds.) *Oceanic Hotspots*. Berlin: Springer.

the Mid-Pacific Mountains, and the Magellan Rise (e.g., Clouard and Bonneville (2005) and references therein). The lack of modern dating methods applied to samples of many of these provinces leads to significant age uncertainties, and the large number of volcanoes scattered throughout the western Pacific makes it difficult to even define volcano groups. Three notable examples show nonprogressive volcanism with ages confirmed with modern dating methods. The Line Islands and Cook–Austral groups are oceanic chains that both involve volcanism over tens of millions of years with synchronous or near-synchronous events spanning distances >2000 km (**Figure 6**) (Schlanger *et al.*, 1984; McNutt *et al.*, 1997; Davis *et al.*, 2002; Devey and Haase, 2004; Bonneville *et al.*, 2006). The Cameroon line, which extends from Africa to the SW on to the Atlantic seafloor (**Figure 7**) (Marzoli *et al.*, 2000), may represent a continental analog to the former oceanic cases.

The remaining oceanic hot spots in **Table 1** do not have sufficient chronological data to test for time–space relations. This list includes cases that are geographically localized (e.g., Discovery, Ascension/Circe, Sierra Leone, Conrad, Bermuda), have spatial distributions due to interactions with spreading centers (e.g., Bouvet, Shona, Balleny), or have elongated geographic trends but have simply not been adequately dated (Socorro, Tuamotu, Great Meteor).

7.09.2.1.4 Continental hot spots

In addition to the intraplate oceanic volcanism there are a number of volcanic regions in the continents that are not directly associated with present-day subduction or continental rifting. In **Figure 1** we included a number of these areas such as the Yellowstone (YEL)–Snake River volcanic progression, the European Eifel hot spot (EIF), and African hot spots such as expressed by the volcanic

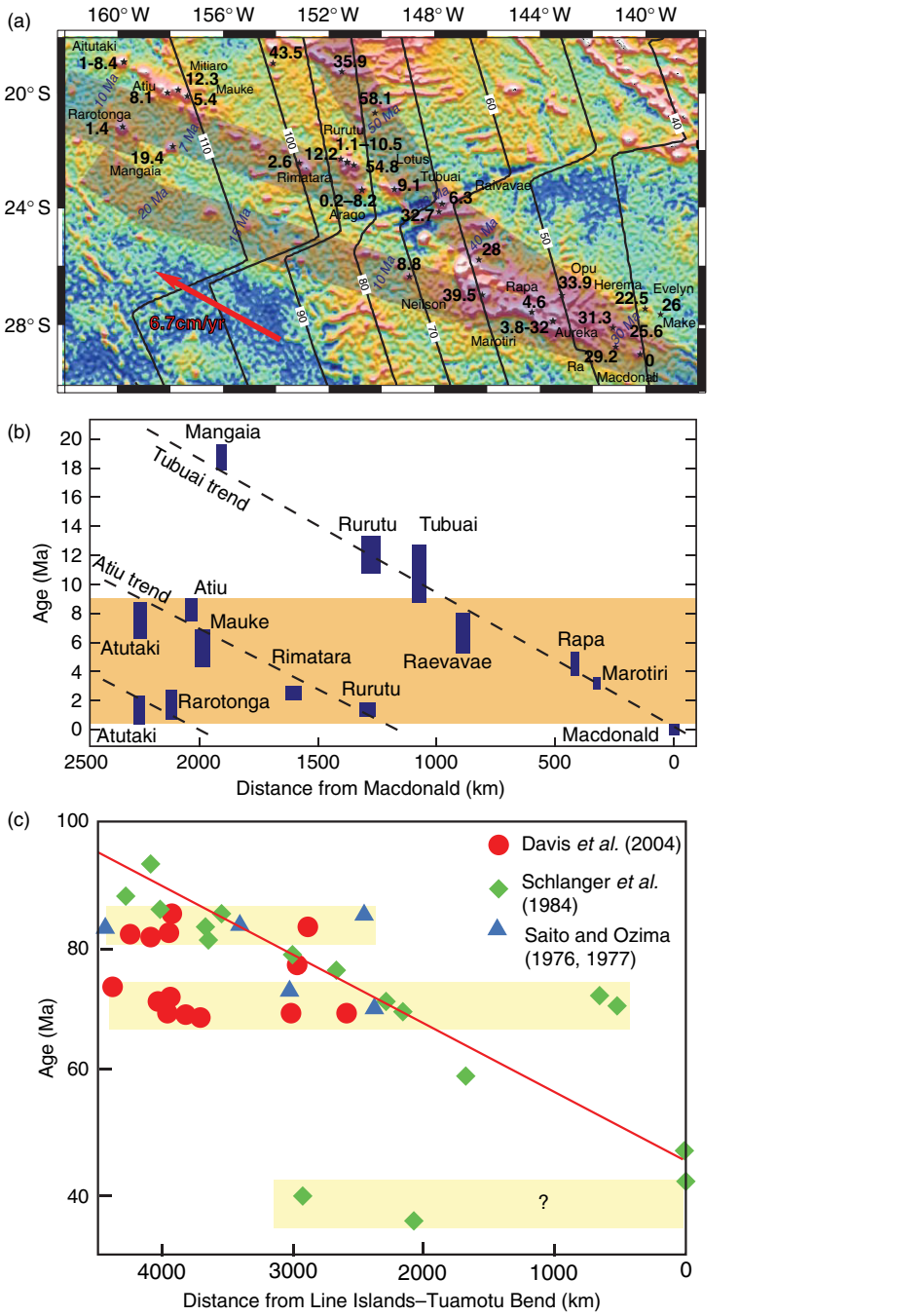

Figure 6 (a) Map of Cook–Austral group with age dates marked near sample locations. Shaded bands show possible hot-spot tracks using stage poles for absolute Pacific Plate motion of Wessel and Kroenke (1997). (b) A subset of the above dates vs distance from Macdonald seamount . This plot omits the ages >20 Ma along the northernmost hot-spot track shown in (a). Dashed lines have slopes of 110 km My^{-1}. (c) Age vs distance along the Line Islands. Diagonal red line represents a volcanic propagation rate of 96 km My^{-1} as proposed by Schlanger *et al*. (1984). Yellow bands show at least two and possibly three episodes of nearly sychronous volcanism. (a) Reproduced from Clouard V and Bonneville A (2005) Ages of seamounts, islands, and plateaus on the Pacific Plate. In: Foulger G., Natland JH, Presnall DC, and Anderson DL (eds.) *Plumes, Plates, and Paradigms,* pp. 71–90. Boulder, CO: GSA, with permission from GSA. (b) From Devey CW and Haase KM (2004) The sources for hotspot volcanism in the South Pacific Ocean. In: Hekinian R, Stoffers, P and Cheminee J-L (eds.) *Oceanic Hotspots*, pp. 253–280. New York: Springer. (c) Reproduced from Davis AS, Gray LB, Clague DA, and Hein JR (2002) The Line Islands revisited: New $^{40}Ar/^{39}Ar$ geochronologic evidence for episodes of volcanism due to lithospheric extension. *Geochemistry Geophysics Geosystems* 3(3), 10.1029/2001GC000190, with permission from AGU.

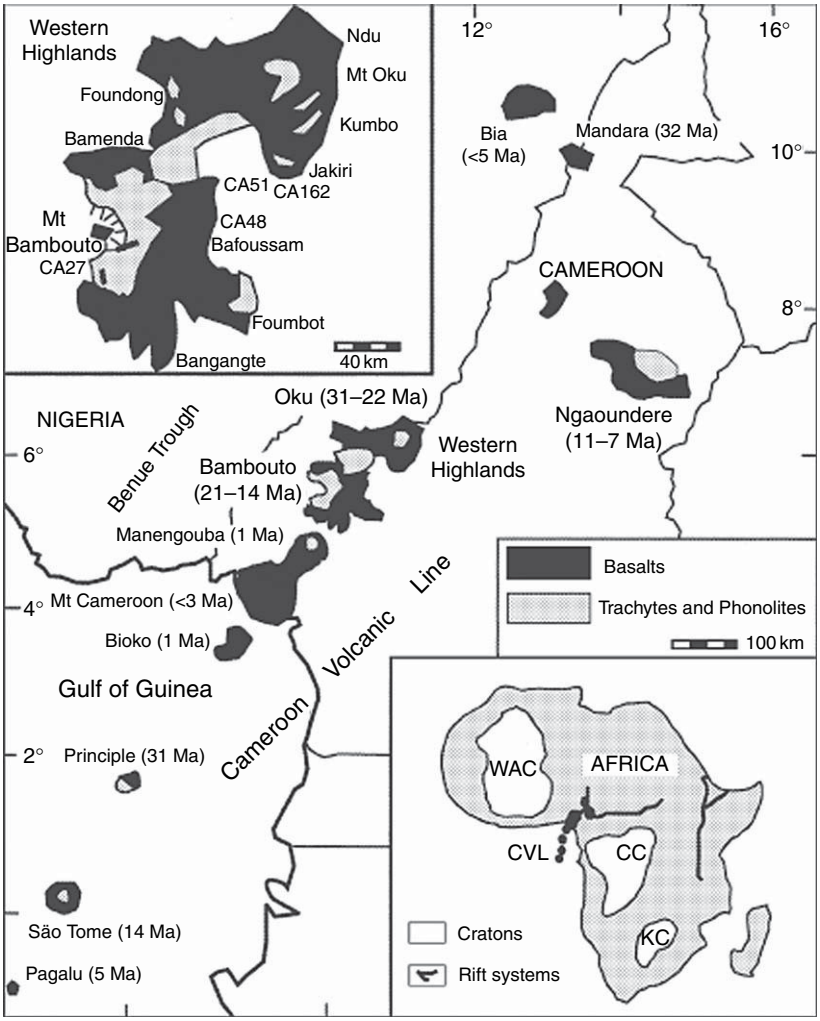

Figure 7 Sketch map of the Cameroon Line. Reported ages refer to the volcanism on the continent and to the onset of basaltic volcanism on the ocean islands. Inset, top left: sketch map of Western Cameroon Highlands showing location of basaltic samples used for $^{40}Ar/^{39}Ar$ dating. Inset, bottom right: West African Craton (WAC), Congo Craton (CC) and Kalahari Craton (KC). Reproduced from Marzoli A, Piccirillo EM, Renne PR, Bellieni G, Iacumin M, Nyobe JB, and Tongwa AT (2000) The Cameroon volcanic line revisited; petrogenesis of continental basaltic magmas from lithospheric and asthenospheric mantle sources. *Journal of Petrology* 41: 87–109, by permission of Oxford University Press.

mountains of Jebel Mara (DAR), Tibesti (TIB), and Ahaggar (AHA) (Burke, 1996). The Yellowstone hot spot is the only one with a clear age progression. The lack of age progression of the other hot spots could indicate very slow motion of the African and European Plates.

The Yellowstone hot spot is centered on the caldera in Yellowstone National Park. Its signatures include a topographic bulge that is 600 m high and approximately 600 km wide, high heat flow, extensive hydrothermal activity, and a 10–12 m positive geoid anomaly (Smith and Braile, 1994). The trace of the Yellowstone hot spot is recorded by silicic-caldera-forming events starting at 16–17 My at the Oregon–Nevada border, ~700 km WSW of the hot spot (**Figure 8**). The original rhyolitic volcanism is followed by long-lived basaltic volcanism that now forms the Snake River Plain. The effective speed of the hot-spot track is 4.5 cm yr^{-1}, which is interpreted to include a component of the present-day plate motion (2.5 cm yr^{-1}) and a component caused by the Basin and Range extension. The excess topography of the Snake River Plain decays systematically and is consistent to that of a cooling and thermally contracting lithosphere following the progression of the American Plate over a hot spot (Smith and Braile, 1994).

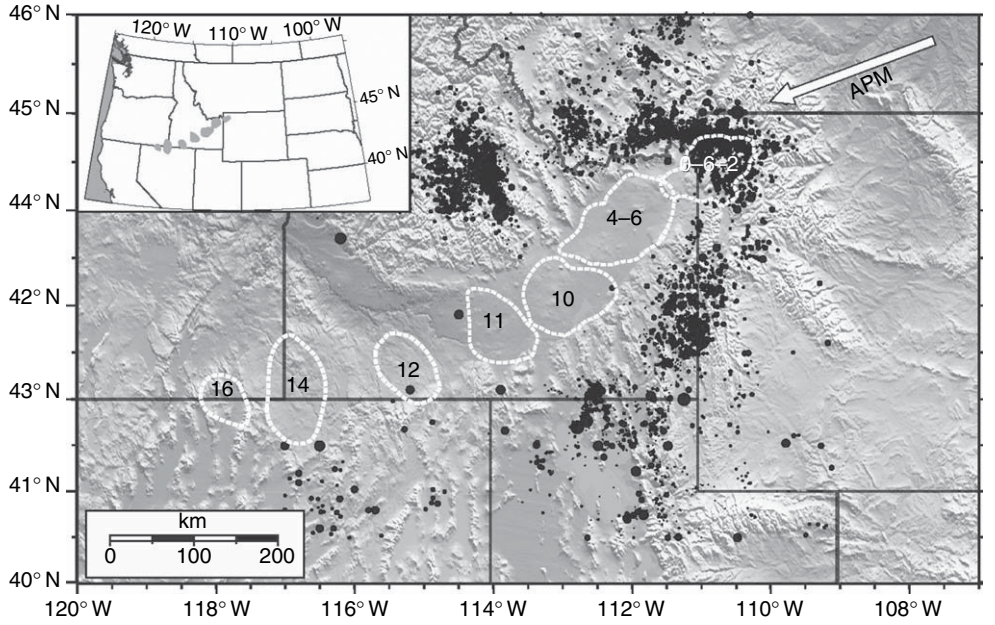

Figure 8 Shaded relief topography, seismicity (black circles), and calderas (white dashed lines with age indication in Ma) of the Yellowstone–Snake River province. Reproduced from Waite GP, Smith RB, and Allen RM (2006) V–P and V–S structure of the Yellowstone hot spot from teleseismic tomography: Evidence for an upper mantle plume. *Journal of Geophysical Research* 111: B04303, with permission from AGU.

7.09.2.1.5 The hot-spot reference frame

The existence of long-lived volcano chains with clear age progression led Morgan (1971, 1972) to suggest that hot spots remain stationary relative to one another and therefore define a global kinematic reference frame separate from the plates (Morgan, 1983; Duncan and Clague, 1985). However, ongoing studies have established that hot spots do move relative to the Earth's spin-axis and that there is motion between the Pacific and Indo-Atlantic hot spots with speeds comparable to the average plate speed (Molnar and Stock, 1987; Acton and Gordon, 1994; Tarduno and Gee, 1995; DiVenere and Kent, 1999; Raymond *et al.*, 2000; Torsvik *et al.*, 2002). Paleomagnetic evidence (Tarduno *et al.*, 2003; Pares and Moore, 2005) suggests rapid southward motion of the Kerguelen hot spot in the past 100 My and of the Hawaiian hot spot prior to the Hawaiian–Emperor Bend at 50 Ma (Sharpe and Clague, 2006). Southward motion of the Hawaiian hot spot appears to have slowed or nearly ceased since this time (Sager *et al.*, 2005). Combined with a possible shift in plate motion (Norton, 2000; Sharpe and Clague, 2006) this change most likely contributes to the sharpness of the Hawaiian–Emperor Bend (Richards and Lithgow-Bertelloni, 1996). Near present-day (i.e., <4–7 Ma) motion between hot spots globally is unresolvable or at least much slower than it has been in the geologic past (Wang and Wang, 2001; Gripp and Gordon, 2002).

While past rapid motion between groups of hot spots in different oceans is likely, rapid motion between hot spots on single plates is not. Geometric analyses of volcano locations suggest no relative motion, to within error, between some of the larger Pacific hot spots (Harada and Hamano, 2000; Wessel and Kroenke, 1997). Such geometric methods are independent of volcano ages and therefore have the advantage of using complete data sets of known volcano locations, unhindered by sparse age dating of variable quality. Koppers *et al.* (2001), however, argue that geometric analyses alone are incomplete and that when age constraints are considered as well, motion between the large Hawaiian and Louisville hot spots is required. But Wessel *et al.* (2006) show that the hot-spot track predicted by Koppers *et al.* (2001) misses large sections of both chains and present an improved plate-motion model derived independently of age dating. Thus, at this point, there appears to be little or no motion between the prominent Hawaiian and Louisville hot spots. Shorter chains in the Pacific do appear to move relative to larger chains (Koppers *et al.*, 1998;

Koppers and Staudigel, 2005) but as noted above, the existence of age progression along many short-lived chains is questionable. One enigma, in particular, is the apparent motion required between Iceland and both the Pacific and Atlantic hot spots (Norton, 2000; Raymond *et al.*, 2000). For a more complete description of the methods and above issues regarding absolute plate motion, *see* Chapter 6.02.

7.09.2.2 Topographic Swells

Figure 1 illustrates that most oceanic hot spots and melt anomalies show anomalously shallow topography extending several hundred kilometers beyond the area of excess volcanism. The prominence of hot-spot swells as established in the 1970s was initially attributed to heat anomalies in the mantle (Crough, 1978, 1983; Detrick and Crough, 1978). The evidence for their cause is somewhat ambiguous: for one, heat flow data fail to show evidence for heated or thinned lithosphere (Stein and Stein, 1993, 2003; DeLaughter *et al.*, 2005). However, it is likely that hydrothermal circulation associated with volcanic topography obscures the deep lithospheric signal (McNutt, 2002; Harris and McNutt, 2007). Seismic studies are limited but provide some clues. Rayleigh-wave dispersion shows evidence for a lithosphere of normal thickness beneath the Pitcairn hot spot (Yoshida and Suetsugu, 2004), whereas an S-wave receiver function study argues for substantial lithospheric thinning a few hundred kilometers up the Hawaiian chain from the hot spot (Li *et al.*, 2004).

Shallower-than-normal topography along the axes of hot-spot-influenced ridges indicates another form of hot-spot swell. Gravity and crustal seismic evidence indicate that topography along the ridges interacting with the Galápagos (Canales *et al.*, 2002) and Iceland (White *et al.*, 1995; Hooft *et al.*, 2006) hot spots are largely caused by thickened oceanic crust. In the case of the Galápagos spreading center, a resolvable contribution to topography likely comes from the mantle (Canales *et al.*, 2002), but for Iceland, it appears that crustal thickness alone can explain the observed topography (Hooft *et al.*, 2006).

An example of a much larger-scale swell is the South Pacific Superswell (McNutt and Fischer, 1987) which spans a geographic extent of ~3000 km and encompasses the hot spots in French Polynesia. Other swells of comparable size include the ancient Darwin Rise in the far northwestern Pacific (McNutt *et al.*, 1990) and the African Superswell (e.g., Nyblade and Robinson, 1994), which encompasses the southern portion of Africa and the South Atlantic down to the Bouvet Triple Junction. Both the South Pacific and African Superswells involve clusters of individual hot spots. The hot spots in the South Pacific (French Polynesia) are mostly short lived, including some without simple age progressions (see Section 7.09.2.1) (McNutt, 1998; McNutt *et al.*, 1997). This region is also known to have anomalously low seismic wave speeds in the mantle (e.g., Hager and Clayton, 1989; Ritsema and Allen, 2003) and relatively high geoid (McNutt *et al.*, 1990) suggesting an origin involving anomalously low densities but without substantially thinned lithosphere (e.g., McNutt, 1998). The African Superswell, on the other hand, does not show a seismic anomaly in the upper mantle but rather a broad columnar zone of slow velocities in the lower mantle (e.g., Dziewonski and Woodhouse, 1987; Li and Romanowicz, 1996; Ritsema *et al.*, 1999).

For individual hot spots, we identify the presence of a swell if residual topography exceeds an arbitrarily chosen value of 300 m and extends appreciably (>~100 km) away from volcanic topography (**Figure 1**). We find that such hot-spot swells are very common (**Table 1**). Swells are even apparent on chains with very small volcanoes such as the Tasmandid tracks and the Pukapuka (**Figure 5**) and Sojourn Ridges (Harmon *et al.*, 2007).

One characteristic of hot-spot swells is that they are not present around extremely old volcanoes (**Table 1**). The Hawaiian Swell for example is prominent in the youngest part of the chain but then begins to fade near ~178° W, disappears near the Hawaiian–Emperor Bend (50 Ma), and is absent around the Emperor chain (**Figure 1**). Swells also appear to fade along the Louisville chain (near a volcano age of ~34 Ma), along the Tristan chain near Walvis Ridge (62–79 Ma), and possibly along the Kerguelen track as evident from the shallow seafloor that extends away from the Kerguelen Plateau on the Antarctic Plate but that is absent around the southernmost portion of Broken Ridge (~43 Ma) on the Indian Plate. A swell appears to be present over the whole length of the St Helena chain out to ~80 Ma, but it is not possible with the current data to separate the swell around the oldest portion of this chain with that around the Cameroon line. The SE portion of the Line Islands (ages ranging from 35 to 91 Ma) most likely has a swell but the NE portion (55–128 Ma) may not. Given the diversity of possible times of volcanism in the Line Islands, however, it is not clear which episode is associated with the current

swell. Old chains that lack swells in our analysis include the Japanese–Wake seamounts (>70 Ma), the Magellan Seamounts (>70 Ma), the Mid-Pacs (>80 Ma), and the Musician Seamounts (>65.6 Ma). Overall, it thus appears that if a swell forms at a hot spot, it decreases in height with time until it can no longer be detected at an maximum age of 80 Ma, but often even after <50 Ma.

While swells are very prominent even around small or short-lived volcano chains, the Madeira and Canary hot spots are two cases that break the rule. The lack of obvious swells around these large and long-lived volcano chains is indeed very puzzling.

7.09.2.3 Flood Basalt Volcanism

LIPs provide further constraints on the nature of hot spots and mantle dynamics. In this chapter we use the term LIP to represent continental flood basalt provinces, oceanic plateaus, and volcanic passive margins, which are typified by massive outpourings and intrusions of basaltic lava, often occurring within a couple of million years. Reviews of the nature and possible origin of LIPs are provided by Richards *et al.* (1989); Coffin and Eldholm (1994); Mahoney and Coffin (1997); and Courtillot and Renne (2003). As characterized by Coffin and Eldholm (1994), continental LIPs, such as the Siberian Traps or the Columbia River Basalts, often form by fissure eruptions and horizontal flows of massive tholeiitic basalts. Volcanic passive margins, such as those of the North Atlantic Volcanic Province or Etendeka–Paraná, form generally just before continental rifting. The initial pulse is rapid and can be followed by a longer period of excess oceanic crust production and long-term generation of a seamount chain. Oceanic LIPs form broad, flat-topped features of thickened oceanic crust with some eruptions being subaerial (Kerguelen oceanic plateau) and others seeming to be confined to below sea level (e.g., Ontong Java Plateau (OJP) and Shatsky Rise). This section reviews some basic geophysical and geological observations of LIPs that formed since the Permian. For information on older LIPs we refer the reader to other reviews (Ernst and Buchan, 2001, 2003). **Figure 1** shows locations (abbreviations defined in the following text), and **Figure 9** summarizes the areas and volumes of the provinces described as follows.

7.09.2.3.1 Continental LIPs

Columbia River Basalts (*CRBs*). The CRBs erupted a volume of ~0.17 Mkm^3 between 16.6–15.3 Ma (Courtillot and Renne, 2003). Excellent exposures provide insights into flow structures and relationships to feeder dikes. Individual eruptions have volumes in excess of 2000 km^3 and flow over distances up to 600 km (Hooper, 1997). Lack of collapse structures suggests that large amounts of magma were rapidly derived from a deep source without being stored in the crust (Hooper, 1997).

Emeishan (*EM*). The EM province in west China is estimated to have spanned an area of at least 2 Mkm^2 and volume of 1 Mkm^3 when it first formed (Zhou *et al.*, 2002). Eruption ages are dated at 251–255 Ma and ~258 Ma (e.g., see Courtillot and Renne (2003), and Zhang *et al.* (2006) and references therein), with a date of ~259 Ma being confirmed by a Zircon U–Pb dating (Ali *et al.*, 2005). A rapid, kilometer scale uplift appears to have preceded the basalt eruption by

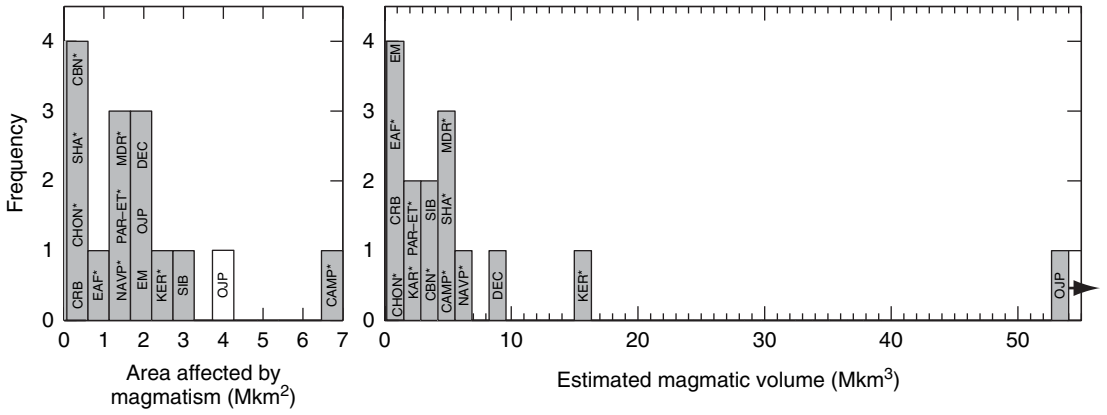

Figure 9 Histograms of estimated areas affected by magmatism and magmatic volumes of the large igneous provinces discussed in the text. The OJP–Manihiki–Hikurangi LIP would have the area shown by white bar and an even larger volume than shown, as indicated by arrow. Asterisks indicate provinces with voluminous magmatism that could have endured for >3 My to a few tens of millions of years; no asterisks indicate cases that mostly likely erupted in <3 My.

~3 My (Xu *et al.*, 2004; He *et al.*, 2003). Basalts erupted rapidly and were accompanied by high MgO basalts (He *et al.*, 2003; Zhang *et al.*, 2006). Since, the Emeishan traps have been fragmented and eroded, they currently encompass an area of only ~0.3 Mkm^2 (Xu *et al.*, 2001).

Siberia (*SIB*). The Siberian Traps are presently exposed over an area of only 0.4 Mkm^2 and have an average thickness of 1 km (Sharma, 1997). There are strong indications that the volcanics extend below sedimentary cover and into the West Siberian Basin (Reichow *et al.*, 2005). Additional dikes and kimberlites suggest a maximum extent of 3–4 Mkm^2 with a possible extrusive volume of >3 Mkm^3. Lack of significant sedimentary rocks or paleosols between flows suggests rapid extrusion (Sharma, 1997). Most of the province probably erupted within ~1 My coinciding with the Permo-Triassic boundary at 250 Ma (Courtillot and Renne, 2003). Individual flows can be as thick as 150 m and can be traced over lengths of hundreds of kilometers. Use of industry seismic and borehole data in the West Siberian Basin indicates that the basin elevation remained high during rifting, suggesting dynamic mantle support (Saunders *et al.*, 2005).

Yemen/Ethiopia/East Africa Rift System (*EAF*). An early volcanic episode in southernmost Ethiopia starting ~45 Ma was followed by widespread flood basalt volcanism in Northwest Ethiopia ~30 Ma and in Yemen starting 31–29 Ma. The 30 Ma Ethiopia event consisted of tholeiites and ignimbrites (Pik *et al.*, 1998) that erupted within 1–2 My (Hofmann *et al.*, 1997; Ayalew *et al.*, 2002). In Yemen, 0.35–1.2 Mkm^3 of mafic magmas were produced, followed by less voluminous silicic volcanism starting ~29 Ma (Menzies *et al.*, 1997). Flood volcanism appears to have occurred several million years prior to the onset of extension along the EAR ~23 Ma (Morley *et al.*, 1992; Hendrie *et al.*, 1994) and in the Gulf of Aden ~26 Ma (Menzies *et al.*, 1997). The volcanism is bimodal with shield volcanoes forming on top of tholeiitic basalts (Courtillot and Renne, 2003; Kieffer *et al.*, 2004). Currently, the Ethiopian and Kenyan Rift Systems are on an area of elevated topography ~1000 km in diameter. A negative Bouguer gravity anomaly suggests this topography is dynamically supported in the mantle (Ebinger *et al.*, 1989).

Older continental flood basalts. These are often more difficult to detect in the geological record due to the effects of surface uplift and erosion. A general characteristic that is attributed to continental LIPs is radiating dike swarms (Mege and Korme, 2004; Mayborn and Lesher, 2004). These dike swarms provide the main pathways for basaltic magmas vertically from the mantle, as well as laterally over distances up to 2500 km, as suggested for the 1270-My-old Mackenzie dike swarm in N. America (Lecheminant and Heaman, 1989; Ernst and Baragar, 1992). The longest dikes usually extend well beyond the original boundaries of the main lava field.

7.09.2.3.2 LIPs near or on continental margins

Central Atlantic Magmatic Province (*CAMP*). The CAMP is primarily delineated by giant dike swarms and is associated with the early breakup of Gondwana between North Africa, North America, and Central South America. Widely separated eruptions and dike swarms are present over an area of ~7 Mkm^2 with an estimated magmatic volume of ~2 Mkm^3 (Marzoli *et al.*, 1999), while seismic and magnetic studies on the eastern margin of North America suggest that this offshore portion of the CAMP could have a volume as large as 3 Mkm^3 (Holbrook and Kelemen, 1993). These estimates bring the total volume to near 5 Mkm^3. $^{40}Ar/^{39}Ar$ dates spanning 197–202 Ma suggests an emplacement episode lasting ~5 My (Hames *et al.*, 2000; Marzoli *et al.*, 1999; Courtillot and Renne, 2003). Only the offshore portion is mapped in **Figure 1**.

Chon Aike (*CHON*). In contrast to the other large igneous provinces discussed in the chapter, the Chon Aike Province in Patagonia is primarily silicic with rhyolites dominating over minor mafic and intermediate lavas. The rhyolites may have formed due to intrusion of basalts into crust that was susceptible to melting. The province is relatively small with an area of 0.1 Mkm^2 and total volume of 0.235 Mkm^3 (Pankhurst *et al.*, 1998). Chon Aike had an extended and punctuated eruptive history from Early Jurassic through Early Cretaceous (184–140 Ma). Pankhurst *et al.* (2000) recognize episodic eruptions with the first coinciding with the Karoo and Ferrar LIPs. The province potentially extends into present-day West Antarctica.

Deccan (*DEC*). The Deccan Traps provide one of the most impressive examples of continental flood basalts. It formed by primarily tholeiitic magmatism over Archean crust interspersed over an area of ~1.5 Mkm^2, with an estimated volume of 8.2 Mkm^3 (Coffin and Eldholm, 1993). Eruptions straddle the magnetic chrons C30n, C29r, C29n within 1 My

around the K–T boundary, as confirmed by ^{40}Ar–^{39}Ar and Re–Os dating (Allégre *et al.*, 1999; Courtillot *et al.*, 2000; Hofmann *et al.*, 2000). An iridium anomaly embedded between flows suggests that the Chicxulub impact happened while the Deccan Traps were active (Courtillot and Renne, 2003). Seafloor spreading between India and the Seychelles started a few million years after the major Deccan event, ~63 Ma (Vandamme *et al.*, 1991; Dyment, 1998). Unlike older continental flood basalts associated with the breakup of Gondwana, the Deccan basalts that are least contaminated by continental lithosphere closely resemble hot-spot basalts in oceanic areas and the major element contents agree with predictions for high-temperature melting (Hawkesworth *et al.*, 1999).

Karoo–Ferrar (*KAR–FER*). The Karoo province in Africa and Ferrar basalts in Antarctica record a volume of 2.5 Mkm^3 which erupted at ~184 Ma (Encarnacion *et al.*, 1996; Minor and Mukasa, 1997), possibly followed by a minor event at 180 Ma (Courtillot and Renne, 2003). The short (<1 My) duration is questioned by Jourdan *et al.* (2004, 2005) who obtained ages of ~179 Ma for the northern Okavango dike swarm in Botswana and consequently prefer a longer-lived initial activity that propagated from the south to the north. In Africa, tholeiitic basalts dominate but some picrites and some rhyolites occur (Cox, 1988). The triple-junction pattern of the radiating dike swarm that supplied the Karoo basalt was likely controlled by pre-existing lithospheric discontinuities that include the Kaapvaal and Zimbabwe Craton boundaries and the Limpopo mobile belt (Jourdan *et al.*, 2006). The Ferrar Province spans an area of ~0.35 Mkm^2 (Elliot and Fleming, 2004) in a linear belt along the Transantarctic Mountains. The two provinces were split by continental rifting and then seafloor spreading ~156 Ma.

Madagascar (*MDR*). Wide-spread voluminous basaltic flows and dikes occurred near the northwestern and southeastern coasts of Madagascar during its rifting from India around 88 Ma (Storey *et al.*, 1997). The oldest seafloor magnetic anomaly to form is chron 34 (84 Ma). Flood volcanism was probably prolonged as it continued to form the Madagascar Plateau to the south, perhaps 10–20 My later as inferred from the reconstructed positions of Marion hot spot.

North Atlantic Volcanic Province (*NAVP*). The NAVP covers ~1.3 Mkm^2 (Saunders *et al.*, 1997) with an estimated volume of 6.6 Mkm^3 (Coffin and Eldholm, 1993) and is closely linked to continental rifting and oceanic spreading (e.g., Nielsen *et al.*, 2002) (**Figure 2**). Prior to the main pulse of flood volcanism, seafloor spreading was active south of the Charlie–Gibbs fracture zone at 94 Ma and propagated northward into the Rockall Trough, which stopped in the late Cretaceous near or prior to the earliest eruptions of the NAVP. The early NAVP eruptions occurred as large picritic lavas in West Greenland and Baffin Island (Gill *et al.*, 1992, 1995; Holm *et al.*, 1993; Kent *et al.*, 2004) soon followed by massive tholeiitic eruptions in West and Southeast Greenland, British Isles, and Baffin Island at 61 Ma (2 Mkm^3) and in East Greenland and the Faeroes at 56 Ma (>2 Mkm^3) (Courtillot and Renne, 2003). The initial episodes were followed by rifting between Greenland and Europe recorded by Chron 24, 56–52 Ma, continental margin volcanisms, and ocean crust formation, which included the formation of thick seaward-dipping seismic reflection sequences. Spreading slowed in Labrador Sea ~50 Ma, stopped altogether at 36 Ma, but continued further to the west on the Aegir Ridge and eventually along the Kolbeinsey Ridge at ~25 Ma, where it has persisted since. This provides an intriguing suggestion that the presence of hot spots can guide the location of seafloor spreading following continental breakup.

Many of the volcanic margin sequences erupted subaerially or at shallow depths, suggesting widespread regional uplift during emplacement (Clift and Turner, 1995; Hopper *et al.*, 2003). Uplift in the Early Tertiary is documented by extensive erosion and changes in the depositional environments as far as the North Sea Basin (e.g., see Nadin *et al.* (1997) and Mackay *et al.* (2005) and references therein). Reconstructions from drill cores show that uplift was rapid and synchronous and preceded the earliest volcanism by >1 My (Clift *et al.*, 1998).

Paraná–Etendeka (*PAR–ET*). Paraná and Etendeka are conjugate volcanic fields split by the breakup of South America and Africa. The Paraná field in South America covers 1.2 Mkm^2 with estimated average thickness of 0.7 km (Peate, 1997). Extensive dike swarms surrounding the provinces suggest the original extent could have been even larger (Trumbull *et al.*, 2004). Volcanism is bimodal with dominating tholeiitic lavas and rhyolites. ^{40}Ar–^{39}Ar dates suggest a peak of eruption ~133–130 Ma (Turner and al., 1994; Renne *et al.*, 1996; Courtillot and Renne, 2003), preceded by minor eruptions in the northwest of the Paraná basin at 135–138 Ma (Stewart *et al.*, 1996). Younger magmatism persisted along the coast

(128–120 Ma) and into the Atlantic Ocean, subsequently forming the Rio Grande (RIO) and Walvis (WAL) oceanic plateaus.

The Etendeka province covers 0.08 Mkm^2 and is very similar to the Paraná flood basalts in terms of eruptive history, petrology, and geochemistry (Renne *et al.*, 1996; Ewart *et al.*, 2004). Seafloor spreading in the South Atlantic progressed northward, with the oldest magnetic anomalies near Cape Town (137 or 130 Ma). Earliest magnetic anomaly near Paraná is ~127 Ma. The formation of onshore and offshore basins suggests a protracted period of rifting well in advance of the formation of oceanic crust and the emplacement of the Paraná basalts (Chang *et al.*, 1992).

7.09.2.3.3 Oceanic LIPs

Caribbean (*CBN*). The Caribbean LIP is a Late Cretaceous plateau, which is now partly accreted in Colombia and Equador. Its present area is 0.6 Mkm^2 with thickness of oceanic crust ranging from 8–20 km. A volume of 4 Mkm^3 of extrusives erupted in discrete events from 91–88 Ma (Courtillot and Renne, 2003). The full range of $^{40}Ar/^{39}Ar$ dates of 69–139 Ma (e.g., Sinton *et al.*, 1997; Hoernle *et al.*, 2004), however, suggests a protracted volcanic history that is poorly understood. The cause volcanism has been attributed to the Galápagos hot spot, which is currently in the Eastern Pacific.

Kerguelen (*KER*). The Kerguelen hot spot has a fascinating history of continental and oceanic flood eruptions and rifting, as well as prolonged volcanism (**Figure 2**). The breakup of India, Australia, and Antarctica coincided closely in time with the eruption of the Bunbury basalts in southwest Australia, dated at 123 and 132 Ma (Coffin *et al.*, 2002). The first massive volcanic episode formed the Southern Kerguelen Plateau at 119 Ma, the Rajmahal Traps in India at 117–118 Ma followed by lamprophyres in India and Antarctica at 114–115 Ma (Coffin *et al.*, 2002; Kent *et al.*, 2002). The Central Kerguelen Plateau formed by ~110 Ma and Broken Ridge formed by 95 Ma (Coffin *et al.*, 2002; Frey *et al.*, 2000; Duncan, 2002). The above edifices represent the most active period of volcanism with a volcanic area and volume of 2.3 Mkm^2 and 15–24 Mkm^3, respectively (Coffin and Eldholm, 1993), but unlike many other flood basalt provinces, it spanned tens of millions of years. Another unusual aspect is the presence of continental blocks as suggested from wide-angle seismics (Operto and Charvis, 1996) and more directly from trace-element and isotopic data of xenoliths and basalts from Southern Kerguelen Plateau and Broken Ridge (Mahoney *et al.*, 1995; Neal *et al.*, 2002; Frey *et al.*, 2002). During 82 to 43 Ma northward motion of the Indian Plate formed the Ninetyeast Ridge on young oceanic lithosphere, suggesting the Kerguelen hot spot stayed close to the Indian–Antarctic spreading center (Kent *et al.*, 1997). At ~40 Ma, the Southeast Indian Ridge formed and separated Kerguelen and Broken Ridge. Volcanism has since persisted on the Northern Kerguelen Plateau until 0.1 Ma (Nicolaysen *et al.*, 2000). Dynamic uplift of the plateau in the Cretaceous is indicated by evidence for subaerial environment, but subsidence since then is not much different than normal oceanic subsidence (Coffin, 1992).

Ontong Java Plateau (*OJP*). A recent set of overview papers on the origin and evolution of the OJP is provided by Fitton *et al.* (2004) and Neal *et al.* (1997). This plateau extends across ~2 Mkm^2, has crust as thick as 36 km, and has volumes estimated at 44 Mkm^3 and 57 Mkm^3 for accretion off, and on a mid-ocean ridge, respectively (Gladczenko *et al.*, 1997). The majority of the basalts were erupted in a relatively short time (~1–2 My) near 122 Ma as revealed by ^{40}Ar–^{39}Ar (Tejada *et al.*, 1996), Re–Os isotope (Parkinson *et al.*, 2002), and paleomagnetic (Tarduno *et al.*, 1991) studies. Basalts recovered from Site 803, and the Santa Isabel and Ramos Islands indicate a smaller episode of volcanism at 90 Ma (Neal *et al.*, 1997). Age contrasts between the surrounding seafloor and OJP suggest it erupted near a mid-ocean ridge. Furthermore, rifting is evident on some of its boundaries and Taylor (2006) suggests that the OJP is only a fragment of what was originally an even larger edifice that included Manihiki (MAN) and Hikurangi (HIK) Plateaus. The inferred original size of the edifice makes it, by far, the largest of any flood basalt province in the geologic record, approaching an order of magnitude more voluminous than any continental flood basalt.

The plateau has been sampled on the tectonically uplifted portions in the Solomon Islands (e.g., Tejada *et al.*, 1996, 2002; Petterson, 2004) and with eight ocean drill holes (most recently during Ocean Drilling Program Leg 192; Mahoney *et al.* (2001)). The volcanics are dominated by massive flows of low-K tholeiitic basalts. Petrological modeling is consistent with the primary magmas formed by 30% melting of a peridotitic source (Fitton and Godard, 2004; Herzberg, 2004b; Chazey III and Neal, 2004), which would require a hot (1500°C) mantle under thin lithosphere. The low volatile

content of volcanic glasses (Roberge *et al.*, 2004, 2005), as well as the range and limited variability of Pb, Sr, Hf, and Nd isotope compositions (Tejada *et al.*, 2004) resemble characteristics of many MORB.

Besides its gigantic volume, the other aspect that makes OJP extremely enigmatic is that it appears to have erupted below sea level with little evidence for hot-spot-like uplift (Roberge *et al.*, 2005; Korenaga, 2005b; Ingle and Coffin, 2004; Coffin, 1992; Ito and Clift, 1998). These aspects must be explained by any successful model for the origin of this flood basalt province.

Shatsky–Hess Rise (*SHA–HES*). Shatsky Rise is one of the large Pacific oceanic plateaus with an area of 0.48 Mkm^2 and volume of 4.3 Mkm^3. The initial eruption is associated with the jump of a triple junction between the Pacific, Izanagi, and Farallon Plates toward the plateau (Nakanishi *et al.*, 1999; Sager, 2005) near 145 Ma (Mahoney *et al.*, 2005). Subsequently, volcanism progressed northeast together with the triple junction (which migrated with repeated jumps as indicated by seafloor magnetic lineation) until ~128 Ma. The most voluminous portion of the plateau is the central-southwest portion. Magmatism appears to have diminished toward the northeast (**Figure 1**). Thus Shatsky appears to show a short-lived age-progressive volcanism on timescales much like many smaller volcano groups (e.g., Cook–Austral and Pukapuka). Volcanism, however, may have continued with a renewed pulse starting some 10–20 My later with the formation of the Hess Rise, which is comparable in area to Shatsky. Age constraints on Hess Rise are poor because of the lack of sampling and its location on Cretaceous Quite Zone seafloor. The possible coincidence of both plateaus at a mid-ocean ridge suggests a dynamic linkage between their formation and seafloor spreading. Another notable aspect is that Pb and Nd isotope compositions for Shatsky Rise are indistinguishable from those of the present-day East Pacific Rise (Mahoney *et al.*, 2005).

7.09.2.3.4 Connections to hot spots

The possible links between hot spots and LIPs are important for testing the origin of both phenomena, with particular regard to the concept of a starting mantle plume head and trailing, narrower plume stem. While linkages are clear for some cases, a number of proposed connections are obscured by ridge migrations or breakup of the original LIP. Below we list the connections of hot spots to LIPs, in approximate order of decreasing reliability.

At least six examples have strong geographical, geochronological, and geochemical connections between hot-spot volcanism and flood basalt provinces. These are: (1) Iceland and the North Atlantic Volcanic Province, including Greenland, Baffin Island, Great Britain volcanics, Greenland–UK (Faeroe) Ridge (Saunders *et al.*, 1997; Smallwood and White, 2002); (2) Kerguelen, and Bunbury, Naturaliste, Rajmahal (E. India), Broken Ridge, and Ninetyeast Ridge (Kent *et al.*, 1997); (3) Réunion and Deccan (Roy, 2003), W. Indian, Chagos–Laccadive, Mascarenas, Mauritius; (4) Marion and Madagascar (Storey *et al.*, 1997); (5) Tristan da Cunha and Paraná, Etendeka, Rio Grande, Walvis Ridge (Peate, 1997); (6) Galapagos and Caribbean (Feigenson *et al.*, 2004; Hoernle *et al.*, 2004).

In addition to these six examples, a tentative link exists between Yellowstone and the early eruptive sequence of the CRBs based on geochemistry (Dodson *et al.*, 1997), but the paleogeographical connection is somewhat indirect since the main CRB eruption occurred up to 500 km north of the hot-spot track. This may suggest a mechanism for the formation of the flood basalts that is independent of the Yellowstone hot spot (Hales *et al.*, 2005). Yet, the earliest manifestation of the CRBs is possibly the Steens Mountain basalt (Oregon) which is located well to the south of the main eruptive sequences (Hooper, 1997; Hooper *et al.*, 2002) and closer to the proposed location of the Yellowstone hot spot. This suggests a south-to-northward propagation of the basalts and supports the suggestion that flood basalts may have been forced sideways from their mantle source by more competent continental lithosphere toward a weaker 'thin spot' in the lithosphere (Thompson and Gibson, 1991).

The links are less clear – in part due to lack of data – for other flood basalt provinces. The Bouvet hot spot has been linked to the Karoo–Ferrar; the Balleny hot spot may be connected to the Tasmanian Province or to Lord Howe Rise (Lanyon *et al.*, 1993); and the Fernando hot spot has been linked to the Central Atlantic Magmatic Province. Only three Pacific hot spots possibly link back to LIPs: Louisville–OJP, Easter–Mid-Pac, and Marquesas–Hess-Shatsky (Clouard and Bonneville, 2001). The Louisville–OJP connection is doubtful at best: kinematic arguments against such a link have been made (Antretter *et al.*, 2004) and geochemical distinctions between the oldest Louisville seamounts and OJP would require distinct geochemistry between plume head and tail or a difference in melting conditions (Mahoney *et al.*,

1993; Neal *et al.*, 1997). Finally, some hot spots such as Hawaii, Bowie–Kodiak, and Cobb terminate at subduction zones, so any record of a possible LIP has been destroyed.

It is interesting to note that the strongest connections between hot-spot chains and LIPs involve flood basalt provinces near continental margins. The possible exception is Kerguelen, for which most of the magmatism occurred away from any continental margins. The presence of continents probably plays a key role in the origin of many flood basalt provinces (Anderson, 1994b).

7.09.2.4 Geochemical Heterogeneity and Distinctions from MORB

The geochemistry of MORBs and basalts from hot spots and melting anomalies has played a key role in our understanding of mantle dynamics. Isotope ratios of key trace elements reflect long-term (10^2–10^3 My) concentration ratios between parent and daughter elements and therefore have been used to fingerprint the mantle from which different lavas arise. We will focus on three commonly used ratios: $^{87}Sr/^{86}Sr$, $^{206}Pb/^{204}Pb$, and $^{3}He/^{4}He$. High (or low) $^{87}Sr/^{86}Sr$ is associated with mantle material that is enriched (or depleted) in highly incompatible elements (i.e., those that partition mostly into melt when in equilibrium with the solid during partial melting) relative to moderately incompatible elements (e.g., Rb/Sr). High (or low) $^{206}Pb/^{204}Pb$ ratios are associated with mantle with a long-term high (or low) U/Pb. The $^{3}He/^{4}He$ ratio is a measure of the amount of primordial helium (^{3}He, which was present in the presolar nebula and is only lost from the Earth to space via degassing) relative to ^{4}He, which is primarily generated by radioactive decay of U and Th.

MORB is well characterized by low and small variability in the above ratios. **Figure 10** shows frequency distributions of basalts from the three major oceans; the data are from http://www.petdb.org/ and absolutely no data (e.g., Iceland) are excluded. One standard deviation about the median for all three datasets combined defines the MORB range for $^{87}Sr/^{86}Sr$ of 0.7025–0.7033, for $^{206}Pb/^{204}Pb$ of 17.98–18.89, and for $^{3}He/^{4}He$ of 7.08–10.21 (where $^{3}He/^{4}He$ is given in multiples of the atmosphere ratio, R_a). Significantly, while the median values from the three major spreading systems vary individually, each fall within the above ranges for all three isotope ratios. In contrast, ocean-island basalts (OIBs) have much larger variability, extending from MORB values to much higher values (**Figure 10**). By comparing the median hot-spot compositions (solid bar) with the MORB ranges, it becomes clear that, with few exceptions, the hot spots and melting anomalies have compositions that are distinguishable from MORB by at least one of the three isotope ratios (see also **Table 1**). This result appears to be independent of the duration of age-progression (e.g., Tristan vs. Marquesas), the presence or absence of a swell (Hawaii vs. Canaries), or even volcano size (Kerguelen vs. Pukapuka (Janney *et al.* (2000)) and Foundation (Maia *et al.* (2000)).

There are at least four possible exceptions: Cobb, Bowie–Kodiak, the Caroline seamounts, and the Shatsky Rise. Helium isotopes are not yet available at these locations but $^{87}Sr/^{86}Sr$ and $^{206}Pb/^{204}Pb$ compositions for each case fall within or very near to the MORB range. These examples span a wide range of forms, from a small, short-lived seamount chain (Caroline), to longer-lived, age-progressive volcanism (Cobb, Bowie–Kodiak), to an oceanic LIP (Shatsky). The possibility that these cases are geochemically indistinguishable from MORB has far-reaching implications about mantle processes and chemical structure; it clearly needs testing with further sampling.

7.09.2.5 Mantle Seismic Anomalies

7.09.2.5.1 Global seismic studies

Seismic wave propagation is generally slowed by elevated temperature, volatile content, the presence of melt, and mafic (primarily garnet) content of the mantle (e.g., Anderson, 1989). Seismology is therefore the primary geophysical tool for probing the mantle signature of hot spots and melting anomalies. Seismic tomography has become a popular method of 'imaging' the mantle. While it has provided important insights into the deep transport of subducting slabs (e.g., Grand *et al.*, 1997; Bijwaard *et al.*, 1998), seismic tomography has yet to produce robust images with sufficient spatial resolution in the deep mantle beneath hot spots (Nataf, 2000; Ritsema and Allen, 2003). The lack of methods that can probe the lower mantle with sufficient resolution makes it particularly difficult to address questions regarding the putative lower-mantle source for hot spots.

Global seismic models provide a first attempt to trace the surface expressions of hot spots to seismic anomalies into the mantle (Niu *et al.*, 2002; Zhao, 2001; DePaolo and Manga, 2003; Montelli *et al.*, 2004). The most robust features are the voluminous low-velocity

Figure 10 Frequency distributions (dark gray, normalized by maximum frequency for each case, so the peaks are at 1.0) of isotope measurements taken from the shown oceanic hot spots and mid-ocean ridges (lower left). Solid lines mark median values and dashed lines encompass 68% (i.e., one standard deviation of a normal distribution) of the samples. Light gray bars denote the range of values encompassing 68% of all of the MORB measurements (sum of the three ridges shown). Most of these data are from the GEOROC database with key references for ^{3}He/^{4}He data given in Ito and Mahoney (2006). Data for the Puka–Puka are from Janney *et al*. (2000) and for the Foundation chain from Maia *et al*. (2000).

anomalies in the lowermost mantle below the South Pacific and Africa Superswell regions (Breger *et al.*, 2001; Ni *et al.*, 2005; van der Hilst and Karason, 1999; Trampert *et al.*, 2004). The sharp edges of these anomalies (Ni *et al.*, 2002; To *et al.*, 2005) and their reproduction in dynamical models (Tan and Gurnis, 2005; McNamara and Zhong, 2005) suggest both a compositional and thermal origin of these anomalies. It is more difficult to identify low-velocity anomalies at smaller spatial scales and shallower depths. For example, Ritsema and Allen (2003) investigated the correlation between seismic low-velocity regions in the global S-wave model S20RTS (Ritsema *et al.*, 1999) and hot spots from a comprehensive list (Sleep, 1990). They confidently detected anomalously low seismic wave speeds in the upper mantle for only a small numbers of hot spots. Stronger correlations between a number of hot spots and deep-mantle anomalies were found using finite-frequency P- and S-wave tomography (Montelli *et al.*, 2004), but the ability of this method to actually improve the resolution with the available data is debated (de Hoop and van der Hilst, 2005; van der Hilst and de Hoop, 2005; Boschi *et al.*, 2006).

The topography of seismic discontinuities in the transition zone may also reflect heterogeneity. A hotter anomaly causes the exothermic phase change at 410 km to occur deeper and the endothermic phase change at 660 km to occur shallower, assuming the olivine system dominates the phase changes (Ito and Takahashi, 1989; Helffrich, 2000). Global observations of the transition zone thickness provide some support for hotter-than-normal mantle below some hot spots (e.g., Helffrich, 2002; Li *et al.*, 2003a, 2003b), although other observations suggest that global seismic data can resolve strong correlations between topography of the 410 km discontinuity and seismic velocities only at wavelengths larger than those of individual hot spots (Chambers *et al.*, 2005).

7.09.2.5.2 Local seismic studies of major hot spots

Improved insights into the upper mantle beneath hot spots can be obtained using regional or array studies, including the use of surface waves (e.g., Pilidou *et al.*, 2005).

Iceland. Regional seismic studies have confidently imaged a body of anomalously slow seismic wave speeds in the upper mantle beneath Iceland. Conventional ray theory was used to first image the anomaly (Allen *et al.*, 1999a, 2002; Foulger *et al.*, 2001; Wolfe *et al.*, 1997) but improved finite-frequency techniques (Allen and Tromp, 2005) resolve the feature to be roughly columnar with lateral dimension of 250–300 km and peak P- and S-wave anomalies of −2.1% and −4.2%, respectively (Hung *et al.*, 2004) (**Figure 11**). Recent studies using Rayleigh waves and local earthquakes confirm these high amplitudes, which most likely require a combination of excess temperature and melt (Yang and Shen, 2005; Li and Detrick, 2006).

In addition, studies of surface waves and shear-wave splitting reveal significant seismic anisotropy in the Icelandic upper mantle (Li and Detrick, 2003; Bjarnason *et al.*, 2002; Xue and Allen, 2005). Overall, they find that the fast S-wave propagation directions are mostly NNE–SSW in central Iceland with stronger E–W components to the west and east. The anisotropy in west and eastern Iceland deviates significantly from the directions of motion of the two plates and thus could indicate a large-scale mantle flow in the region (Bjarnason *et al.*, 2002). However, in central Iceland, the strong rift-parallel anisotropy near the active rift zones is interpreted to indicate ridge-parallel flow associated with a mantle plume (Li and Detrick, 2003; Xue and Allen, 2005).

The anomalous seismic structure extends well below 410 km as evidenced by the thinning of the transition zone beneath Iceland (Shen *et al.*, 1998) (**Figure 12**). While Shen *et al.* (1998) show evidence for both a deepening 410- and shoaling 660-discontinuity, Du *et al.* (2006) argue that the discontinuity at 660 km is instead flat. The precise nature of both discontinuities is important in determining whether the Iceland anomaly initiates in the upper mantle or is present below 660 km (Shen *et al.* 1998). One global tomography model suggests that the anomaly extends into the lower mantle (Bijwaard and Spakman, 1999) and another study identifies an ultralow-velocity zone near the core–mantle boundary (CMB) below Iceland (Helmberger *et al.*, 1998). The available seismic data, however, leave a lower mantle origin open to debate (e.g., Foulger *et al.*, 2001) and a robust test awaits improved regional seismic experiments.

Other Atlantic hotspots. Slow surface-wave speed anomalies extend to 200 km below the Azores hot spot as part of an along-strike perturbation of the velocity structure beneath the MAR (Pilidou *et al.*, 2004). Receiver function analysis at Cape Verde (Lodge and Helffrich, 2006) indicates a thickened crust (∼15 km) and a high-velocity, low-density zone to a depth of ∼90 km. The oldest volcanoes sit on top of the thickest parts of the crust and the high-velocity layer. Such high velocities in the shallow mantle beneath active hot spots are unusual. They

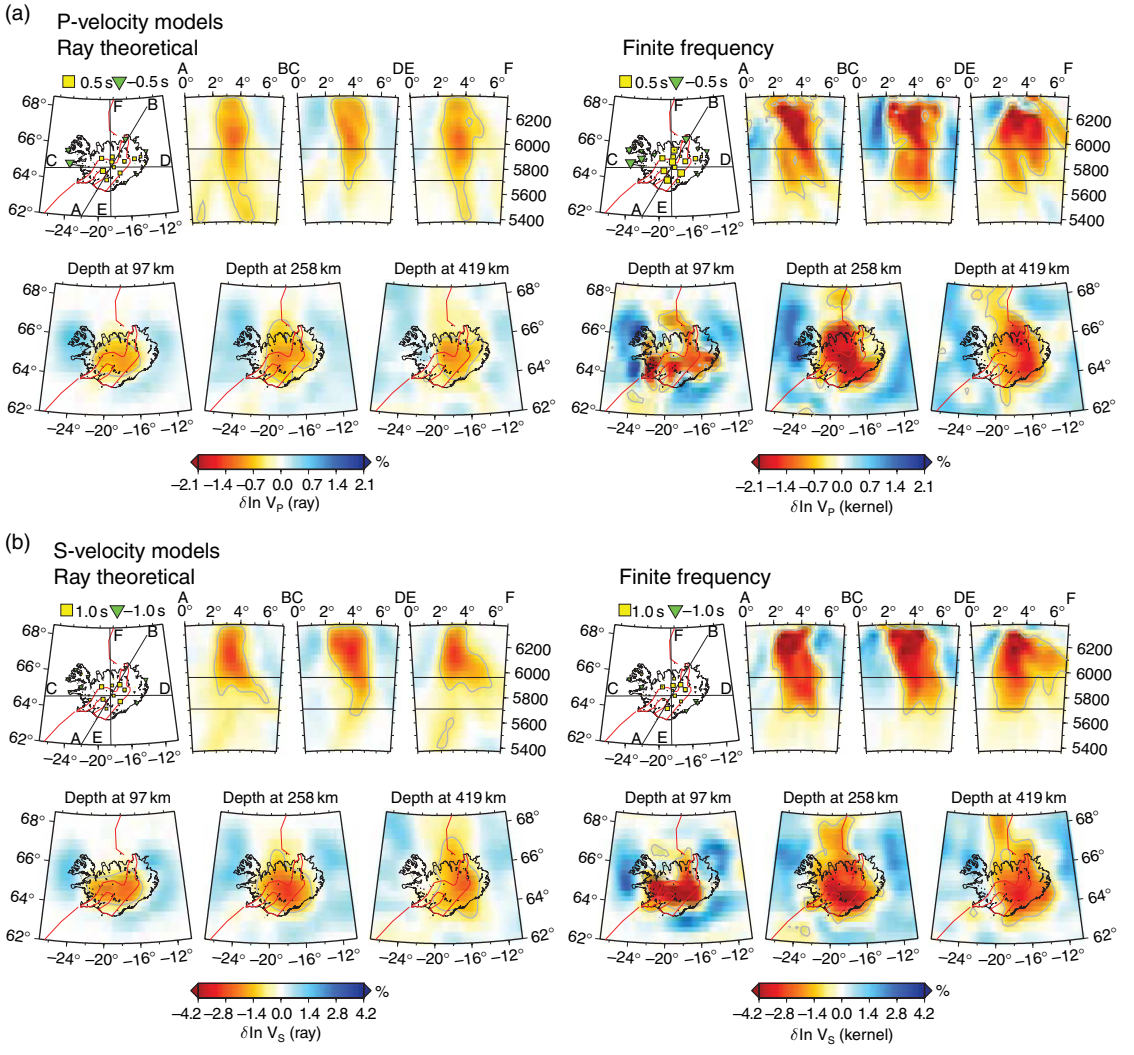

Figure 11 Tomographic inversions of the mantle below the Iceland hot spot imaged by suggesting major improvement in the resolving power using a finite frequency approach (right) compared to traditional ray based methods (left) in both P- (top) and S- (bottom) wave models. Reproduced from Hung SH, Shen Y, and Chiao LY (2004) Imaging seismic velocity structure beneath the Iceland hot spot: A finite frequency approach. *Journal of Geophysical Research* 109: B08305 (doi:10.1029/2003JB002889), with permission from AGU.

suggest major-element heterogeneity (e.g., due to melt depletion) dominate over other effects such as the presence of volatiles, melt, or excess temperature.

Hawaii. Anomalously low seismic wave speeds beneath the Hawaiian hot spot have been found from preliminary surface wave (Laske *et al.*, 1999) and tomographic (Wolfe *et al.*, 2002) studies. The anomaly imaged by tomography appears broader and higher in amplitude for S-waves (200 km diameter and up to −1.8%) than it does for P-waves (100 km diameter and −0.7%). A significant low S-wave speed (<4 km s^{-1}) is observed below 130 km suggesting the presence of partial melt below this depth (Li *et al.*, 2000). Additional evidence for an upper-mantle melt anomaly is provided by a seafloor magnetotelluric study (Constable and Heinson, 2004) which suggested a columnar zone of 5–10% partial melting with a radius <100 km and a depth extent of 150 km. Insights into the deeper structure using seismic tomography are currently hindered by poor coverage of stations and earthquake sources, but resolution tests indicate that the anomaly is unlikely to be restricted to the lithosphere (Wolfe *et al.*, 2002). A deep origin is suggested by evidence for a thinning of the transition zone by 40–50 km (Li *et al.*, 2000, 2004; Collins *et al.*, 2002). These studies, as well as a

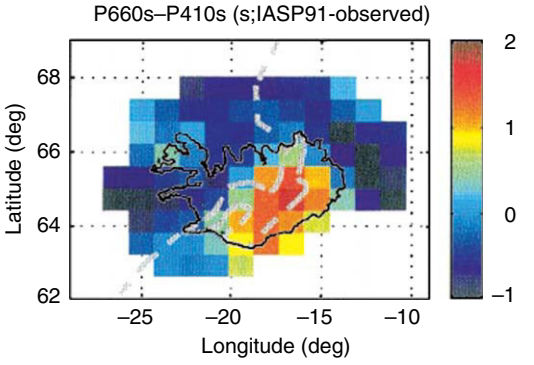

Figure 12 Difference in travel time between PS conversions at depths of 660 and 410 km with respect to the IASPEI91 (Kennett and Engdahl, 1991) reference model in seconds. The sharp decrease in velocity in a focused zone below Iceland suggests a strong thinning of the transition zone which is best explained by a significant increase in local mantle temperature. Reprinted by permission from Macmillan Publishers Ltd: (Nature) Shen Y, Solomon SC, Bjarnason IT, and Wolfe C 1998) Seismic evidence for a lower mantle origin of the Iceland plume. *Nature* 395: 62–65, copyright (1998).

combined seismic and electromagnetic inversion show that the transition-zone anomaly is consistent with an excess temperature of 200–300 K (Fukao *et al.*, 2004). A still deeper origin, possibly to the CMB, is suggested by a recent tomographic study that incorporates core phases (Lei and Zhao, 2006).

Galápagos. The Galápagos hot spot is part of a broad region in the Nazca and Cocos Basins with significantly reduced long-period Love and Rayleigh wave speeds (Vdovin *et al.*, 1999; Heintz *et al.*, 2005). The transition zone surrounding the Galápagos has similar thickness to that of the Pacific Basin except for a narrow region of ~100 km in radius slightly to the west of the Galápagos archipelago where it is thinned by ~18 km. This amount of thinning suggests an excess temperature of 130 K (Hooft *et al.*, 2003). Preliminary results of a regional tomography study indicate a low-velocity feature of comparable dimension, extending above the transition zone into the shallow upper mantle (Toomey *et al.*, 2001). The western edge of the archipelago shows shear-wave splitting of up to 1s with a direction consistent with E–W plate direction. The anisotropy disappears beneath the archipelago where the upper-mantle wave speeds are anomalously low, suggesting that melt or complex flow beneath the hot spot destroy the plate-motion derived anisotropy (Fontaine *et al.*, 2005).

Yellowstone. Early tomographic studies revealed a complex velocity structure in the upper mantle beneath the Snake River Plain, southwest of the Yellowstone hot spot. This structure was interpreted to represent compositional variability restricted to the upper mantle associated with melting (Saltzer and Humphreys, 1997). More recent work suggests that a narrow, low-velocity feature extends from the upper mantle into the top of the transition zone (Waite *et al.*, 2006; Yuan and Dueker, 2005). The shallow upper-mantle anomaly is present over a distance of more than 400 km, spanning from the northeastern extent of the Snake River Plain to Yellowstone National Park, including a short segment to the northeast of the Yellowstone caldera. The anomaly is strongest at depths 50–200 km with peak anomalies of −2.3% for Vp and −5.5% for Vs (Waite *et al.*, 2006). The velocity reductions are interpreted to represent 1% partial melt at a temperature of 200 K above normal (Schutt and Humphreys, 2004). Initial transition-zone studies showed significant topography of the 410 discontinuity throughout the region (Dueker and Sheehan, 1997). More recent studies show that the 410 discontinuity deepens by 12 km near the intersection of the low-velocity anomaly identified by Waite *et al.* (2006) and Yuan and Dueker (2005), but interestingly, the 660 km discontinuity appears flat in this area (Fee and Dueker, 2004). Shear-wave splitting measurements around the Yellowstone–Snake River Plain show fast S-wave speeds primarily aligning with apparent plate motion, except for two stations in the Yellowstone caldera, perhaps due to local melt effects (Waite *et al.*, 2005).

Eifel. The Eifel region in Western Germany is characterized by numerous but small volcanic eruptions with contemporaneous uplift by 250 m in the last 1 My. Tomographic imaging indicates a mantle low-velocity anomaly extending to depths of at least 200 km (Passier and Snieder, 1996; Pilidou *et al.*, 2005). Inversions using a high-resolution local array study indicate a fairly narrow (100 km) P-wave anomaly of −2% that possibly extends to a depth of 400 km (Ritter *et al.*, 2001; Keyser *et al.*, 2002). The connection with the deeper mantle is unclear but has been suggested to include the low-velocity structure in the lower mantle below central Europe (Goes *et al.*, 1999) (**Figure 13**). Shear-wave splitting measurements show the largest split times for S-waves polarized in the direction of absolute plate motion, but the pattern is overprinted by complex orientations, suggestive of parabolic mantle flow around the hot spot (Walker *et al.*, 2005). A comparison of the seismic anomaly structure below the Eifel, Iceland, and Yellowstone is provided in **Figure 14** (from Waite *et al.*, 2006).

East Africa. Body and surface-wave studies indicate a strong regional low-velocity anomaly in the mantle

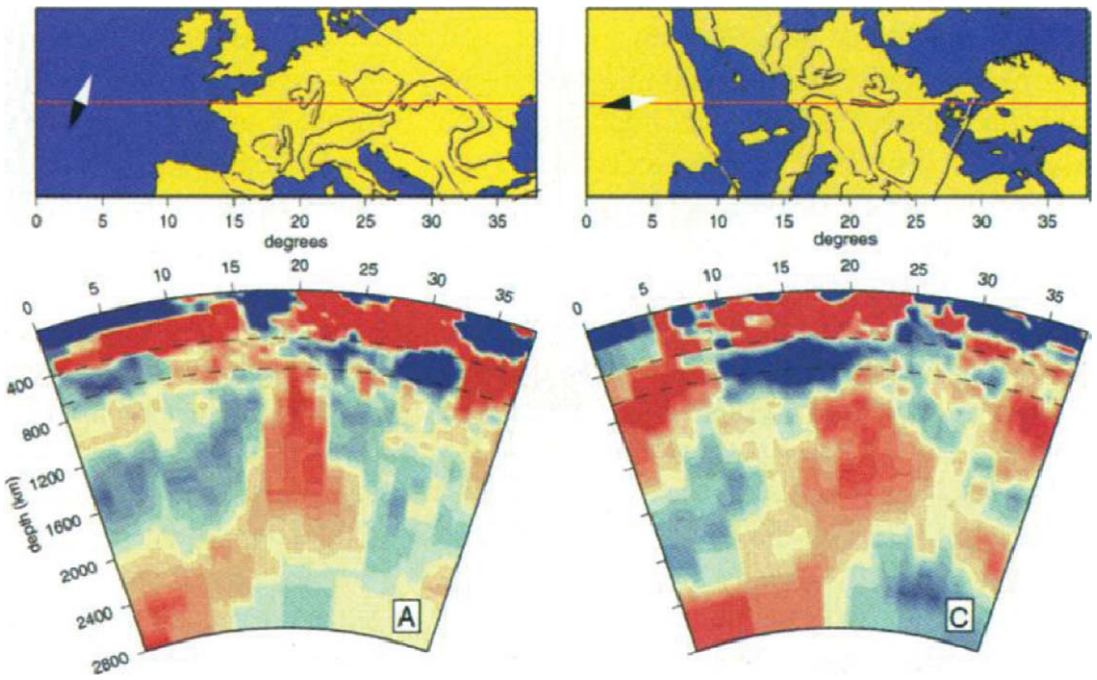

Figure 13 Whole-mantle P tomography below Europe showing possible connections of mid-European volcanism to deep seated low-velocity anomalies in the lower mantle. Reprinted with permission from Goes S, Spakman W, and Bijwaard H (1999) A lower mantle source for central European volcanism. *Science* 286: 1928–1931. Copyright (1999) AAAS.the AAAS.

below the East Africa Rift System. Below Afar, surface-wave studies image anomalous velocities ($\leq -6\%$ in vertically polarized S-waves) extending to a depth of ~200 km (Sebai *et al.*, 2006). In the North Ethiopian Rift, a narrow (75–100 km) tabular feature extends to depths >300 km and is slightly broader in the northern portion which trends toward Afar. Between the flanks the rift zones, P-wave speeds are reduced by 2.5% and S-wave speeds by 5.5% (Bastow *et al.*, 2005). Independent P-wave tomography confirms the general trend and amplitude of the anomaly with a tentative suggestion that it trends to the south and west (Benoit *et al.*, 2006) toward the broad lower-mantle seismic anomaly below Africa (Ritsema *et al.*, 1999; Grand, 2002). The Tanzania Craton, to the northwest, is imaged as having high P- and S-wave speeds to depths of at least 200 km (Ritsema *et al.*, 1998), is thinner than other African cratons, and is surrounded by the slow seismic-wave speeds associated with the East African Rift System (Sebai *et al.*, 2006). The transition zone shows complicated variations but is generally thinner below the Eastern Rift by 30–40 km compared to the more normal thickness under areas of the Tanzania Craton (Owens *et al.*, 2000; Nyblade *et al.*, 2000). Combined, these results suggest that the mantle below the rifts is hotter than normal mantle by 200–300 K with partial melt in the shallow upper mantle.

Seismic anisotropy is dominantly parallel to the main Ethiopian Rift, in an area that extends to nearly 500 km away from the ridge axis, which likely rules out simple extension-driven asthenospheric flow (Gashawbeza *et al.*, 2004). The regional anisotropy is most likely caused by pre-existing features in the late Proterozoic Mozambique Belt but may be locally enhanced by aligned melt in the Ethiopian and Kenyan Rifts (Gashawbeza *et al.*, 2004; Walker *et al.*, 2004; Kendall *et al.*, 2005).

South Pacific Superswell. Recordings of French nuclear explosions in French Polynesia provide evidence for seismically fast velocities in the shallow mantle which suggest compositional heterogeneity without evidence for excess temperature (Rost and Williams, 2003). Rayleigh-wave dispersion measurements across the Pitcairn hot-spot trail suggest an absence of lithospheric thinning (Yoshida and Suetsugu, 2004). Underside reflections of S-waves at the 410- and 660-discontinuities show normal thickness of the mantle transition zone, except in a 500-km-wide area beneath the Society hot spot (Niu *et al.*, 2002). Seismic anisotropy in French Polynesia generally aligns with apparent plate motion, although

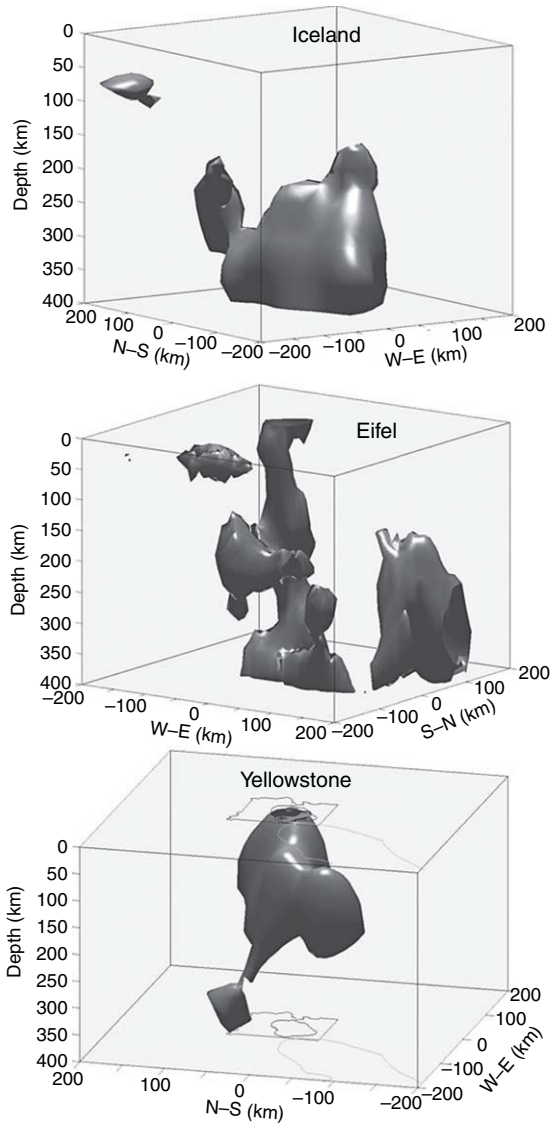

Figure 14 Contours of −1% P-wave velocity anomaly below the Eifel, Iceland, and Yellowstone hot spots. Reproduced from Waite GP, Smith RB, and Allen RM (2006) V–P and V–S structure of the Yellowstone hot spot from teleseismic tomography: Evidence for an upper mantle plume. *Journal of Geophysical Research* 111: B04303, with permission from AGU.

the absence of anisotropy beneath Tahiti and minor deviations beneath other islands could indicate the presence of local flow or magma (Russo and Okal, 1998).

Bowie. The presence of a narrow, low-velocity zone near the base of the transition zone below the Bowie hot spot is based on delays in seismic records of Alaskan earthquakes measured in the NW United States (Nataf and VanDecar, 1993). The delays are consistent with a zone of 150 km diameter with an excess temperature of 200 K.

LIPs. Beneath the Deccan Traps, seismic speeds in the shallow upper-mantle are anomalously low to a depth of at least 200 km (Kennett and Widiyantoro, 1999). The anomaly appears to be absent at depths near the transition zone (Kumar and Mohan, 2005). The Paraná Province is underlain by a distinct region of low seismic-wave speeds in the upper mantle (VanDecar *et al.*, 1995; Schimmel *et al.*, 2003). The OJP has an upper-mantle velocity anomaly of −5% with respect to Preliminary Reference Earth Model (PREM) (Dziewonski and Anderson, 1981) with a maximum depth extent of 300 km (Richardson *et al.*, 2000), whereas ScS reverberations show that this region is less attenuating than 'normal' Pacific asthenosphere (Gomer and Okal, 2003). Seismic anisotropy beneath the OJP is weak, which is interpreted to indicate that the residual mantle root has remained largely undeformed since it formed ~120 Ma (Klosko *et al.*, 2001). The presence of anomalously slow mantle beneath such old flood basalts is enigmatic in that any thermal anomaly is expected to have diffused away.

7.09.2.6 Summary of Observations

Long-lived (>50 My) age-progressive volcanism occurs in 13 hot spots. At present day, these hot spots define a kinematic reference frame that is deforming at rates lower than average plate velocities. Over geologic time, however, there has been significant motion between the Indo-Atlantic hot spots, the Pacific hot spots, and Iceland. Short-lived (≤22 My) age progressions occur in at least eight volcano chains. The directions and rates of age progression in the short-lived chains suggest relative motion between these hot spots, even on the same plate. Finally, a number of volcano groups, which sometimes align in chains (e.g., Cook–Austral, Cameroon), fail to show simple age–distance relations but instead show episodic volcanism over tens of millions of years.

Anomalously shallow topographic swells are very common among hot spots and melting anomalies. These swells are centered by the volcanoes and span geographic widths of hundreds of kilometers to >1000 km. Swells appear to diminish with time; they are usually present around volcanoes with ages <50 Ma and are typically absent around volcanoes older than ~70 My. Conspicuously, the Madeira and Canary hot spots are two active volcano chains without substantial swells.

Large igneous provinces represent the largest outpourings of magma but also show a huge range in magmatic volumes and durations. They can be as large as 50 Mkm^3 (OJP) to <2 Mkm^3 (CRB) (see **Figure 9**). Voluminous magmatism can occur in dramatic short bursts, lasting 1–2 My (CAMP, CRB, EM, OJP, SIB) or can be prolonged over tens of millions of years (e.g., CHON, CBN, KER, NAVP, SHA). Main eruptive products are tholeiitic basalts which, on the continents, typically are transported through radiating dike swarms. High-MgO basalts or picrites are found in a number of provinces (NAVP, OJP, CAR) which indicate high degrees of melting. Smaller rhyolitic eruptions in continental flood basalts (KAR, PAR, CHON, EARS) indicate melting of continental crust. Dynamic topographic uplift is evident around the main eruptive stages of some LIPs (EM, NAVP, SIB, KER) but may not have occurred at some oceanic plateaus (OJP, SHA). While an appreciable amount of the geologic record is lost to subduction, a half-dozen recently active hotspot chains are confidently linked to LIPs with the remainder having tenuous or non-existent links. Those volcano chains that clearly backtrack to LIPs involve those at the centers or margins of continents; Kerguelen is one of the possible exception. Also, most of the LIPs we have examined are associated with rifting, either between continents (PAR, KAR, CAMP, NAVP, DEC, MDR) or at mid-ocean ridges (OJP–MAN–HIK, KER, SHA–HES). The above characteristics compel substantial revisions and/or alternatives to the hypothesis of an isolated head of a starting mantle plume as the only origin of LIPs.

Basalts from hot spots and other melting anomalies, for the most part, are more heavily influenced by mantle materials that are distinct in terms of $^{87}Sr/^{86}Sr$, $^{206}Pb/^{204}Pb$, and/or $^{3}He/^{4}He$ ratios from the MORB source. Four possible exceptions, which show MORB-like $^{87}Sr/^{86}Sr$ and $^{206}Pb/^{204}Pb$ compositions (but lack constraints from $^{3}He/^{4}He$) are the Shatsky Rise and the Bowie–Kodiak, Cobb, and Caroline chains.

Most hot spots are associated with anomalously low seismic-wave speeds below the lithosphere and in the upper mantle. The transition zone below hot spots is often thinned by tens of kilometers. The above findings are consistent with elevated mantle temperature by 150–200 K and with excess partial melt in the shallow upper mantle. Improved understanding of mineral physics at appropriately high pressure and temperature are needed to better constrain the magnitude of the possible temperature anomalies and to quantify the potential contribution of compositional heterogeneity. Finally, while there are hints of seismic anomalies extending into the lower mantle and even to the CMB, definitive tests of a deep origin for some melting anomalies require more extensive regional seismic experiments and modern methods of interpretation.

The key characteristics described above provide information needed to test various proposed dynamical mechanisms for the formation of hot spots and melting anomalies. Some trends and generalities are apparent but substantial deviations likely reflect a range of interacting processes. In other words, it is very unlikely that a single overarching mechanism applies to all cases.

7.09.3 Dynamical Mechanisms

This section reviews the mechanisms proposed to generate hot spots and melting anomalies. We begin with a summary of methods used to quantitatively explore the mechanisms (Section 7.09.3.1). We then discuss the shallower processes of melting (Section 7.09.3.2) and swell formation (Section 7.09.3.3) before addressing the possible links to the deeper mantle, with specific focus on the extensive literature on mantle plumes (Section 7.09.3.4). In the context of whole mantle convection, we discuss possible causes of volcano age progressions and the inferred approximately coherent motion among hot spots on the same (Indo-Atlantic and the Pacific) plates (Section 7.09.3.5). Proposed mechanisms for generating LIPs and their possible connection to hot spots are explored in Section 7.09.3.6. The diversity of observations of hot spots and LIPs requires important modifications to the thermal plume hypothesis, as well as alternative possibilities as presented in Section 7.09.3.7. In light of these possibilities we discuss possible causes for the differences in geochemistry between hot-spot basalts and MORB in Section 7.09.3.8.

7.09.3.1 Methods

The origin and evolution of hot spots and melting anomalies can be constrained by studying the transport of energy, mass, and momentum in the solid and partially molten mantle (*see* Chapter 7.02). Key parts of the above processes can be described mathematically by the governing equations and solved with analytical or numerical approaches, or can be studied by simulation in laboratory experiments using analog materials.

Analytical approaches provide approximate solutions and scaling laws that reveal the main

relationships between phenomena and key parameters (*see* Chapter 7.04). Relevant examples of applications include boundary layer analysis, which is important to quantifying the time and length scales of convection, and lubrication theory, which has been instrumental in understanding hot-spot swell formation. A separate approach uses experimental methods (*see* Chapter 7.03), involving analog materials such as corn syrup and viscous oils to simulate mantle dynamics at laboratory timescales. Analog methods were instrumental in inspiring the now-classic images of plumes, with voluminous spherical heads followed by narrow columnar tails. Numerical techniques are necessary to solve the coupling between, and non-linearities within the equations such as those caused by strongly varying (e.g., temperature, pressure, and composition-dependent) rheology (*see* Chapter 7.05), phase transitions, and chemical reactions. Numerical models are therefore well suited for simulating more-or-less realistic conditions and for allowing quantitative comparisons between predictions and observations. In this way, numerical techniques provide a means to directly test conceptual ideas against the basic laws of physics and to delineate the conditions under which a proposed mechanism is likely to work or has to be rejected based on observations.

Unfortunately, fully consistent modeling is difficult to achieve and is hampered by multiple factors. First, the constitution of the Earth's mantle can only be approximated. Information about material properties such as density, rheology, and thermal conductivity, are essential for quantitative modeling but is not precisely known and becomes increasingly imprecise with depth. Second, the transition from the brittle lithosphere to the viscous asthenosphere involves a rapid temperature increase; the common assumption that the deformation of the Earth's mantle can be approximated as creeping viscous flow is only correct at high temperatures and the details of the lithosphere–asthenosphere interaction depend on poorly known processes that are difficult to model self-consistently. Finally, the problem is multiscale, involving processes occurring from scales as small as individual grains (e.g., fluid–solid interaction, chemical transport), to as large as the whole mantle (*see* Chapters 7.02, 2.06, and 2.14). Addressing these challenges will require careful comparisons between the different techniques, adjustments according to improved insights from experimental and observational work, and smart use of increasing computating technology.

7.09.3.2 Generating the Melt

Understanding of the causes for excess melt generation is essential for our understanding of the dynamics of hot spots and melting anomalies. The rate that an infinitesimal bulk quantity of mantle melts to a fraction F can be described by

$$\begin{aligned} \mathrm{D}F/\mathrm{D}t = {} & (\partial F/\partial T)_{P,\,C}\,(\mathrm{D}T/\mathrm{D}t) \\ & + (\partial F/\partial C)_{P,\,T}\,(\mathrm{D}C/\mathrm{D}t) \\ & + (-\partial F/\partial P)_S(-\mathrm{D}P/\mathrm{D}t) \end{aligned} \qquad [1]$$

The first two terms on the right-hand side describe nonisentropic processes. The first term describes the melt produced by heating and is proportional to the change in F with temperature T at constant pressure P (i.e., isobaric productivity); melting by this mechanism may occur in a variety of settings but is likely to be comparatively small and thus has not been a focus of study. The second term describes melt generated by the open-system change in composition. This term may be important behind subduction zones where the addition of fluids into the mantle wedge causes 'flux' melting and the formation of arc and back-arc volcanism. Finally, the third term describes isentropic decompression melting, which is perhaps the most dominant process of melt generation at mid-ocean ridges, hot spots, and other melting anomalies.

For decompression melting, the rate of melt generation is controlled by the melt productivity $-\partial F/\partial P$, which is positive if temperature exceeds the solidus. Both the solidus and value of $\partial F/\partial P$ (e.g., McKenzie, 1984; Hirschmann *et al.*, 1999; Phipps Morgan, 2001) depend on the equilibrium composition of the solid and liquid at a given pressure. The rate of decompression $-\mathrm{D}P/\mathrm{D}t$ is controlled by mantle dynamics and is primarily proportional to the rate of mantle upwelling. The total volumetric rate of melt generation is approximately proportional to $\mathrm{D}F/\mathrm{D}t$ integrated over the volume V of the melting zone,

$$\dot{M} = \frac{\rho_\mathrm{m}}{\rho_\mathrm{c}} \int_V (\partial F/\partial P)_S(\mathrm{D}P/\mathrm{D}t)\,\mathrm{d}V \qquad [2]$$

where ρ_m is mantle density and ρ_c is igneous crustal density. Melting anomalies thus require one or more of the following conditions: excess temperature, presence of more fusible or fertile material, and mantle upwelling. Higher temperatures increase V by increasing the pressure at which the solidus is intersected, more fusible mantle can change both $(-\partial F/\partial P)_S$ and increase V, and both factors may influence $\mathrm{D}P/\mathrm{D}t$ through their effects on mantle buoyancy.

7.09.3.2.1 Temperature

Melting caused by an increase in temperature has been a major focus of previous studies. One way to estimate mantle temperature is based on comparisons between predicted and observed melt-production rates at different settings. Another way involves using compositions of primitive lavas. Given an assumed starting source composition and a model for melt–solid interaction as the melt migrates to the surface (e.g., 'batch', 'fractional', 'continuous' melting), the liquid concentrations of key oxides (e.g., Na_2O, CaO, Al_2O_3, SiO_2, FeO, MgO) as well as incompatible trace elements can be predicted based on their dependence on P, T, and F, which are related through solid mineralogy and liquid composition. The above relationships can be established by thermodynamic theory and constrained with laboratory experiments.

Estimates of temperature variations at mid-ocean ridges are aided by the relative simplicity of lava compositions, relatively straightforward measurements of magma production rate (e.g., crustal thickness times spreading rate), and the ability to correlate variations in the above observational parameters in space (i.e., along mid-ocean ridges). In addition, spreading rate provides a constraint on the rate of mantle upwelling, for example, if one assumes, to first order, that mantle upwelling is a passive (kinematic) response to plate spreading. Based on the conditions needed for a lherzolitic mantle to yield observed crustal thicknesses and major element variations near Iceland, excess mantle temperatures beneath Iceland relative to normal mid-ocean ridges are estimated to range from about 100°C to >250°C (e.g., Klein and Langmuir, 1987; McKenzie and Bickle, 1988; Langmuir *et al.*, 1992; Shen and Forsyth, 1995; Presnall *et al.*, 2002; Herzberg and O'Hara, 2002). Excess temperature estimates based on inversions of crustal thickness and incompatible trace-element compositions also fall within the above range for Iceland (White *et al.*, 1995; Maclennan *et al.*, 2001) and other hot spots (White *et al.*, 1992).

Beneath Hawaii, the maximum mantle potential temperatures (i.e., temperature at zero pressure after removing the effects of adiabatic decompression) is estimated at 1500–1600°C based on predicted melt production rates from numerical models of mantle upwelling, driven by thermal buoyancy (Ribe and Christensen, 1999; Watson and McKenzie, 1991). This temperature range is 200–300°C higher than the estimated potential temperature of 1280°C beneath normal mid-ocean ridges using the same melting model (McKenzie and Bickle, 1988).

Another method of estimating mantle temperatures is based on Fe–Mg content of primary melts and the olivine phenocrysts with which they equilibrate. This method depends on experimentally constrained partitioning of Fe and Mg between liquid and olivine, measured forsterite content of olivine crystals, and estimated Fe and Mg content of primary magmas (i.e., magmas that segregated from the mantle melting zone and have not been further modified by shallow processes such as crystal fractionation or accumulation). One group suggests that the mantle is no hotter beneath Hawaii than beneath many mid-ocean ridges (Green *et al.*, 2001). Other groups, however, suggest elevated temperatures of 50–100°C (Herzberg and O'Hara, 2002; Herzberg, 2004a) and 100–200°C (Putirka, 2005) beneath Hawaii and Iceland. As essentially all sampled lavas have evolved to varying degrees after they left the mantle source, an important uncertainty is the MgO content of the primary liquids. Putirka (2005) argues, for example, that the lower MgO contents derived by Green *et al.* (2001) for Hawaii could lead to an underestimate of temperature. A recent critical evaluation of the criteria for determining mantle potential temperatures below ridges and hot spots is provided by Herzberg *et al.* (in press).

7.09.3.2.2 Composition

A major source of uncertainty for all of the above temperature estimates is the composition of the mantle source. Water and CO_2, for example, can dramatically reduce melting temperatures even in the small proportions (i.e., well below saturation) likely to be present in the MORB source (Asimow and Langmuir, 2003; Dasgupta and Hirschmann, 2006). While such small concentrations of volatiles are not likely to increase the total extent of melting significantly, they can enhance the amount of melt produced for a given temperature by appreciably expanding the volume of the melting zone. As the mantle beneath hot spots is likely to be more volatile rich, temperature estimates based on dry peridotite may be too high. For example, excess temperatures beneath the hot-spot-influenced Galápagos spreading center may be reduced from ~50°C for anhydrous melting models to <40°C when water is considered (Cushman *et al.*, 2004; Asimow and Langmuir, 2003). Similarly, estimates for the mantle excess temperature beneath Azores have been revised from ~75°C to ~55°C (Asimow

and Langmuir, 2003). Hydrous melting models have yet to be explored in detail for the larger Iceland and Hawaii hot spots.

The mantle beneath hot spots may also contain more fusible, mafic lithologies, such as those generated by the recycling of subducted oceanic crust. The presence of such 'fertile' mantle has been suggested for hot spots such as Hawaii (Hauri, 1996; Takahashi, 2002), Iceland (Korenaga and Kelemen, 2000), the CRBs (Takahashi *et al.*, 1998), Galápagos (Sallares *et al.*, 2005), and others (Hofmann, 1997). Pyroxenite lithologies have both a lower solidus and greater productivity ($\partial F/\partial P$) than peridotite (Pertermann and Hirschmann, 2003) and therefore require much lower temperatures to produce the same volume of melt as peridotite.

Some have argued that fertile mantle melting could generate many melting anomalies with very small or zero excess temperatures (Korenaga, 2005b). An important difficulty with this hypothesis is that mafic materials will tend to form eclogite, which is significantly denser than lherzolite in the upper mantle (Irifune *et al.*, 1986). This material must therefore produce substantial melt at depths where upwelling (i.e., $-DP/Dt$, eqn [2]) is not appreciably impeded by negative buoyancy. It has been suggested that eclogite becomes neutrally buoyant near the base of the upper mantle (~660 km) (Hirose *et al.*, 1999; Ringwood and Irifune, 1988) (*see* Chapter 2.18). To reach the solidus and initiate melting at this depth most likely requires temperatures >300 K higher than normal (e.g., Hirose and Fei, 2002). Alternatively, it has been suggested that rapid upwelling driven by shallow thermal convection (Korenaga, 2004) (**Figure 15**) or fast seafloor spreading (Korenaga, 2005b) could entrain eclogite upward from a neutrally buoyant layer at 660 km and cause melting in the upper mantle without usually hot mantle. More recent experiments, however, suggest that subducted basalt is actually denser than peridotite throughout the upper mantle (Aoki and Takahashi, 2004) and thus would unlikely accumulate near 660 km. It is clear that a more complete understanding of the properties and phase relations of different lithologies at a range of mantle pressures and temperatures is needed to test the importance of fertile mantle melting.

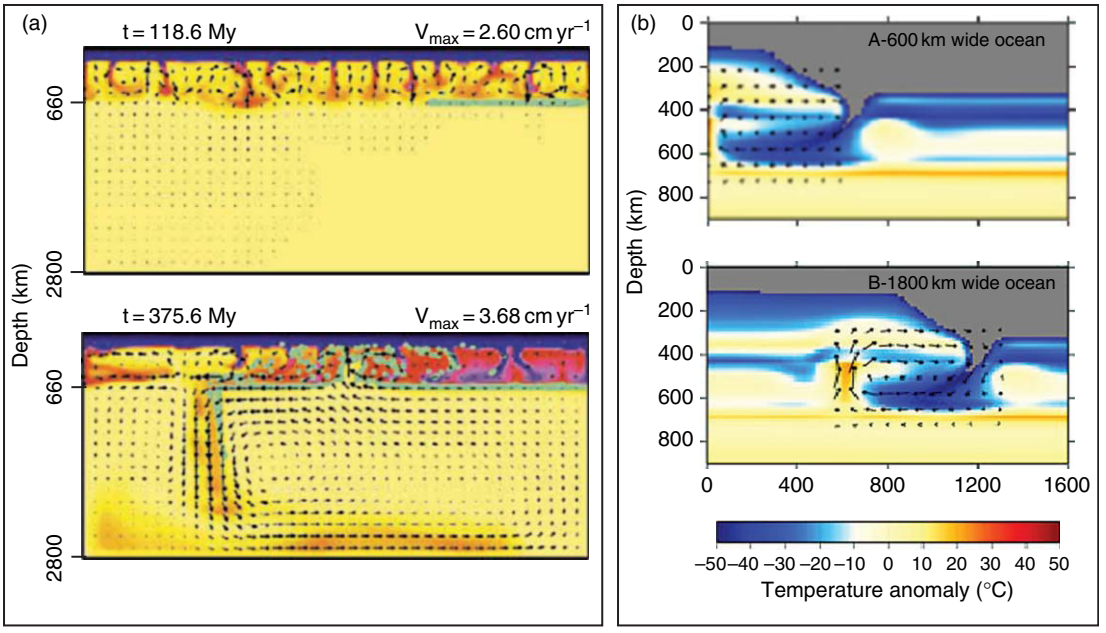

Figure 15 Two forms of small-scale convection in the upper mantle. (a) Solutions of 2-D numerical models in which sublithospheric thermal instabilities drive convection (arrows show mantle flow) in the upper mantle at two time steps as labeled. Colors show temperature with blue being cold (lithosphere) and light yellow being hottest. Green tracers of subducted crustal fragments first form a layer at 660 km; some eventually sink into the lower mantle and some are drawn upward where they could melt. (b) Predictions of 2-D numerical models in which small-scale convection is driven by the edge of thick lithosphere (gray). Colors show temperature contrast from the mantle adiabat. (a) From Korenaga J (2004) Mantle mixing and continental breakup magmatism. *Earth and Planetary Science Letters* 218: 463–473. (b) From King S and Anderson DL (1998) Edge-driven convection. *Earth and Planetary Science Letters* 160: 289–296.

7.09.3.2.3 Mantle flow

The final major factor that can lead to melting anomalies is enhanced mantle upwelling ($-DP/Dt$). Thermal buoyancy can cause rapid upwelling and dramatically enhance melt production (e.g., Ito *et al.*, 1996; Ribe *et al.*, 1995). Compositional buoyancy could also enhance upwellings (Green *et al.*, 2001). However, compositionally lighter material such as those with less iron and dense minerals (i.e., garnet), perhaps due to prior melt depletion (Oxburgh and Parmentier, 1977; Jordan, 1979), are likely to be less fusible than undepleted or fertile mantle. Behaving in complimentary fashion to fertile mantle, depleted mantle must be light enough such that the associated increase in upwelling rate ($-DP/Dt$) overcomes the reduction in fusability (V and $(-\partial F/\partial P)_S$ in eqn [2]).

Buoyancy-driven upwelling, however, only requires enhanced lateral variations in density. Besides hot, plume-like upwellings from the deep mantle, large density variations can occur near the lithospheric thermal boundary layer (TBL). Sublithospheric boundary layer instabilities can drive small-scale convection in the upper mantle (e.g., Richter, 1973; Korenaga and Jordan, 2003; Huang *et al.*, 2003; Buck and Parmentier, 1986) (**Figure 15(a)**). A related form of small-scale convection can occur where there are large variations in lithospheric thicknesses such as that near rifted continental margins (Buck, 1986; King and Anderson, 1998) (**Figure 15(b)**). While the physics of convection in such situations have been explored to some degree, the volumes, timescales, and compositions of magmatism that could be produced have not.

The process of thinning the continental lithosphere can also cause rapid passive upwelling in the underlying asthenosphere. Thinning could occur by the foundering and delamination of the lower lithosphere or by continental rifting. Both mechanisms have been proposed to form flood volcanism on continents or continental margins without elevated mantle temperatures (Hales *et al.*, 2005; van Wijk *et al.*, 2001) (see Section 7.09.3.6).

Another form of enhanced mantle upwelling can occur in response to melting itself. Partial melting reduces the density of the solid residue (discussed above) and generates intergranular melt. Both factors can reduce the bulk density of the partially molten mantle and drive buoyant decompression melting (**Figure 16**). Buoyant decompression melting has been shown to be possible beneath mid-ocean ridges but could also occur away from mid-ocean ridges (Tackley and Stevenson, 1993; Raddick *et al.*, 2002). The key requirements for buoyant decompression melting to occur mid-plate is the presence of an appreciable thickness of mantle to be very near its

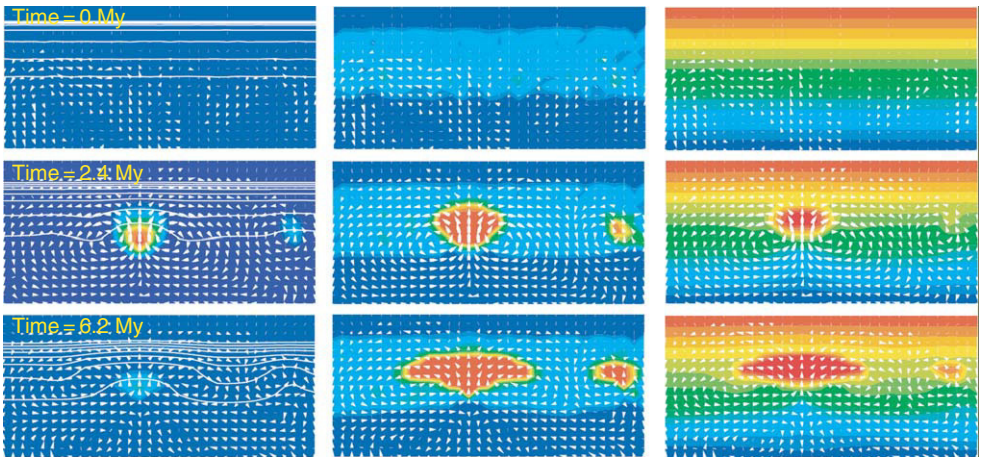

Figure 16 Predictions of 2-D numerical models which simulate buoyant decompression melting for three time steps as labeled. Left column shows fractional melting rate (red = 0.0021 My^{-1}, blue = 0), middle column shows melt fraction retained in the mantle ϕ (red = 0.02), and right column shows volume fraction of melt extracted ξ (red = 0.108). Density decreases as linear functions of both ϕ and ξ, and lateral density variations are what drive upwelling. Melting is therefore limited by the accumulated layer low-density residue. Reproduced from Raddick MJ, Parmentier EM, and Scheirer DS (2002) Buoyant decompression melting: A possible mechanisms for intra plate volcanism. *Journal of Geophysical Research* 107: 2228 (doi: 1029/2001JB000617), with permission from AGU.

solidus and a perturbation to initiate upwelling and melting. Perturbations could be caused by rising small bodies of hotter or more fusible mantle, the flow of mantle from beneath the old and thick side of a fracture zone to the young and thin side (Raddick *et al.*, 2002), or even sublithospheric convection.

Lastly, mantle upwelling can be driven by vertical motion of the lithosphere, such as that due to lithospheric flexure. The flexural arch around large intraplate volcanoes, for example, is caused by the growth of volcanoes which not only pushes the underlying lithosphere downward but causes upward flexing in a donut-shaped zone around the volcano. Flexural arching also occurs on the seaward side of subduction zones. Decompression melting can occur beneath flexural arches, again, if an appreciable thickness of asthenosphere is near or at its solidus (Bianco *et al.*, 2005).

7.09.3.3 Swells

One of the more prominent characteristics of hot spots and melting anomalies is the presence of broad seafloor swells. One indication of the possible origin is an apparent dependence of swell size with the rate of plate motion. We measure swell widths using the maps of residual topography (**Figure 1**) with the criterion that the swell is defined by the area that exceeds a height of +300 m in the direction perpendicular to volcano chains. This direction usually corresponds to the direction in which the swell is least wide (except for Trindade). The parallel bars in **Figure 1** mark the widths we measure for different hot spots. **Figure 17(a)** shows how swell width $\bar{W}$ varies with the plate speed U_p at the hot spot, relative to the hot-spot reference frame (compiled by Kerr and Mériaux (2004)). For plate speeds $<80\,\mathrm{km\,My^{-1}}$, $\bar{W}$ appears to decrease with increasing plate speed. The prominent Pacific hot spots (Hawaii, Marquesas, Easter, Pitcairn, and Louisville) break the trend and have widths comparable to many of the swells in the Atlantic. We now test whether the observations can be explained by buoyant, asthenospheric material ponding beneath the lithosphere.

7.09.3.3.1 Generating swells: Lubrication theory

Lubrication theory is a simplifying approach of solving the equations governing fluid flow against a solid interface. The method eliminates partial derivatives with respect to depth by assuming that fluid layers are thin compared to their lateral dimension, and therefore describes fluid-layer thickness in map view. This theory was first applied to the formation of hot-spot swells by Sleep (1987) and Olson (1990) (*see* Chapter 7.04). Here, buoyant asthenosphere is introduced at the base of a moving, rigid (lithospheric) plate. The buoyant material is dragged laterally by plate motion and expands by self-gravitational spreading away from the source such that the extent W perpendicular to plate motion increases with distance x from the source (**Figure 18(a)**). Without plate motion the material would expand axisymmetrically like a pancake.

As confirmed with laboratory experiments and numerical models, the width of the buoyant material and swell far from the source can be approximated by the dimensionless equation (**Figure 18(a)**):

$$W/L_0 = C_1(x/L_0)^{1/5} \quad [3]$$

where C_1 is a constant ($\sim$3.70) and L_0 is the characteristic length scale of the problem defined as (Ribe and Christensen, 1994)

$$L_0 = \left(\frac{B^3 g}{96\pi^3 \Delta\rho^2 \eta U_p^4}\right)^{1/4} \quad [4]$$

This length scale contains information about the key parameters controlling the width of the flow: buoyancy flux $B\,(\mathrm{kg\,s^{-1}})$, acceleration of gravity g, density contrast between the buoyant and normal mantle $\Delta\rho$, viscosity of the buoyant mantle η, and plate speed U_p. Alternatively, if the buoyant material is introduced along a semi-infinite line, then W will increase more rapidly with distance. Using the same reasoning as Kerr and Mériaux (2004), this case can be directly compared to [3], using the length scale L_0

$$W/L_0 = C_2 L_0^{3/5}(x/L_0)^{4/5} \quad [5]$$

where C_2 is a constant (in **Figure 18(a)** $C_2 L_0^{3/5} = 1.23$).

In either case, W is predicted to be of the same order as $L_0 \propto B^{3/4}/U_p$. This relation predicts L_0 and thus W to be inversely proportional to U_p because faster plates allow less time for the layer to expand while it is dragged a distance x. The above relations also show an important dependence on B, which is not considered in our initial plot in **Figure 17(a)**. Larger buoyancy fluxes (proportional to Q) lead to larger W primarily by enhancing the rate of gravitational expansion.

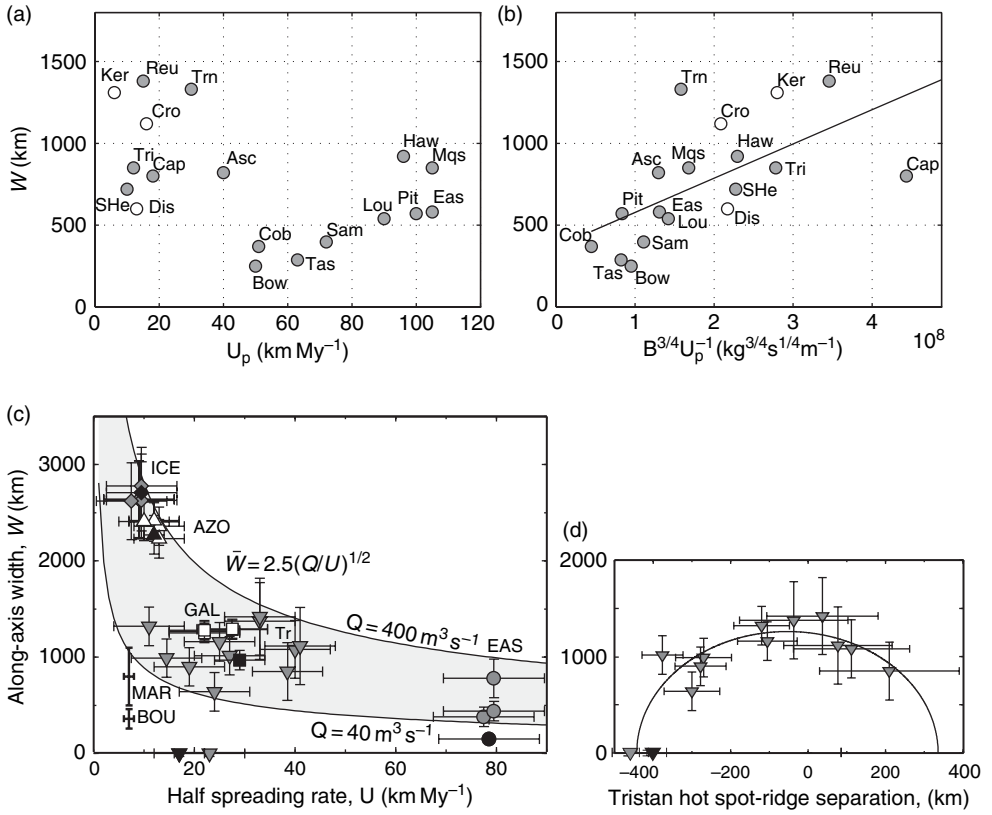

Figure 17 (a) Average widths $\bar{W}$ of intraplate hot-spot swells measured by lines shown in **Figure 1** versus the rate U_p of plate motion relative to the hot spots. (b) Lubrication theory of buoyant mantle expanding beneath the lithosphere predicts a swell width scale $L_0 \propto B^{-3/4}/U_p$, where B is buoyancy flux. Line shows best fitting regression to the data, but excluding Cape Verde. (c) Widths W for hot-spot–ridge interaction are the total along-isochron span of positive residual topography: diamonds, Iceland; white triangles, Azores; white squares, Galápagos; inverted triangles, Tristan; circles, Easter. Plate rate U is the half spreading rate of the ridge during times corresponding to isochron ages (Ito and Lin, 1995). Black symbols mark present-day ridge-axis anomalies. Bold error bars show along-axis mantle-Bouguer gravity anomaly widths along the Southwest Indian Ridge near the Bouvet (black) and Marion (purple) hot spots (Georgen *et al.*, 2001). Curves show predictions of scaling laws based on lubrication theory for a range of volume fluxes of buoyant mantle Q. (d) Along-isochron widths of residual bathymetric anomalies vs plume-ridge separation distance at times corresponding to isochron ages for the Tristan–MAR system. Curve is best fitting elliptical function $E(x/W_0)$ in eqn [7]. (c, d) Reproduced from Ito G, Lin J, and Graham D (2003) Observational and theoretical studies of the dynamics of mantle plume-mid-ocean ridge interaction. *Review of Geophysics* 41: 1017 (doi:10.1029/2002RG000117), with permission from AGU.

Buoyancy flux can be estimated based on the volumetric rate of swell creation, (Davies, 1988; Sleep, 1990)

$$B = \bar{h}\bar{W}U_p(\rho_m - \rho_w) \quad [6]$$

where $\bar{h}$ and $\bar{W}$ are averages of swell height and width, respectively, and $\rho_m - \rho_w$ is the density contrast between the mantle and water.

Using estimated values for B and U_p (Kerr and Meriaux, 2004), a plot of $\bar{W}$ versus $B^{3/4}/U_p$ indeed shows a positive correlation (**Figure 17(b)**). Some of the scatter could be due to errors in B, perhaps due to uncertainties in swell height (Cserepes *et al.*, 2000) as well as the oversimplifying assumption in [6] that the buoyant material flows at the same speed as the plate (Ribe and Christensen, 1999). Other sources of scatter could be differences in $\Delta\rho$ and η between hot spots.

For hot spots interacting with mid-ocean ridges, swell widths are the extent that positive residual topography extends in the direction parallel to ridges (Ito *et al.*, 2003). Swell widths along hot-spot-influenced ridges and nearby seafloor isochrons appear to depend on the full spreading rate U as well as hot-spot–ridge separation (**Figures 17(c) and 17(d)**). Lubrication theory predicts that along-axis 'waist' widths $\bar{W}$ will reach a steady state when the volume flux of buoyant

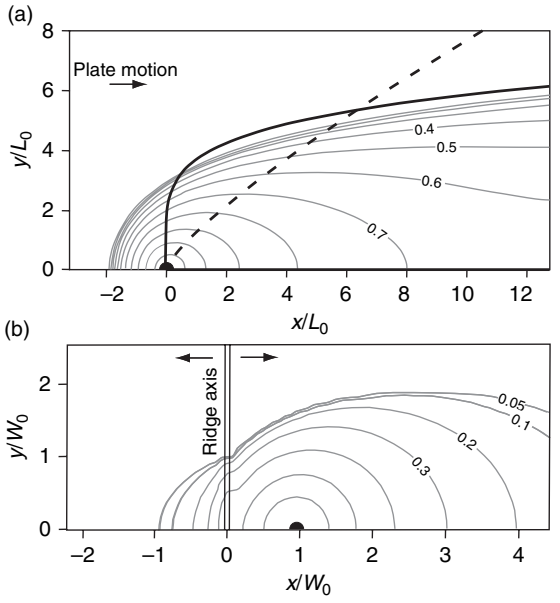

Figure 18 (a) Plan view of predicted thickness (gray contours) of buoyant material expanding by gravitational spreading beneath a moving plate. Horizontal distances (x,y) are normalized by the width scale L_0 given by [4]. Buoyant material is introduced at a point at the origin. Bold curve is the analytical solution for the total width W of the layer far from the source (eqn [3]). Dashed curve shows predicted W for buoyant material emanating from a uniform line source (bold horizontal line) that starts at $x/L_0 = 0$ (eqn [5]). (b) Predicted thickness of buoyant material expanding from a source near two spreading plates. Distances are normalized by the width scale W_0 (eqn [8]). The width along the ridge axis reaches a steady-state value of $\bar{W}$. The numerical model predicts the material to expand away from the source due to its own buoyancy, to be dragged away from the ridge by plate motion, to thin in response to ambient mantle upwelling and lithospheric accretion, and to be channeled toward the ridge by the ridge-ward sloping lithosphere. Reproduced from Ribe NM and Christensen UR (1994) Three-dimensional modelling of plume-lithosphere interaction. *Journal of Geophysical Research* 99: 669–682, with permission from AGU.

material at the source Q is balanced by the sinks associated with lithospheric accretion near the mid-ocean ridge (**Figure 18(b)**). Results of numerical models are well explained by the scaling law (Feighner and Richards, 1995; Ribe, 1996; Ito *et al.*, 1997; Albers and Christensen, 2001; Ribe *et al.*, 2007):

$$\bar{W}/W_0 = C_3 \left(\frac{Q\,\Delta\rho g}{48\eta U^2} \right)^c E(x_r/W_0) \qquad [7]$$

where $C_3 \sim 2$, $c \sim 0.07$, and E is an equation for an ellipse in terms of the normalized distance x_r/W_0 between the source and ridge axis. The characteristic width scale is

$$W_0 = (Q/U)^{1/2} \qquad [8]$$

The curves in **Figure 17(c)** show widths predicting by [7] and [8] for seven cases of hot-spot–ridge interaction. The general inverse relationship between $\bar{W}$ and $U^{1/2}$ explains the data reasonably well. Dispersion of $\bar{W}$ at a given U can be caused by differences in Q and in hot-spot-ridge separation x_r (**Figure 17(d)**).

Overall, the apparent correlations between hot-spot widths, fluxes, and plate rates can be well explained by buoyant material being introduced at the base of the lithosphere. Compositionally or thermally buoyant upwellings rising from below the asthenosphere are possible sources and have been widely explored in context of the mantle-plume hypothesis (see also below). Buoyant mantle could also be generated near the base of the lithosphere, perhaps due to buoyant decompression melting. Such a mechanism for swell generation may be an alternative to deep-seated thermal upwellings.

7.09.3.3.2 Generating swells: Thermal upwellings and intraplate hot spots

Hot mantle plumes provide a straightforward mechanism to explain both the swells and excess volcanism associated with some hot spots. Three dimensional (3-D) numerical models that solve the governing equations of mass, energy, and momentum equilibrium of a viscous fluid have quantified the physics of plume-generated swells (Ribe and Christensen, 1994; Zhong and Watts, 2002; van Hunen and Zhong, 2003). They have, for example, successfully predicted the shape and uplift history of the Hawaiian swell. They also predict the eventual waning of swell topography to occur as a result of the thinning (see also **Figure 18(a)**) and cooling plume material beneath the lithosphere. Such a prediction provides a simple explanation for the disappearance of hot-spot swells along the Hawaiian and Louisville chain, as well as the lack of swells around very old portions of other volcano chains. Ribe and Christensen (1994) also predict minimal thinning of the lithosphere; therefore, the predicted elevation in heat flow is smaller than the variability that can be caused by local crustal or topographic effects (DeLaughter *et al.*, 2005; Harris and McNutt, 2007).

A similar model but with melting calculations defined the range of lithospheric thicknesses, potential temperatures, and buoyancy fluxes needed to generate the Hawaiian magma fluxes, swell width, and swell height (Ribe and Christensen, 1999)

(**Figure 19**). For reference, a plume composed of anhydrous lherzolite requires high potential temperatures of 1500–1600°C to roughly match the observations. In addition to a main (shield) melting phase, this model also predicts a secondary zone of upwelling and melting substantially down the mantle 'wind' of the plume. The location of this melting zone away from the main zone is consistent with it contributing to part of the rejuvenated stages on some Hawaiian Islands.

7.09.3.3.3 Generating swells: Thermal upwellings and hot-spot–ridge interaction

Another series of numerical modeling studies help define the conditions for hot upwelling plumes to explain swells and melting anomalies along hot-spot influenced ridges. Initially, studies showed that the swell width and the crustal thickness along the MAR near Iceland required a very broad upwelling (radius ~300 km) of only modest excess temperature (<100°C above an ambient of 1350° C) (Ribe *et al.*,

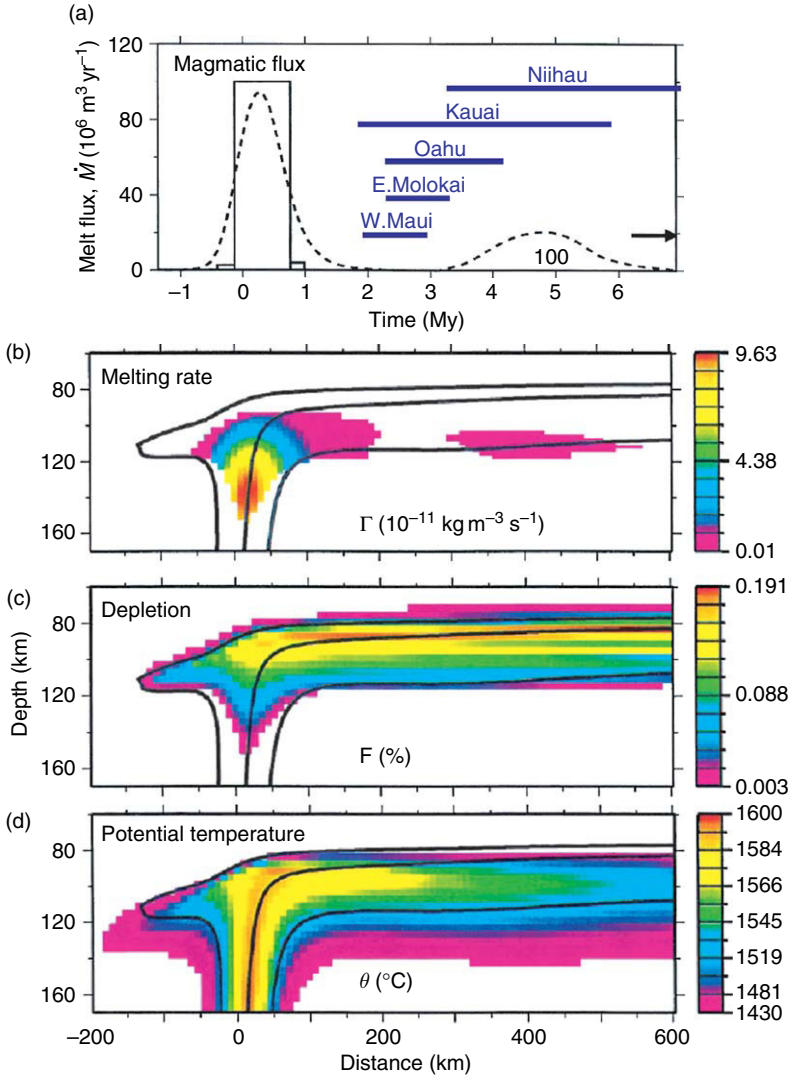

Figure 19 Predictions of a 3-D numerical model for the generation of the Hawaiian swell and volcanism. A thermally buoyant mantle plume is introduced at a model depth of 400 km; it rises, interacts with a moving lithosphere, and melts. (a) Predicted duration and flux of volcanism (eqn [2]) (dashed) is comparable to the pre-shield, shield, and post-shield volcanic stages (three boxes). Blue lines show the spans of rejuvenated volcanism on the five labeled islands at distances from the concurrently active shield volcanoes (Bianco *et al.*, 2005). Cross-sections through the center of the plume show (b) melting rate $\Gamma = \rho_m DF/Dt$, (c) depletion F, and (d) potential temperature. Bold curves are streamlines. From Ribe NM and Christensen UR (1994) Three-dimensional modelling of plume-lithosphere interaction. *Journal of Geophysical Research* 99: 669–682.

1995; Ito *et al.*, 1996). These characteristics appeared to be inconsistent with the evidence from seismic tomography for a much narrower and hotter body (Wolfe *et al.*, 1997; Allen *et al.*, 1999b, 2002). However, calculations involving such a narrow and higher temperature upwelling predict crustal thicknesses that are several times that measured on Iceland – even assuming dry lherzolite as the source material.

One solution is provided by the likelihood that water that was initially dissolved in the unmelted plume material is extracted at the onset of partial melting, and this dramatically increases the viscosity of the residue (Hirth and Kohlstedt, 1996). Numerical models that simulate this effect predict that the lateral expansion of the plume material occurs beneath the dry solidus and generates the observed swell width along the MAR (Ito *et al.*, 1999). Above the dry solidus, where most of the melt is produced, the mantle rises slowly enough to generate crustal thicknesses comparable to those at Iceland and along the MAR (**Figure 20**). A similar model, but with a variable flux of material rising in the plume produces

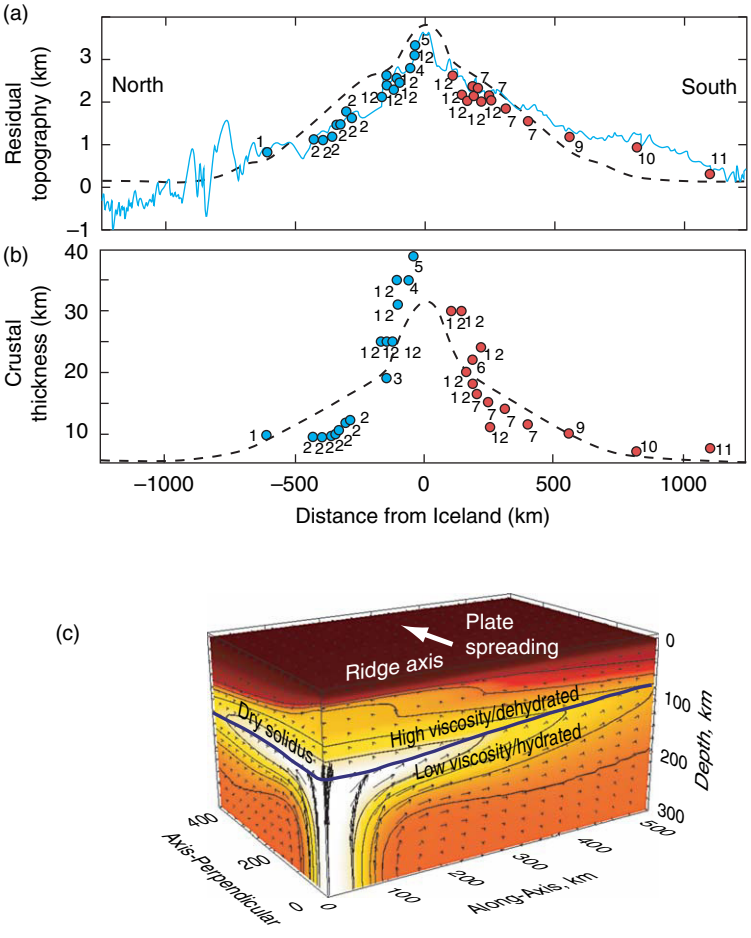

Figure 20 (a)–(c) Comparisons between observations and predictions of a 3-D numerical model of a hot mantle plume rising into the upper mantle, interacting with two spreading plates, and melting. (a) Observed (light blue from gridded bathymetry and dots from refraction experiments) residual topography along the MAR, compared to the predictions, which assumes isostatic topography due to the thickened crust and low-density mantle. Dots show height above the seismically determined crustal thicknesses that are shown in (b). Dashed curve in (b) is predicted crustal thickness. (c) Perspective view of potential temperatures (white > ~1500° C, orange = 1350° C) within the 3-D model. The vertical cross-sections are along (left) and perpendicular (left) to the ridge. Viscosity decreases with temperature and increases at the dry solidus by 10^2 because water is extracted from the solid with partial melting (Ito *et al.*, 1999). (a, b) Reproduced from Hooft EEE, Brandsdóttir B, Mjelde R, Shimamura H, and Murai Y (2006) Asymmetric plume-ridge interaction around Iceland: The Kolbeinsey Ridge Iceland Seismic Experiment. *Geophysics*, *Geochemistry*, *and Geosystems* 7: Q05015 (doi:10.1029/2005GC001123), from AGU. (c) Reproduced from Ito G. Shen Y, Hirth G, and Wolfe CJ (1999) Mantle flow, melting, and dehydration of the Iceland mantle plume. *Earth and Planetary Science Letters* 165: 81–96.

fluctuations in crustal production at the ridge that propagates away from the plume source along the ridge axis (Ito, 2001). This behavior was shown to explain V-shaped ridges that straddle the MAR north and south of Iceland for hundreds of kilometers (Vogt, 1971; Jones *et al.*, 2002b). A north–south asymmetry in crustal thickness documented by Hooft *et al.* (2006) is not predicted by the above models and could hold clues to larger-scale mantle flow, heterogeneity, or both.

7.09.3.4 Dynamics of Buoyant Upwellings

Our discussion of hot spots and melting anomalies is set amidst the background of larger-scale processes of plate tectonics and mantle convection. The cooling of the oceanic lithosphere is the main driving force for plate motion and the associated convection in the mantle. While the volume of mantle that participates in the plate-tectonic cycle is still debated, a consensus model has emerged of moderated whole-mantle convection, with significant material exchange between the upper mantle with relatively low viscosity and the more sluggishly convecting lower mantle. Observational evidence for whole-mantle convection is based on geoid and topography (e.g., Richards and Hager, 1984; Davies, 1998), geodynamic inversions (Mitrovica and Forte, 1997), seismological observations of slab extensions in to the lower mantle (Creager and Jordan, 1986), and seismic tomography (Grand, 1994; Su *et al.*, 1994, Grand *et al.*, 1997). Geodynamic models of whole-mantle convection show reasonable agreement with seismic tomography (Lithgow-Bertelloni and Richards, 1998; McNamara and Zhong, 2005), seismic anisotropy in the lower mantle (McNamara *et al.*, 2002), as well as surface heat flux and plate motions (e.g., van Keken and Ballentine, 1998). Hot spots and melting anomalies represent smaller-scale processes that likely involve mantle plumes.

The lack of detailed knowledge about lower-mantle properties, such as rheology, and thermal conductivity and expansivity, provides speculative opportunities about dynamical behavior; but numerical calculations can be used to map out the likely range of outcomes. For example, whole-mantle convection models with reasonable degrees of internal heating can satisfactorily explain both the average surface heat flow and plate velocities, but only when a higher-viscosity mantle is assumed (e.g., van Keken and Ballentine, 1998). Mineral physics (*see* Chapter 2.06) provide strong suggestions for a reduction in thermal expansivity and increase in thermal conductivity with pressure. The combined effects will reduce convective vigor, but models that incorporate reasonable depth variations of these properties predict that this does not render the lower mantle immobile (e.g., van Keken and Ballentine, 1999; van den Berg *et al.*, 2005; Matyska and Yuen, 2006a). Dynamical theory provides an essential stimulus for the mantle-plume hypothesis, since thermal plumes form naturally from hot boundary layers in a convecting system. The CMB is the main candidate to have a significant TBL (e.g., Boehler, 2000), but other boundary layers may exist at locations where sharp transitions in material properties or composition occur, such as the bottom of the transition zone at 670 km depth and the proposed thermochemical layer at the base of the mantle. We will first summarize the fluid dynamics of plumes rising from a TBL before addressing the consequences of chemical buoyancy forces and depth-dependent mantle properties.

7.09.3.4.1 TBL instabilities

In it simplest form, the growth of an upwelling instability from a hot boundary layer can be approximated as a Rayleigh–Taylor instability with the onset time and growth rate controlled by the local (or boundary) Rayleigh number,

$$Ra_\delta = \frac{\rho g \alpha \Delta T \delta^3}{\mu \kappa} \qquad [9]$$

The instability is enhanced by thermal expansivity α (ρ is density and g is acceleration of gravity), the temperature jump across the boundary layer ΔT, and the layer thickness δ, and is hampered by viscosity μ, and thermal diffusivity κ (including potential radiative effects in the deep mantle). Large-scale mantle flow tends to suppress the growth of instabilities but the temperature dependence of rheology will enhance its growth. For more specifics on governing equations for boundary layer instabilities and examples of their modeling with laboratory and numerical techniques see chapters 6 and 11 of Schubert *et al.* (2001). Indeed, analytical methods provide important insights to the rate of formation of the instability and the dependence on ambient conditions (see e.g., Whitehead and Luther, 1975; Ribe and de Valpine, 1994). The growth of a diapir to a full plume can be understood with nonlinear theory; for example, Bercovici and Kelly (1997) show that growth is retarded by draining of the

source layer and the diapir can temporarily stall. Experimental and numerical investigations confirm and expand these predictions and, quite importantly, provide direct verification of model predictions made by independent approaches (e.g., Olson *et al.*, 1988; Ribe *et al.*, 2007). In general, most studies find that for reasonable lower-mantle conditions, the boundary layer instabilities will grow on the order of 10–100 My (e.g., Christensen, 1984; Olson *et al.*, 1987; Ribe and de Valpine, 1994).

As the diapir rises it will generally be followed by a tail of hot material that traces back to the boundary layer. The rise speed of the diapir is proportional to its buoyancy, the square of its radius, and is inversely proportional to viscosity. The morphology of the plume head and tail are controlled by the viscosity contrast between the hot and ambient fluid. A more viscous plume will tend to form a head approximately the same width as the tail (a 'spout' morphology) whereas a lower-viscosity plume will tend to form a voluminous plume head much wider than the tail (a 'mushroom' or 'balloon' geometry following terminology by Kellogg and King (1997)). Since mantle viscosity is a strong function of temperature it is generally expected that the mushroom/balloon geometry should dominate, but Korenaga (2005a) proposes an interesting counter argument for grain-size controlled, high-viscosity plumes. As we will discuss below, chemical buoyancy may have significant control on the shape of the plume as well.

Dynamical experiments without large-scale flow generally demonstrate that a boundary layer will become unstable with many simultaneous plumes that interact with each other as they rise through the fluid (e.g., Whitehead and Luther, 1975; Olson *et al.*, 1987; Kelly and Bercovici, 1997; Manga, 1997; Lithgow-Bertelloni *et al.*, 2001). To study the dynamics of a single plume, it has become common to use a more narrow or point source of heat, which in laboratory experiments can be achieved by inserting a small patch heater at the base of the tank (e.g., Kaminski and Jaupart, 2003; Davaille and Vatteville, 2005) or to inject hot fluid through a small hole in the base of the tank (Griffiths and Campbell, 1990). The latter work showed that with strongly temperature-dependent viscosity the plume head entrains ambient fluid, forming a characteristic mushroom-shaped head. Interestingly, this same shape was observed also by Whitehead and Luther (1975) but for mixing of fluids with similar viscosity (their figure 9). Van Keken's (1997) replication of Griffiths and Campbell's (1990) laboratory experiment also showed that this form of plume is retained when it originates from a TBL or when olivine, rather than corn syrup rheology, was assumed. Other relevant numerical experiments are provided by Davies (1995) and Kellogg and King (1997).

7.09.3.4.2 Thermochemical instabilities

Studies of thermal plumes originating from TBLs have guided much of the classic descriptions of mantle upwellings and represent a logical starting point for understanding them. The Earth, however, is more complex since density is likely to be controlled by composition, as well as temperature. The seismic structure in the deep mantle beneath the African and South Pacific Superswell regions provides evidence for such deep compositional heterogeneity. Mantle convection models suggest that dense layers are likely to form distinct large blobs or piles that are away from areas of active downwellings (Tackley, 2002; McNamara and Zhong, 2005). Due to the spatial and temporal interaction between chemical and thermal buoyancy forces, the upwellings that form from a thermochemical boundary layer can be dramatically different from the classical thermal plume and interaction with the lower-viscosity upper mantle can significantly alter their shape (Farnetani and Samuel, 2005). The stable topography of high-density layers could provide an anchoring point above which thermal plumes can rise and thus define a fixed reference frame for different hot-spot groups (Davaille *et al.*, 2002; Jellinek and Manga, 2002).

A compelling cause for compositional heterogeneity is the recycling of oceanic crust in subduction zones (e.g., Christensen and Hofmann, 1994). The density of the mafic (eclogitic) crust likely remains higher than that of the ambient mantle through most of the lower mantle (Ono *et al.*, 2001). A layer generated by oceanic crust recycling is likely to remain stable if its density is in the range of 1–6% greater than that of the ambient mantle (Sleep, 1988; Montague and Kellogg, 2000; Zhong and Hager, 2003; Brandenburg and van Keken, in press). Entrainment of this layer by plumes provides a straightforward explanation for the geochemically observed oceanic crust component in OIBs (Shirey and Walker, 1998; Eiler *et al.*, 2000). The potential for entrainment of a deep chemical boundary was studied systematically by Lin and van Keken (2006a, 2006b) who found that with strongly temperature-dependent viscosity the entrainment would become

episodic under a large range of conditions. The style of entrainment ranged from nearly stagnant large plumes in the lower mantle to fast episodic pulsations traveling up the pre-existing plume conduit, which provides an explanation for the pulses of LIP volcanism (Lin and van Keken, 2005). Oscillatory instabilities in starting plumes can be caused by the competing effects of thermal and chemical buoyancy with particularly interesting effects where the effective buoyancy is close to zero (Samuel and Bercovici, 2006).

7.09.3.4.3 Effects of variable mantle properties

Large variations in material properties can lead to complex forms and time dependence of buoyant upwellings. For example, the combination of increasing ambient viscosity, thermal conductivity, and decreasing thermal expansivity with depth will likely cause plumes to be relatively broad in the deep mantle but become thinner when migrating upward (Albers and Christensen, 1996). Changes in rheology fundamentally alter plume dynamics. The sharp decrease of ambient viscosity for a plume rising from the lower, to the upper mantle will cause a rapid increase in speed and resulting drop in plume width (van Keken and Gable, 1995). Such necking may also cause the formation of a second boundary layer with episodic diapirism with timescales on the order of 1–10 My (van Keken *et al.*, 1992, 1993). The viscosity change can also completely break apart a starting mantle-plume head into multiple diapirs, perhaps contributing to multiple flood basalt episodes (Bercovici and Mahoney, 1994). An important aspect of mantle rheology is the non-Newtonian behavior, which is characterized by a viscosity that has a strong, nonlinear function of stress in addition to temperature and pressure. The strong stress dependence can dramatically enhance the deformation rate of boundary layer instabilities and lead to much higher rise speeds than is observed in Newtonian fluids (where strain rate and stress are linearly related) (Larsen and Yuen, 1997; Van Keken, 1997; Larsen *et al.*, 1999). Such behavior can cause starting plume heads to rise sufficiently fast to almost completely separate from the smaller tail, thus providing an alternative explanation for the observed LIP episodicity (Van Keken, 1997).

The transition zone is also characterized by major phase changes in the upper-mantle mineral assemblages, dominated by the exothermic 400 km discontinuity and the endothermic 670 km discontinuity. The phase changes provide a dynamical influence that can strongly modify plume flow, with predictions for more episodic or faster plume flow in the upper mantle (Nakakuki *et al.*, 1997; Brunet and Yuen, 2000). One model provides a source for plumes even just below the 660 km discontinuity (Cserepes and Yuen, 2000), an intriguing possibility for hot spots with sources above the CMB.

The sluggish nature of the lower mantle may be enhanced if heat radiation becomes efficient at high temperature. This has been explored for mantle plumes by Matyska *et al.* (1994) who suggest that the radiative components will strongly enhance the stability and size of large 'super'plume regions in the lower mantle, even without chemical stabilization. The plume stability may be enhanced by the possible post-perovskite transition at the base of the lower mantle (Matyska and Yuen, 2005, 2006a).

Thus, the concept of a cylindrical plume, rising vertically from the CMB to the lithosphere, is probably far too simple. Upwellings are likely to take on complex shapes, have a wide range of sizes, be strongly time dependent, and originate from different depths in the mantle. We will revisit such issues in Section 7.09.3.7.

7.09.3.4.4 Plume buoyancy flux and excess temperature

A long-standing question concerns the efficiency of heat transport in mantle plumes. If hot spots are dynamically supported by plumes that rise from the CMB, then we can use surface observations to estimate the heat from the core. The topography of hotspot swells provides a fundamental constraint on the buoyancy flux of plumes. Davies (1988) estimated, from swell heights of 26 hot spots provided by Crough (1983), that new topography is being generated at a rate $S = 17.5\,\mathrm{m^3\,s^{-1}}$ (in comparison to $300\,\mathrm{m^3\,s^{-1}}$ for the total mid-oceanic ridge system). Iceland was excluded from this compilation and the overall flux was dominated by the Pacific hot spots and in particular by Hawaii, Society, and the Marquesas. The total buoyancy flux follows by multiplication with the density difference between mantle and sea water, $B = (\rho_m - \rho_w)S = 40\,\mathrm{Mg\,s^{-1}}$, assuming $(\rho_m - \rho_w) = 2300\,\mathrm{kg\,m^{-3}}$. The estimated heat flux carried by the plumes q_p follows from $q_\mathrm{p} = \rho_m C_p S/\alpha$, which is around 2 TW, assuming $C_\mathrm{p} = 1000\,\mathrm{J\,kg^{-1}\,K^{-1}}$ and $\alpha = 3 \times 10^{-5}\,\mathrm{K^{-1}}$. Sleep (1990) provided a similar analysis for 34 hot spots, including Iceland, and found a slightly larger value of $55\,\mathrm{Mg\,s^{-1}}$ for the total buoyancy flux, implying a

core heat loss of ~2.7 TW. The plume heat flux is therefore significantly smaller than the total heat flux of the Earth of 44 TW (Pollack *et al.*, 1993).

The low estimates for plume heat flux are suggestive of only a minor contribution of plumes to the cooling of the Earth, and potentially a small contribution of core cooling, under the assumption that hot-spot heat is related to the heat from the core. However, the role of compressible convection, internal heating modes, and interaction with the large-scale flow and plate tectonics may be important in masking heat rising from the core. For example, a large-scale mantle circulation associated with plate tectonics could be drawing heat from the CMB toward mid-ocean ridges rather than allowing it to rise in vertical plumes to form mid-plate hot spots (Gonnermann *et al.*, 2004). Statistical arguments for the power-law distribution of plumes have been used to debate that many small plumes are entrained in the large-scale flow and do not express themselves as hot spots (Malamud and Turcotte, 1999). This idea has been supported by mantle convection models that simulate a wide range of heating modes (Labrosse, 2002; Mittelstaedt and Tackley, 2006).

The temperature increase across the TBL at the CMB can be estimated based on the adiabatic extrapolation of upper-mantle temperatures and mineral physics constraints on the temperature of the core. An estimate exceeding 1000 K (Boehler, 2000) is much greater than the temperature anomalies expected in the upper mantle beneath the major hot spots of only 200–300 K (see Section 7.09.3.2.1). If plumes rise from the CMB, what then is the mechanism for reducing the plume temperature by the time it reaches the base of the lithosphere? While entrainment of, and diffusive heat loss to the surrounding cooler mantle will reduce the plume excess temperature, most calculations based on the classical plume model suggest only modest reductions (e.g., Leitch *et al.*, 1996; Van Keken, 1997).

In our view, the likely important role of thermochemical convection and the variable properties of the mantle (see Sections 7.09.3.4.2 and 7.09.3.4.3) can provide a self-consistent resolution to the above discrepancy. For example, Farnetani (1997) showed that if a compositionally dense layer stabilizes at the base of D″, plumes will tend to rise from only the top of the TBL, which is substantially less hot than the CMB. In addition, decompression and subadiabaticity can enhance the cooling of plumes as they rise through the mantle and further reduce their surface expression (Zhong, 2006).

7.09.3.5 Chains, Age Progressions, and the Hot-spot Reference Frame

Thermal plumes rising from below the upper mantle to the lithosphere provide a reasonably straightforward explanation for a source of at least some hot-spot swells and age-progressive volcano chains. An origin residing below the asthenosphere allows for the possibility of a kinematic reference frame that is distinct from the plates. On the other hand, if thermal plumes rise from the deep, convecting mantle, it should be intuitive that hot spots are not stationary (Section 7.09.2).

A series of studies initiated by Steinberger (Steinberger and O'Connell, 1998; Steinberger, 2000) have used numerical models to simulate plumes rising in a convecting mantle. Their calculations of a spherical Earth assume that mantle flow is driven kinematically by the motion of the plates with realistic geometries, and dynamically by internal density variations estimated from different seismic tomography models. The viscosity structure includes high viscosities in the lower mantle ($\sim 10^{21}-10^{23}$ Pa s) and lower viscosities in the upper mantle ($\sim 10^{20}-10^{21}$ Pa s). A plume is simulated by inserting a vertical conduit in the mantle at a specified time in the past. Velocities at each point along the conduit are the vector sum of the ambient mantle velocity and the buoyant rise speed of the conduit, which is computed based on scaling laws derived from theory and laboratory experiments. For simplicity, the ambient mantle flow is not influenced by the plumes. Plume conduits therefore deform with time and where they intersect the base of the lithosphere defines the location of the hot spots (**Figure 21**).

This method was applied to examine the evolution of the Hawaiian, Louisville, and Easter hot spots in the Pacific ocean (Steinberger, 2002; Koppers *et al.*, 2004). A mantle flow model was found to optimize fits between predicted and observed age progressions along the whole lengths of all three chains. For the Hawaiian hot spot, the models predict absolute southward motion that was rapid (average ~40 km My^{-1}) during 50–80 Ma (prior to the Hawaiian–Emperor Bend) and slower (<20 km My^{-1}) since 50 Ma, thereby providing an explanation for the paleomagnetic evidence (Tarduno *et al.*, 2003; Pares and Moore, 2005; Sager *et al.*, 2005). The models also predict slow eastward motion of Louisville, consistent with the observed nonlinear age progression (Koppers *et al.*, 2004), as well as WSW motion of the Easter hot spot at rates of ~20 km My^{-1}.

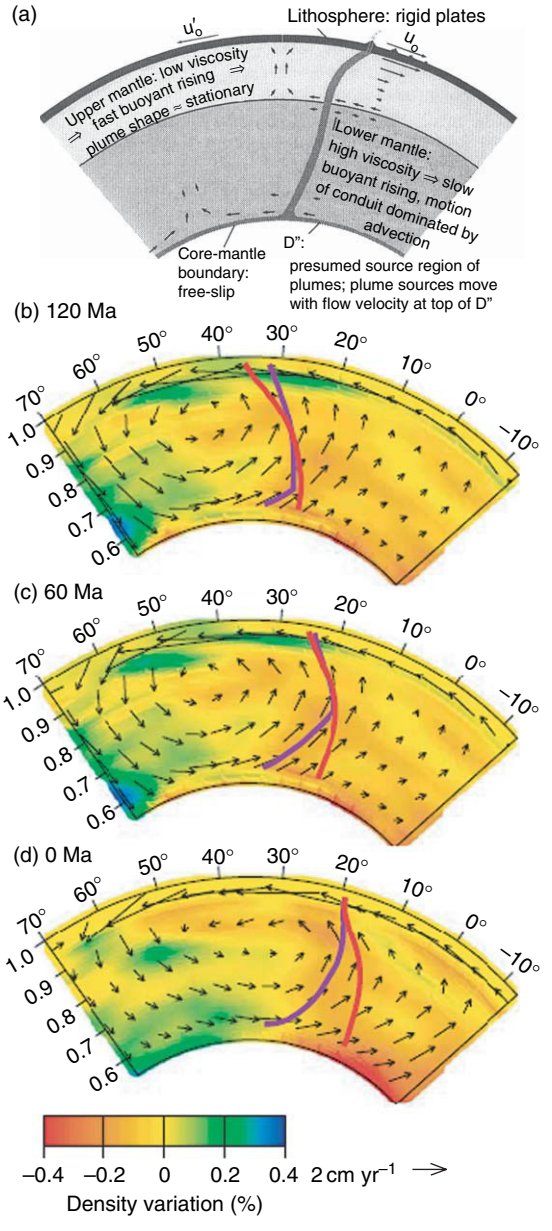

Figure 21 (a) Cartoon illustrating the rise and deformation of plumes through a flowing mantle with layered viscosity and surface plate motion. (b)–(d) show predicted mantle flow (arrows), density variations (colors), and deformation of the Hawaiian plume rising from the CMB at a location that is fixed (purple, initiated 150 Ma, or moving with the mantle (red, initiated 170 Ma). Times in the past are labeled. (a) Reproduced from Steinberger B and O'Connell RJ (2000) Effects of mantle flow on hotspot motion. *Geophysical Monograph* 121: 377–398, with permission from AGU. (b)–(d) Reprinted by permission from Macmillan Publishers Ltd: (Nature) Steinberger B, Sutherland R, and O'Connell RJ (2004) Prediction of Emperor-Hawaii seamount locations from a revised model of global plate motion and mantle flow. *Nature* 430: 167–173, copyright (2004).

The above studies addressed one group of hot spots but a key challenge is to explain the age progressions of both the Pacific and Indo-Atlantic hot spots in a single whole-mantle flow model. Steinberger *et al.* (2004) started this by considering two kinematic circuits to define the relative motions between the Pacific and African Plates: (1) through Antarctica, south of New Zealand and (2) through the Lord Howe Rise, north of New Zealand, Australia, and then Antarctica. The reference case of fixed hot spots predicts hot-spot tracks that deviate substantially from observed locations (dotted curves in **Figure 22**) for both plate circuits. Considering moving hot spots derived from mantle flow simulations with plate circuit (1) yields reasonable matches to the tracks for ages <50 Ma but predicts a track too-far west of the Emperor chain for ages >50 Ma. Finally, predicted tracks with moving hot spots using plate circuit (2) provide the closest match to the observed tracks. This model successfully predicts the geographic age progressions along most of the Tristan, Réunion, and Louisville tracks, and for the Hawaiian track since 50 Ma, including a bend between the Hawaiian and Emperor seamounts. But the bend is not sharp enough: the models still predict a trajectory for the Emperor seamounts too far west.

The above studies illustrate that models of plumes rising in a geophysically constrained, mantle flow field can explain many key aspects of apparent hot-spot motion. The studies, however, underscore the importance of uncertainties in defining relative plate motions, particularly in the presence of diffuse plate boundaries – for example, that near Lord Howe Rise. Still more uncertainties are associated with the locations of volcanism in time and in paleomagnetic latitudes. The models are sensitive to a number of properties such as mantle viscosity structure, the choice of seismic tomography model, the mapping between seismic velocities and density, as well as the buoyancy and dimensions (which control the rise speed) of the mantle plumes. A recent study has just begun to quantify the observational uncertainties and to use them to define statistically robust mantle flow solutions (O'Neill *et al.*, 2003). But many observations remain poorly understood, including the location and trend of the older portion of the Emperor chain.

7.09.3.6 Large Igneous Provinces

The rapid and massive magmatic production of many LIPs, combined with their strong connection to continental breakup, but inconsistent connection to

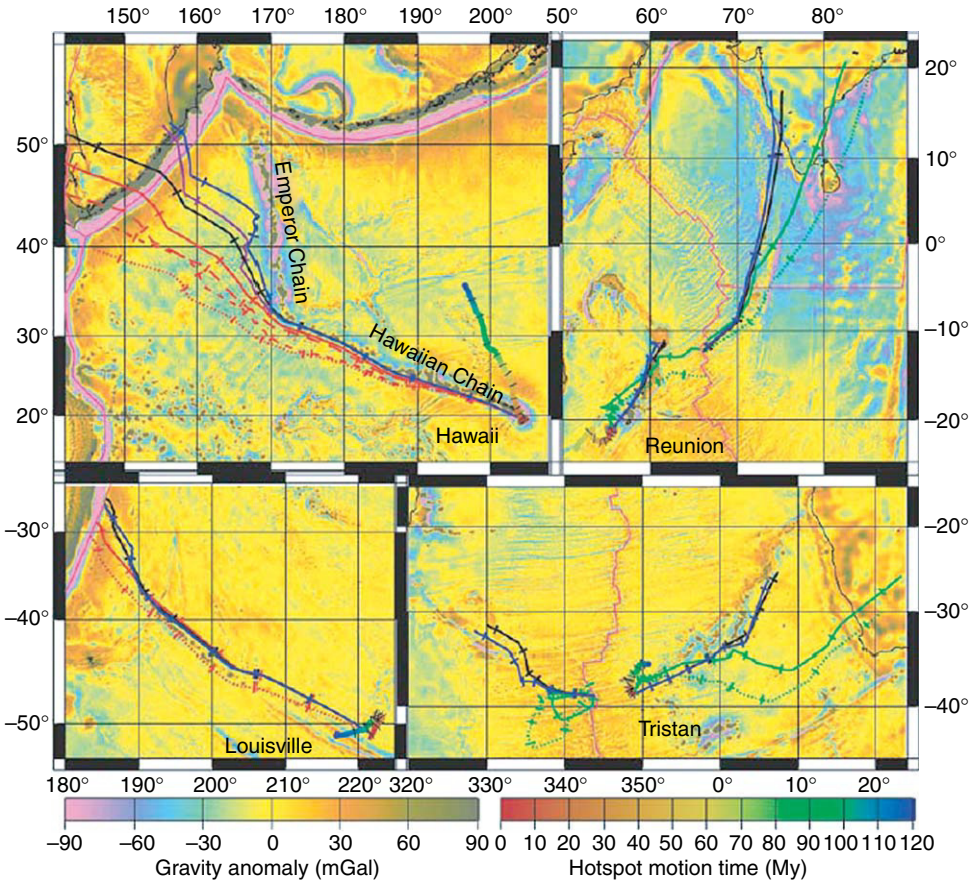

Figure 22 Computed hot-spot motion (rainbow colored bands with color indicating position in time according to scale on the lower right) and tracks overlain on gravity maps (left color scale). Tracks are plotted on all plates regardless of whether a hot spot was actually on the plates during those times. Ticks along tracks are every 10 My. Dotted (red and green) lines are solutions assuming fixed hot spots. Solid red lines (plate circuit (1) shown for Hawaii and Louisville) and purple lines (plate circuit (2) shown for Hawaii) are for moving hot spots in mantle flowing in response to absolute plate motions that optimize fits to only the Tristan and Réunion hot-spot tracks. Green lines (shown for Réunion and Tristan) are best fit solutions to only the Hawaii and Louisville tracks using plate circuit (1). Black (plate circuit (1)) and blue (plate circuit (2)) are solutions that optimize fits to all four tracks. A least-squares method is used to optimize the fit to locations and radiometric ages of seamounts. Reprinted by permission from Macmillan Publishers Ltd: (Nature) Steinberger B, Sutherland R, and O'Connell RJ (2004) Prediction of Emperor-Hawaii seamount locations from a revised model of global plate motion and mantle flow. *Nature* 430: 167–173, copyright (2004).

present-day hot-spot volcanism are challenging to understand. Moreover, the wide range of eruptive volumes (**Figure 8**) and durations suggest that there may not be just one overarching mechanism.

The observation of large plume heads followed by thin tails in fluid dynamical experiments has traditionally been used to explain the LIP-hotspot connection (Richards *et al.*, 1989) and remains, because of its simplicity and plausibility, an attractive base model for the formation of many LIPs. Its strengths include that: (1) it is supported by fluid dynamics for increasingly realistic assumptions about mantle composition and rheology (see Section 7.09.3.4), in fact these modifications to the base model allow for an explanation of some of the diversity seen in the geological record (**Figure 23**); (2) it offers a dynamical cause for the common disconnect between LIP and hotspot volcanism (Farnetani and Samuel, 2005) (i.e., some plume heads rise to the surface without plume tails and some upwellings form narrow plume tails without heads, **Figure 23**). (3) It predicts the hottest material of rising plume heads will erupt first (Farnetani and Richards, 1995) which explains high MgO basalts early in the LIP record; and (4) it

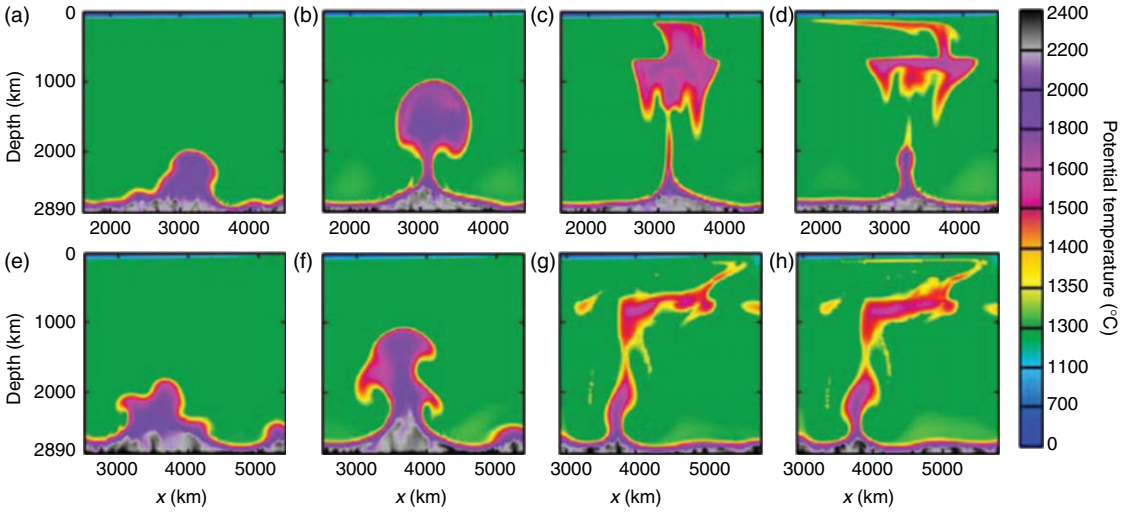

Figure 23 Temperatures of upwelling instabilities rising from the CMB predicted by 3-D numerical models. The CMB is heated from below and is blanked by a layer initially 200 km in thickness and containing material with an intrinsic, compositional density that is 1% greater than that of the surrounding lower mantle. Upwelling through a depth of 670 km is inhibited by an endothermic phase change with a Clapeyron slope of –2.5 MPa K^{-1}. In the top row a large, roughly spherical plume head rapidly rises and could generate flood volcanism at the surface. The head detaches from the stem and this may delay or prevent the formation of a chain of volcanoes extending away from the flood basalts. In the bottom row, only a narrow upwelling rises into the upper mantle. Reproduced from Farnetani CG and Samuel H (2005) Beyond the thermal plume hypothesis. *Geophysical Research Letters* 32: L07311 (doi:10.1029/2005GL022360), with permission from AGU.

predicts that the arrival of the plume at the surface leads to uplift and extension which is observed in the geological record of many LIPs (see Section 7.09.2.3). Plume-based models, however, have yet to adequately explain the strong correlation between LIPS and continental breakup and the lack of uplift during the OJP eruptions (d'Acremont *et al.*, 2003).

There are a number of alternative mechanisms that address the above issues, which include shallow, sublithospheric processes or metorite impacts. While the plume model has received significant attention and quantitative hypothesis testing, the majority of the alternatives are currently still in rather qualitative form.

The first alternative to thermal plumes pertains to LIPs formed on continental margins. Anderson (1994b) proposes that excess heat can build below continents during tectonic quiescence and/or supercontinent formation, which then causes the massive eruptions during continental breakup. This hypothesis addresses the correlation between LIPs and continental breakup and the lack of connection of some continental LIPs to hot-spot trails. One aspect not addressed specifically is why the volcanism is typically not margin-wide but, instead, is more restricted in total extent. Nevertheless, the correlation between the LIPs and continental breakup is intriguing and it is quite likely that regional variations in the composition and strength of the lithosphere have an important control on the location of magma eruption.

Second, delamination of continental lithosphere and secondary convection at rifted margins (**Figure 15(b)**) have been forwarded to generate LIPs near continents (King and Anderson, 1995, 1998; van Wijk *et al.*, 2001; Hales *et al.*, 2005; Anderson, 2005). Like the above concept of subcontinental mantle incubation, these models can explain continental LIPs without hot-spot tracks, but have yet to show how they could form LIPs with hot-spot tracks. Indeed, more quantitative modeling of shallow mantle processes needs to be done.

A third alternative, which could apply to LIPs that form near sites of continental or oceanic rifting, is that compositional, rather than thermal effects cause excess melting, for example, more fertile mantle such as eclogite and/or water in the source (e.g., Anderson, 1994a, 2005; Cordery *et al.*, 1997; Korenaga, 2004; 2005b) (**Figure 15(a)**). The strengths of this possibility include that some compositional effects are expected and these can strongly enhance melt

production (see Section 7.09.3.2.2); the lack of uplift of OJP could be explained if dense eclogite occurs in the source; and it can explain the formation of LIPs not connected to long-lived hot-spot tracks. Again, a key dynamic weakness of models invoking eclogite in the source is that eclogite is dense and requires some mechanism to stay near, or be brought back up to the surface.

Fourth, the enigmatic nature of the OJP has led to the suggestion that a meteorite impact could be responsible for the emplacement of LIPs (Rogers, 1982; Jones *et al.*, 2002a; Tejada *et al.*, 2004; Ingle and Coffin, 2004). The strengths are that the decompression of mantle following impact may generate extensive melting (although perhaps with some qualifications (Ivanov and Melosh, 2003)) with less uplift than expected from a hot plume head and without a connection to a hot-spot track. It is rare, however, to find direct evidence for meteorite impact during LIP emplacement. One of the few convincing observations is the iridium anomaly embedded in the Deccan Traps, but if this impact signal is related to the Chixculub impact, it post-dates the start of volcanism (Courtillot and Renne, 2003). Also, it is statistically unlikely that the majority of Phanerozoic LIPs can be explained by impacts (Ivanov and Melosh, 2003; Elkins-Tanton and Hager, 2005). Finally, a cursory investigation of planetary impact cratering suggests that many large craters on the Moon, Mars, and Venus form without contemporaneous volcanism. An interesting recent speculation is that the formation of the lunar impact basins and (much) later volcanic activity that formed the maria are indeed related and caused by the long term storage of heat in the lunar mantle (Elkins-Tanton *et al.*, 2004).

7.09.3.7 Hot Spots: Modifications and Alternatives

7.09.3.7.1 Variable hot-spot durations from transient thermal plumes

Section 7.09.2.1 showed that the duration of hot-spot activity varies significantly from <10 to >100 My with numerous cases falling near both extremes. A broad range of timescales is generally consistent with the variable scales of flows that characterize mantle convecting at high Rayleigh numbers ($\geq 10^7$). Thermal upwellings, for example, are, in general, transient phenomena as shown by laboratory experiments of basally heated viscous fluids. An excellent example is provided by Davaille and Vatteville (2005); they find that well-developed plumes in the laboratory often detach from their bases on timescales comparable to, but less than, that needed to initiate the instability from the TBL (**Figure 24(a)**). Laboratory experiments show that this timescale is approximately (e.g., Sparrow *et al.*, 1970; Manga *et al.*, 2001)

$$\tau = \frac{H^2}{\pi\kappa}\left(\frac{Ra_c}{Ra}\right)^{2/3} \quad [10]$$

where H is the thickness of the fluid, Ra_c is the critical Rayleigh number (i.e., the minimum needed to grow an instability and is of order 10^3), and Ra is the Rayleigh number of the system. This is essentially the time it takes heat diffusion to sufficiently thicken the TBL (to a thickness $\delta = \sqrt{\pi\kappa\tau_c}$) such that the local Rayleigh number (eqn [8]) equals Ra_c. If the TBL is at the CMB, then $H = 2800$ km, $Ra = 10^7$, and plume life times are expected to be $\tau \sim 200$ My, which is sufficient to maintain long-lived hot-spot chains. If the TBL is near the base of the upper mantle ($H = 660$ km, $Ra = 1e7$), then $\tau \sim 10$ My is comparable to the duration of many short-lived volcano chains.

There are a few ways to initiate plumes from boundary layers internal to the mantle. High-resolution 2-D convection simulations by Matyska and Yuen (2006b) predict large-scale (10^3–10^4 km), superplume-like upwellings as a result of relatively low local Rayleigh numbers caused by high viscosities, low thermal expansivity, and radiative heat transfer in the lower mantle (**Figure 24(b)** and **24(d)**). As superplumes rise through the lower mantle, further rise can be inhibited by the endothermic phase change at 660 km. The hot tops of the superplumes can generate a TBL from which smaller scale (10^2 km) upper-mantle upwellings can originate. Another possible surface for a mid-mantle TBL is the top of a chemically dense layer in the lower mantle (see Section 7.09.3.4.2). Laboratory experiments show that when an initially chemically stratified system is heated from below and cooled from above, a variety of forms of upwellings and downwellings occur, depending on the ratio of chemical-to-thermal buoyancy (Davaille, 1999). When the negative chemical buoyancy of the lower layer is ~0.35–0.55 times the positive buoyancy due to the basal heating, the two layers remain separate but the surface between them undulates to form broad downwellings and superplume upwellings. Above the upwellings, smaller instabilities can rise into the upper layer and to the surface (**Figure 24(e)**). In both of the two examples described above, smaller upper-mantle plumes are shown to rise from the top of broad

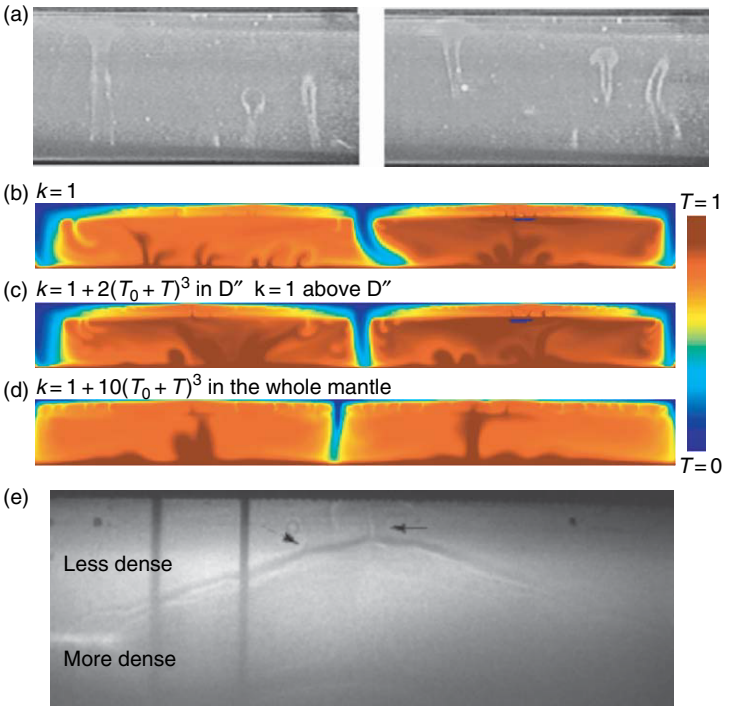

Figure 24 (a) Photographs, the left taken prior to the right, of a laboratory experiment involving sucrose solution heated from the base. Isotherms (white streaks) outline the hot upwellings that detach from the base, as imaged using suspended liquid crystals and glass particles. (b) 2-D numerical simulations of whole-mantle convection in which the mantle is heated internally, at its base, and is cooled at the surface. Viscosity is temperature- and pressure-dependent. Calculations also include an endothermic phase change at 670 km and an exothermic phase change at 2650 km. Coefficient of thermal expansion decreases by >10 times from the surface to the CMB. (b) A thermal conductivity $k = 1$ corresponds to that due to heat diffusion, whereas (c) and (d) include an additional term (dependent on temperature) for radiative heat transfer. (e) Laboratory experiments involving a chemically dense and more viscous fluid underneath a chemically less dense and less viscous fluid. The system is heated from below and cooled from above. Dark and light bands show the interface between the two fluids, which bows upward and resembles the upper surface of a mantle superplume. Smaller plumes are imaged to be rising from this surface into the upper layer. (a) Reproduced from Davaille A and Vatteville (2005) On the transient nature of mantle plumes. *Geophysical Research Letters* 32, doi:1029/2005GL023029, with permission from AGU. (b)–(d) Reproduced from Matyska C and Yuen DA (2006b) Upper-mantle versus lower-mantle plumes: are they the same? In: Foulger GR and Jurdy DM (eds.) *The Origins of Melting Anomalies*: *Plates*, *Plumes*, *and Planetary Processes*. GSA, with permission from GSA. (e) Reprinted by permission from Macmillan Publishers Ltd: (Nature) Davaille A (1999) Simultaneous generation of hotspots and superswells by convection in a heterogeneous planetary mantle. *Nature* 402: 756–760, copyright (1999).

superplumes. Such a situation could provide an explanation for the large frequency of short-lived hot spots in the superswell regions of the South Pacific and Africa (e.g., Courtillot *et al.*, 2003; Koppers *et al.*, 2003).

7.09.3.7.2 Forming melting anomalies by upper-mantle processes

Buoyant upwellings have been the focus of a large number of studies but are probably not the only phenomena giving rise to melting anomalies. Upper-mantle processes that are largely decoupled from the lower mantle undoubtedly contribute to the magmatism in various ways.

Small-scale, sublithospheric convection, as introduced in Section 7.09.3.2, is one possible mechanism. Sublithospheric convection could be evidenced by a number of observations: it could limit the maximum thickness of the lithosphere and slow the subsidence of old seafloor (e.g., Huang *et al.*, 2003); it could give rise to the prominent gravity lineations over the Pacific seafloor (Haxby and Weissel, 1986); and it could explain the periodic fluctuations in upper-mantle seismic structure as imaged perpendicular to hot-spot swells in the Pacific (Katzman *et al.*, 1998). Small-scale sublithospheric convection may explain magmatism along lineaments parallel to plate motion (e.g., Richter, 1973; Huang *et al.*, 2003), but perhaps

without a systematic geographic age progression. Quantitative studies of melting have yet to be done but are needed to quantify the rates and time dependence of magma production, as well as whether small-scale convection could generate seafloor swells.

Another mechanism that has been recently proposed is fingering instabilities of low-viscosity asthenosphere (Weeraratne *et al.*, 2003; Harmon *et al.*, 2006). When two fluids are contained in a thin layer (Hele–Shaw cell in the laboratory and possibly the asthenosphere in the upper mantle) and one fluid laterally displaces a more viscous fluid, the boundary between the two becomes unstable and undulates with increasing amplitude (Saffman and Taylor, 1958). Fingers of the low-viscosity fluid lengthen and penetrate the high-viscosity fluid. Perhaps hot mantle rising beneath the South Pacific Superswell area is supplying hot, low-viscosity asthenosphere that is fingering beneath the Pacific Plate and generating some of the volcanic lineaments such as Pukapuka (Harmon *et al.*, 2006; Weeraratne *et al.*, in press). Weeraratne and Parmentier (2003) explore this possibility using laboratory experiments that simulate asthenospheric conditions.

Finally, numerous studies have suggested that heterogeneity in lithospheric stresses or structure can allow magma that is already present in the asthenosphere to erupt at the surface (e.g., Anguita and Hernan, 2000; Clouard *et al.*, 2003). Lithospheric stress associated with regional (e.g., Sandwell *et al.*, 1995) or local (e.g., Mittelstaedt and Ito, 2005) tectonics, as well as thermal contraction (Gans *et al.*, 2003) could initiate fissures that can propagate and cause volcanic lineaments over a range of scales. Sandwell and Fialko (2004), for example, demonstrate that top-down cooling of the lithosphere generates thermoelastic tensile stress, which is optimally released by local zones of fracturing with spacing comparable to the flexural wavelength of the lithosphere and to the distances between the Pukapuka, Sojourn, and Hotu–Matua Ridges in the South Pacific. Natland and Winterer (2005) propose a lithospheric fissure origin for most or all of the Pacific hot spots, but such a hypothesis has yet to be tested quantitatively.

Another form of stress-influenced magma penetration could redistribute magma from diffuse volumes in the asthenosphere to discrete, localized eruption sites at the surface. The weight of a volcano can draw further magmatism if lithospheric stresses due to loading focuses magma-filled cracks toward the volcano (Muller *et al.*, 2001) or if damage that is related to volcano loading enhances permeability in the lithosphere beneath it (Hieronymus and Bercovici, 1999). Parametrized models of damage-enhanced lithospheric permeability predict volcano chains to form either from a plate moving over a hot-spot-like source of magma (Hieronymus and Bercovici, 1999) or without a hot-spot source, but with nonlithostatic, horizontal tension in the lithosphere related to plate tectonics (Hieronymus and Bercovici, 2000) (**Figure 25**). The latter result provides another

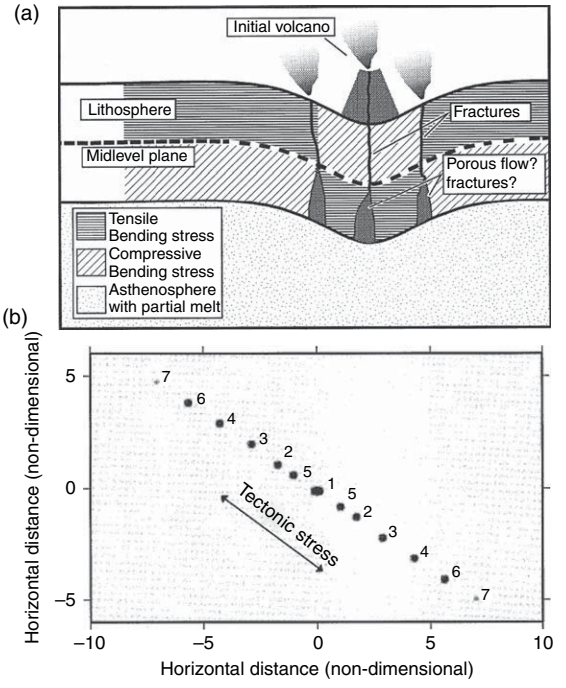

Figure 25 (a) Cartoon of cross-section through the lithosphere, which is being flexed by a growing volcano. Nonlithostatic stresses due to bending are shaded dark for tension and light for compression. The asthenosphere is assumed to be partially molten. Damage-enhanced permeability is high beneath the volcano where bending stresses are largest. New volcanoes are predicted to form where the tension in the upper half of the plate is maximum. Remote, tectonic stresses can cause horizontal, nonlithostatic tension, which is depth independent and can cause new eruptions to occur in lines. (b) Predicted pattern of volcanoes resulting from flexural stresses and nonlithostatic, tectonic stress that is tensile parallel to the volcano lineament (arrows). The location of volcano number 1 was imposed and subsequent volcanoes formed in numerical order as labeled. The model predicts new volcanism to propagate in both directions away from the initial volcano. From Hieronymus CF and Bercovici D (2000) Non-hotspot formation of volcanic chains; control of tectonic and flexural stresses on magma transport. *Earth and Planetary Science Letters* 181: 539–554.

plausible mechanism for forming lineaments without a monotonic age progression, but instead, with testable progressions of decreasing volcano age in both directions along the lineament. Another test is provided by the relationship between tectonic stress and the direction of volcano propagation. Models based on fracture mechanics predict propagation of volcanism perpendicular to the tensile direction, while Hieronymus and Bercovici (2000) predict volcanism to propagate along the tensile direction by the interaction of point-load flexural and background stresses (**Figure 25**).

7.09.3.8 Geochemistry of Hotspots and Melting Anomalies Vs MORB

The geochemical differences between basalts erupted at hot spots and melting anomalies versus MORB provide a vital constraint on the causal mechanisms (*see also* Chapters 7.10 and 2.04). We have focused on $^{87}Sr/^{86}Sr$, $^{206}Pb/^{204}Pb$, $^{3}He/^{4}He$ ratios because they are key to tracing at least five flavors of mantle materials with different, time-averaged, chemical histories (Hart *et al.*, 1992; Hanan and Graham, 1996; Zindler and Hart, 1986). Lavas with low $^{3}He/^{4}He$ and minimal $^{87}Sr/^{86}Sr$ and $^{206}Pb/^{204}Pb$ probably come from depleted mantle material (DM), referring to a long-term ($>10^{2}$ My) depletion in incompatible elements. Enriched (EM1 or EM2, i.e., high $^{87}Sr/^{86}Sr$) and HIMU (i.e., high $^{206}Pb/^{204}Pb$) mantle are thought to be influenced by subducted and recycled material, the former by old oceanic sediments or metasomatized lithosphere, and the latter perhaps by oceanic crust that has been hydrothermally altered and then devolatized during subduction (e.g., Cohen and O'Nions, 1982; Hofmann and White, 1982; Hart *et al.*, 1992; Zindler and Hart, 1986; Hofmann, 1997). High $^{3}He/^{4}He$, moderately low $^{87}Sr/^{86}Sr$, and intermediate-to-high $^{206}Pb/^{204}Pb$ compositions mark the fifth geochemical material; it has been identified with various names and we will refer to it as FOZO (for FOcal ZOne (Hart *et al.*, 1992)). Its origin, however, is not well understood. The 'standard' hypothesis is that $^{3}He/^{4}He$ measures the primordial nature of the source material with low ratios reflecting material that has experienced substantial degassing of primordial ^{3}He and the high ratios indicating relatively undegassed mantle. But more recent evidence weakens the standard hypothesis and instead suggests that FOZO, in fact, has been depleted in highly incompatible elements. In this scenario, the high $^{3}He/^{4}He$ ratio could reflect a low ^{4}He concentration as a result of low U and Th content (Coltice and Ricard, 1999; Stuart *et al.*, 2003; Meibom *et al.*, 2005; Parman *et al.*, 2005).

The key issue is that MORB appears to be heavily influenced by DM and minimally influenced by subducted materials and FOZO, whereas hot spots and melting anomalies appear to be influenced substantially by all five components (albeit to different degrees for different volcano groups). One possibility is that the pressure/temperature dependence of mantle viscosity and mineralogy, as well as density differences between the different mantle materials promotes large-scale layering in mantle geochemistry. DM is likely to be compositionally light and may tend to concentrate in the upper mantle where it is sampled by mid-ocean ridge magmatism. Mantle plumes, which feed hot spots, rise from deeper levels in the mantle and incorporate the other materials in addition to DM.

The formation of the different geochemical components, as well as the possibility of large-scale layering in the presence of vigorous, whole-mantle convection is actively being studied with both computational and laboratory methods (e.g., Christensen and Hofmann, 1994; van Keken and Ballentine, 1999; Davaille, 1999; Ferrachat and Ricard, 2001; Xie and Tackley, 2004). On the one hand, such studies have successfully predicted the formation of deep layers that are concentrated in dense subducted mafic material, which, if entrained in upwelling plumes could explain some of the elevated $^{206}Pb/^{204}Pb$ ratios in hot-spot basalts. On the other hand, it remains to be seen how it is possible to generate and physically separate two (or more) different components that may be depleted of mafic components: one with low $^{3}He/^{4}He$ that is prominent in MORB and the other with high-$^{3}He/^{4}He$ that is weakly expressed in MORB and more prominently expressed in some hot-spot lavas. Another challenge is to reconcile the geochemical character of hot spots/melting anomalies with the possibility that some could be caused by plumes originating very deep in the mantle, some by plumes originating from shallower in the mantle, and others from shallow mechanisms completely unrelated to plumes. Finally, the small heat flux of mantle plumes implied by observations of swell buoyancy flux (Section 7.09.3.4.4), as well as constraints on excess temperatures of plumes in the upper mantle (Zhong, 2006) require that incompatible-element-rich materials are present both above and below the source layer of most mantle plumes.

One key process to consider in addressing the above issues is the chemical extraction of the different components by melting (Phipps Morgan, 1999). Geochemical evidence indicates that heterogeneity is likely to be present over a range of spatial scales, including scales much smaller than the size of upper-mantle melting zones (e.g., Niu *et al.*, 1996; Phipps Morgan, 1999; Saal *et al.*, 1998; Reiners, 2002; Salters and Dick, 2002; Stracke *et al.*, 2003; Kogiso *et al.*, 2004; Ellam and Stuart, 2004). The likelihood that different materials begin melting at different depths for a given mantle temperature makes it probable that differences in lithospheric thickness, as well as the rate of mantle flow through the melting zone can influence the relative proportions of incompatible elements that are extracted from the different components. Mid-ocean ridge magmatism could most substantially melt the refractory component (DM) because the thin lithosphere allows for the greatest amount of decompression melting. Magmatism away from mid-ocean ridges could be less influenced by DM and proportionally more by the other, perhaps less refractory components owing to the thicker lithosphere. Melting of a buoyant upwelling – like a mantle plume – can also emphasize the least refractory components, even beneath relatively thin lithosphere, because the buoyancy pushes mantle through the deepest portions of the melting zone more rapidly than in the shallowest portions (Ito and Mahoney, 2005, 2006). Unraveling the above clues provided by magma geochemistry will thus require integrated geochemical, geophysical, and geodynamic investigations of the character of the mantle source, as well as the mantle convection, melting, and melt extraction.

7.09.4 Conclusions and Outlook

The rich diversity of observations and dynamical behavior makes it likely that a variety of mechanisms cause hot spots and melting anomalies. Our future task is to design observational and theoretical tests of which mechanisms can and cannot explain individual systems. The variety of observational techniques will lead to improved constraints. These observations include volume and durations of volcanism, the nature and depth extent of mantle seismic anomalies, and presence or absence of four key characteristics: swells, age progressions, connections with LIPS, and geochemical distinctions from MORB. We will close this chapter with a short outlook in the form of a wish list for future work.

1. Origin of melting anomalies: We need to explore different mechanisms of mantle flow and melting that include increasingly realistic dynamics (non-Newtonian, time-dependent, and 3-D) and lithologic variability, and we need to test model predictions against observed volumes and durations of volcanism. We need to do this to understand the relative importance of temperature and composition, which are both coupled to the upper-mantle dynamics. Example processes that are relatively less well understood include sublithospheric convection, fertile mantle melting, viscous fingering in the asthenosphere, as well as the role of the lithosphere in controlling magmatism on the surface.
2. Origin of swells: Previous work has shown that plumes can explain many observations of swells but future work is needed to explore whether nonplume mechanisms can cause swells, and in particularly, how they vary with plate speed and buoyancy flux. We are also faced by explaining the presence of melting anomalies without swells, such as the prominent Canaries and Madeira hot spots. Perhaps such systems are dominated by fertile mantle melting.
3. Age progressions and lack thereof: For long-lived age progressions, future challenges involve reducing observational uncertainties with further geophysical studies, more accurate and precise dating, and improving geodynamic models of mantle flow and evolution. The latter will require improved methods of tracking mantle flow further into the past, and in defining the ranges of allowable mantle density and viscosity structures from seismology and mineral physics. For hot spots with short-lived age progressions models will need to consider the possibility of them originating from upwellings from boundary layers above the CMB or nonplume sources. For hot spots without simple age progressions, plume may be unlikely and thus other mechanisms should be explored. In fact some of these mechanisms (e.g., propagating fracture) may predict age progressions and quantitative models are needed to explore these possibilities.
4. LIPs are the most dramatic but potentially the least understood dynamical processes on the planet. It is critical to evaluate how the evolving plume theory can self-consistently address the formation of some LIPs and to which cases alternatives are required.

5. Geochemistry: Differences in isotope geochemistry and in particular the distinctions from MORB of most OIBs require a chemically layered mantle, differences in melting of a nonlayered, heterogeneous mantle, or some combination of above.

6. Seismology: The key challenge is to confidently resolve if any hot spots have seismic anomalies extending into the lower mantle and if so, which ones do and do not. Such information will be critical for evaluating plume versus nonplume mechanisms. Combined with geochemical observations, such information could be the key in addressing the possibility or nature of geochemical layering.

7. Integrated and interdisciplinary work: We need to meet our capabilities of simulating increasingly complex dynamic behaviors with increasing quality of geophysical and geochemical data.

Acknowledgments

This work is partly supported by the National Science Foundation (OCE-0351234 and EAR-0440365 to Garrett Ito and EAR-0229962 to Peter van Keken).

References

Acton GD and Gordon RG (1994) Paleomagnetic tests of Pacific plate reconstructions and implications for motion between hotspots. *Science* 263: 1246–1254.

Albers M and Christensen UR (1996) The excess temperature of plumes rising from the core–mantle boundary. *Geophysical Research Letters* 23: 3567–3570.

Albers M and Christensen UR (2001) Channeling of plume flow beneath mid-ocean ridges. *Earth and Planetary Science Letters* 187: 207–220.

Ali JR, Thompson GM, Zhou MF, and Song XY (2005) Emeishan large igneous province, SW China. *Lithos* 79: 475–489.

Allégre CJ, Birck JL, Capmas F, and Courtillot V (1999) Age of the Deccan traps using Re-187–Os-187 systematics. *Earth and Planetary Science Letters* 170: 197–204.

Allen RM, Nolet G, Morgan WJ, *et al.* (1999a) The thin hot plume beneath Iceland. *Geophysical Journal International* 137: 51–63.

Allen RM, Nolet G, Morgan WJ, *et al.* (1999b) The thin hot plume beneath Iceland. *Geophysical Journal International* 137: 51–63.

Allen RM, Nolet G, Morgan WJ, *et al.* (2002) Imaging the mantle beneath Iceland using integrated seismological techniques. *Journal of Geophysical Research* 107: 10.1029/2001JB000595.

Allen RM and Tromp J (2005) Resolution of regional seismic models: Squeezing the Iceland anomaly. *Geophysical Journal International* 161: 373–386.

Anderson DL (1989) *Theory of the Earth*. Brookline Village, MA: Blackwell.

Anderson DL (1994a) The sublithospheric mantle as the source of continental flood basalts: the case against the continental lithosphere and plume head reservoirs. *Earth and Planetary Science Letters* 123: 269–280.

Anderson DL (1994b) Superplumes or supercontinents? *Geology* 22: 39–42.

Anderson DL (2005) Large igneous provinces, delamination, and fertile mantle. *Elements* 1(5): 271–275.

Anguita F and Hernan F (2000) The Canary Islands origin; a unifying model. *Journal of Volcanology and Geothermal Research* 103: 1–26.

Antretter M, Riisager P, Hall S, Zhao X, and Steinberger B (2004) Modelled paleolatitudes for the Louisville hot spot and the Ontong Java Plateau. *GSA, Special Publication* 299: 21–30.

Aoki I and Takahashi E (2004) Density for MORB eclogite in the upper mantle. *Physics of the Earth and Planetary Interiors* 143–144: 129–143.

Asimow P and Langmuir CH (2003) The importance of water to oceanic melting regimes. *Nature* 421: 815–820.

Ayalew D, Barbey P, Marty B, Reisberg L, Yirgu G, and Pik R (2002) Source, genesis, and timing of giant ignimbrite deposits associated with Ethiopian continental flood basalts. *Geochimica et Cosmochimica Acta* 66: 1429–1448.

Bastow ID, Stuart GW, Kendall JM, and Ebinger CJ (2005) Upper-mantle seismic structure in a region of incipient continental breakup: Northern Ethiopian rift. *Geophysical Journal International* 162: 479–493.

Batiza R (1982) Abundances, distribution and sizes of volcanoes in the Pacific Ocean and implications for the origin of non-hotspot volcanoes. *Earth and Planetary Science Letters* 60: 195–206.

Benoit MH, Nyblade AA, and Vandecar JC (2006) Upper mantle P-wave speed variations beneath Ethiopia and the origin of the Afar hotspot. *Geology* 34: 329–332.

Bercovici D and Kelly A (1997) The non-linear initiation of diapirs and plume heads. *Physics of the Earth and Planetary Interiors* 101: 119–130.

Bercovici D and Mahoney J (1994) Double flood basalts and plume head separation at the 660-kilometer discontinuity. *Science* 266: 1367–1369.

Bianco TA, Ito G, Becker JM, and Garcia MO (2005) Secondary Hawaiian volcanism formed by flexural arch decompression. *Geochemistry Geophysics Geosystems* 6: Q08009 (doi:10.1029/2005GC000945).

Bijwaard H and Spakman W (1999) Tomographic evidence for a narrow whole mantle plume below Iceland. *Earth and Planetary Science Letters* 166: 121–126.

Bijwaard H, Spakman W, and Engdahl ER (1998) Closing the gap between regional and global travel time tomography. *Journal of Geophysical Research* 103: 30055–30078.

Bjarnason IT, Silver PG, Rumpker G, and Solomon SC (2002) Shear wave splitting across the Iceland hot spot: Results from the ICEMELT experiment. *Journal of Geophysical Research* 107: 2382 (doi:10.1029/2001JB000916).

Boehler R (2000) High-pressure experiments and the phase diagram of lower mantle and core materials. *Reviews of Geophysics* 38: 221–245.

Bonneville A, Dosso L, and Hildenbrand A (2006) Temporal evolution and geochemical variability of the South Pacific superplume activity. *Earth and Planetary Science Letters* 244: 251–269.

Boschi L, Becker TW, Soldati G, and Dziewonski AM (2006) On the relevance of Born theory in global seismic tomography. *Geophysical Research Letters* 33: L06302.

Brandenburg JP and van Keken PE (in press) Preservation of oceanic crust in a vigorously convecting mantle. *Journal of Geophysical Research*.

Breger L, Romanowicz B, and Ng C (2001) The Pacific plume as seen by S, ScS, and SKS. *Geophysical Research Letters* 28: 1859–1862.

Brunet D and Yuen DA (2000) Mantle plumes pinched in the transition zone. *Earth and Planetary Science Letters* 178: 13–27.

Buck WR (1986) Small-scale convection induced by passive-rifting: The cause for uplift of rift shoulders. *Earth Planetary and Science Letters* 77: 362–372.

Buck WR and Parmentier EM (1986) Convection beneath young oceanic lithosphere: Implications for thermal structure and gravity. *Journal of Geophysical Research* 91: 1961–1974.

Burke K (1996) The African Plate. *South African Journal of Geology* 99: 339–409.

Campbell IH and Griffiths RW (1990) Implications of mantle plume structure for the evolution of flood basalts. *Earth and Planetary Science Letters* 99: 79–93.

Canales JP, Ito G, Detrick RS, and Sinton J (2002) Crustal thickness along the western Galapagos spreading center and the compensation of the Galapagos hotspot swell. *Earth and Planetary Science Letters* 203: 311–327.

Cannat M, Brias A, Deplus C, *et al.* (1999) Mid-Atlantic Ridge-Azores hotspot interactions: Along-axis migration of a hotspot-derived event of enhanced magmatism 10 to 4 Ma ago. *Earth and Planetary Science Letters* 173: 257–269.

Caroff M, Guillou H, Lamiaux M, Maury RC, Guille G, and Cotten J (1999) Assimilation of ocean crust by hawaiitic and mugearitic magmas: And example from Eiao (Marquesas). *Lithos* 46: 235–258.

Chambers K, Woodhouse JH, and Deuss A (2005) Topography of the 410-km discontinuity from PP and SS precursors. *Earth and Planetary Science Letters* 235: 610–622.

Chang HK, Kowsmann RO, Figueiredo AMF, and Bender AA (1992) Tectonics And stratigraphy of the East Brazil Rift system – An overview. *Tectonophysics* 213: 97–138.

Chazey WJ, III and Neal CR (2004) Large igneous province magma petrogenesis from source to surface: Platinum-group element evidence from Ontong Java Plateau basalts recovered during ODP legs 130 and 192. In: Fitton JG, Mahoney JJ, Wallace PJ, and Saunders AD (eds.) *Origin and Evolution of the Ontong Java Plateau*, pp. 449–484. London: Geological Society.

Christensen U (1984) Instability of a hot boundary-layer and initiation of thermo-chemical plumes. *Annales Geophysicae* 2: 311–319.

Christensen UR and Hofmann AW (1994) Segregation of subducted oceanic crust and the convecting mantle. *Journal of Geophysical Research* 99: 19867–19884.

Clague DA and Dalrymple GB (1987) The Hawaiian-Emperor volcanic chain. In: Decker RW, Wright TL, and Stauffer PH (eds.) *Volcanism in Hawaii*, pp. 5–54. Honolulu: USGC.

Clift PD, Carter A, and Hurford AJ (1998) The erosional and uplift history of NE Atlantic passive margins; constrains on a passing plume. *Journal of the Geological Society of London* 155: 787–800.

Clift PD and Turner J (1995) Dynamic support by the Icelandic Plume and vertical tectonics of the Northeast Atlantic continental margins. *Journal of Geophysical Research* 100: 24473–24486.

Clouard V and Bonneville A (2001) How many Pacific hotspots are fed by deep-mantle plumes? *Geology* 29: 695–698.

Clouard V and Bonneville A (2005) Ages of Seamounts, islands, and plateaus on the Pacific plate. In: Foulger G, Natland JH, Presnall DC, and Anderson DL (eds.) *Plumes, Plates, and Paradigms*, pp. 71–90. Boulder, CO: GSA.

Clouard V, Bonneville A, and Gillot P-Y (2003) The Tarava Seamounts; a newly characterized hotspot chain on the South Pacific Superswell. *Earth and Planetary Science Letters* 207: 117–130.

COFFIN MF (1992) Emplacement and subsidence of Indian Ocean plateaus and submarine ridges. In: Duncan RA, Rea DK, Kidd RB, Rad UV and Weissel JK (eds.) *Synthesis of Results from Scientific Drilling in the Indian Ocean, Geophysical Monograph 70*; pp. 115–125. Washington, DC: American Geophysical Union.

Coffin MF and Eldholm O (1993) Scratching the surface: Estimating dimensions of large igneous provinces. *Geology* 21: 515–518.

Coffin MF and Eldholm O (1994) Large igneous provinces: Crustal structure, dimensions, and external consequences. *Reviews of Geophysics* 32: 1–36.

Coffin MF, Pringle MS, Duncan RA, *et al.* (2002) Kerguelen hotspot magma output since 130 Ma. *Journal Of Petrology* 43: 1121–1139.

Cohen RS and O'nions RK (1982) Identification of recycled continental material in the mantle from Sr, Nd, and Pb isotope investigations. *Earth and Planetary Science Letters* 61: 73–84.

Collins JA, Vernon FL, Orcutt JA, and Stephen RA (2002) Upper mantle structure beneath the Hawaiian Swell; constraints from the ocean seismic network pilot experiment. *Geophysical Research Letters* 29: 1522 (doi:10.1029/2001GL013302).

Coltice N and Ricard Y (1999) Geochemical observations and one layer mantle convection. *Earth and Planetary Science Letters* 174: 125–137.

Condie KC (2001) *Mantle Plumes and Their Record in Earth History*. Cambridge: Cambridge University Press.

Constable S and Heinson G (2004) Hawaiian hot-spot swell structure from seafloor MT sounding. *Tectonophysics* 389: 111–124.

Cordery MJ, Davies GF, and Cambell IH (1997) Genesis of flood basalts from eclogite-bearing mantle plumes. *Journal of Geophysical Research* 102: 20179–20197.

Courtillot V, Davaille A, Besse J, and Stock J (2003) Three distinct types of hotspots in the Earth's mantle. *Earth and Planetary Science Letters* 205: 295–308.

Courtillot V, Gallet Y, Rocchia R, *et al.* (2000) Cosmic markers, Ar-40/Ar-39 dating and paleomagnetism of the KT sections in the Anjar Area of the Deccan large igneous province. *Earth and Planetary Science Letters* 182: 137–156.

Courtillot VE and Renne PR (2003) On the ages of flood basalt events. *Comptes Rendus Geoscience* 335: 113–140.

Cox KG (1988) The Karoo province. In: Macdougall JD (ed.) *Continental Flood Basalts*, 35 p. Dordrecht: Kluwer Academic Publishers.

Creager KC and Jordan TH (1986) Slab penetration into the lower mantle below the Mariana and other island arcs of the Northwest Pacific. *Journal of Geophysical Research* 91: 3573–3589.

Crough ST (1978) Thermal origin of mid-plate hot-spot swells. *Geophysical Journal of the Royal Astronomical Society* 55: 451–469.

Crough ST (1983) Hotspot swells. *Annual Reviews of Earth and Planetary Science* 11: 165–193.

Cserepes L, Christensen UR, and Ribe NM (2000) Geoid height versus topography for a plume model of the Hawaiian swell. *Earth and Planetary Science Letters* 178: 29–38.

Cserepes L and Yuen DA (2000) On the possibility of a second kind of mantle plume. *Earth and Planetary Science Letters* 183: 61–71.

Cushman B, Sinton J, Ito G, and Dixon JE (2004) Glass compositions, plume-ridge interaction, and hydrous melting along the Galapagos spreading center, 90.5 degrees W to 98 degrees W. *Geochemistry, Geophysics, and Geosystems* 5: Q08E17 (doi:10.1029/2004GC000709).

D'acremont E, Leroy S, and Burov EB (2003) Numerical modelling of a mantle plume; the plume head-lithosphere interaction in the formation of an oceanic large igneous province. *Earth and Planetary Science Letters* 206: 379–396.

Dasgupta R and Hirschmann MM (2006) Melting in the Earth's deep upper mantle caused by carbon dioxide. *Nature* 440: 659–662.

Davaille A (1999) Simultaneous generation of hotspots and superswells by convection in a heterogeneous planetary mantle. *Nature* 402: 756–760.
Davaille A, Girard F, and Lebars M (2002) How to anchor hotspots in a convecting mantle? *Earth and Planetary Science Letters* 203: 621–634.
Davaille A and Vatteville (2005) On the transient nature of mantle plumes. *Geophysical Research Letters* 32: (doi:1029/2005GL023029).
Davies GF (1988) Ocean bathymetry and mantle convection 1. Large-scale flow and hotspots. *Journal of Geophysical Research* 93: 10467–10480.
Davies GF (1995) Penetration of plates and plumes through the lower mantle transition zone. *Earth and Planetary Science Letters* 133: 507–516.
Davies GF (1998) Topography: A robust constraint on mantle fluxes. *Chemical Geology* 145: 479–489.
Davies GF (1999) *Dynamic Earth*. Cambridge, UK: Cambridge University Press.
Davis AS, Gray LB, Clague DA, and Hein JR (2002) The Line Islands revisited: New $^{40}Ar/^{39}Ar$ geochronologic evidence for episodes of volcanism due to lithospheric extension. *Geochemistry, Geophysics and Geosystems* 3(3): (doi:10.1029/2001GC000190).
De Hoop MV and van Der Hilst RD (2005) On sensitivity kernels for 'wave-equation' transmission tomography. *Geophysical Journal International* 160: 621–633.
Delaughter JE, Stein CA, and Stein S (2005) Hotspots: A view from the swells. *GSA, Special Publication* 388: 881.
Depaolo DJ and Manga M (2003) Deep origin of hotspots – The mantle plume model. *Science* 300: 920–921.
Desonie DL and Duncan RA (1990) The Cobb–Eickelberg seamount chain: hotspot volcanism with mid-ocean ridge basalt affinity. *Journal of Geophysical Research, B, Solid Earth and Planets* 95: 12697–12711.
Detrick RS and Crough ST (1978) Island subsidence, hot spots, and lithospheric thinning. *Journal of Geophysical Research* 83: 1236–1244.
Devey CW and Haase KM (2004) The sources for hotspot volcanism in the South Pacific Ocean. In: Hekinian R, Stoffers P, and Cheminée J-L (eds.) *Oceanic Hotspots*, pp. 253–280. New York: Springer.
Divenere V and Kent DV (1999) Are the Pacific and Indo-Atlantic hotspots fixed? Testing the plate circuit through Antarctica. *Earth and Planetary Science Letters* 170: 105–117.
Dodson A, Kennedy BM, and Depaolo DJ (1997) Helium and neon isotopes in the Imnaha Basalt, Columbia River Basalt Group; evidence for a Yellowstone plume source. *Earth and Planetary Science Letters* 150: 443–451.
Doucet S, Weis D, Scoates JS, Debaille V, and Giret A (2004) Geochemical and Hf–Pb–Sr–Nd isotopic constraints on the origin of the Amsterdam-St. Paul (Indian Ocean) hotspot basalts. *Earth and Planetary Science Letters* 218: 179–195.
Du Z, Vinnik LP, and Foulger GR (2006) Evidence from P-to-S mantle converted waves for a flat '660-km' discontinuity beneath Iceland. *Earth and Planetary Science Letters* 241: 271–280.
Dueker KG and Sheehan AF (1997) Mantle discontinuity structure from midpoint stacks of converted P to S waves across the Yellowstone hotspot track. *Journal of Geophysical Research, B, Solid Earth and Planets* 102: 8313–8327.
Duncan RA (1978) Geochronology of basalts from the Ninetyeast Ridge and continental dispersion in the Eastern Indian Ocean. *Journal of Volcanology and Geothermal Research* 4: 283–305.
Duncan RA (1984) Age progressive volcanism in the New England Seamounts and the opening of the Central Atlantic Ocean. *Journal of Geophysical Research* 89: 9980–9990.
Duncan RA (1991) Age distribution of volcanism along aseismic ridges in the eastern Indian Ocean. *Proceedings of the Ocean Drilling Program*, *Scientific results*. College Station, TX, USA, Ocean Drilling Program.
Duncan RA (2002) A time frame for construction of the Kerguelen Plateau and Broken Ridge. *Journal of Petrology* 43: 1109–1119.
Duncan RA, Backman J, Peterson LC, *et al.* (1990) The volcanic record of the Reunion hotspot. *Proceedings of the Ocean Drilling Program, Scientific Results* 115: 3–10.
Duncan RA and Clague DA (1985) Pacific plate motion recorded by linear volcanic chains. In: Nairn AEM, Stehli FG, and Uyeda S (eds.) *The Ocean Basins and Margins*, pp. 89–121. New York: Plenum Press.
Duncan RA and Hargraves RB (1984) Caribbean region in the mantle reference frame. In: Bonini W, *et al.* (ed.) *The Caribbean-South American Plate Boundary and Regional Tectonic*, pp. 81–93. Vancouver: Geological Society of America.
Duncan RA and Keller R (2004) Radiometric ages for basement rocks from the Emperor Seamounts, ODP Leg 197. *Geochemistry, Geophysics and Geosystems* 5: Q08L03 (doi:10.1029/2004GC000704).
Duncan RA and Richards MA (1991) Hotspots, mantle plumes, flood basalts, and true polar wander. *Reviews of Geophysics* 29: 31–50.
Dyment J (1998) Evolution of the Carlsberg Ridge between 60 and 45 Ma: Ridge propagation, spreading asymmetry, and the Deccan-reunion hotspot. *Journal of Geophysical Research* 103: 24067–24084.
Dziewonski AM and Anderson DL (1981) Preliminary reference Earth model. *Physics of the Earth and Planetary Interiors* 25: 297–356.
Dziewonski AM and Woodhouse JH (1987) Global images of the Earth's interior. *Science* 236: 37–48.
Ebinger CJ, Bechtel TD, Forsyth DW, and Bowin CO (1989) Effective elastic plate thickness beneath the East African and Afar Plateaus and dynamic compensation of the uplifts. *Journal of Geophysical Research* 94: 2883–2901.
Eiler JM, Schiano P, Kitchen N, and Stolper EM (2000) Oxygen isotope evidence for the origin of chemical variations in the sources of mid-ocean ridge basalts. *Nature* 403: 530–534.
Elkins-Tanton LT and Hager BH (2005) Giant meteoroid impacts can cause volcanism. *Earth and Planetary Science Letters* 239: 219–232.
Elkins-Tanton LT, Hager BH, and Grove TL (2004) Magmatic effects of the lunar heavy bombardment. *Earth and Planetary Science Letters* 222: 17–27.
Ellam RM and Stuart FM (2004) Coherent He-Nd-Sr isotope trends in high $^{3}He/^{4}He$ basalts: Implications for a common reservoir, mantle heterogeneity and convection. *Earth and Planetary Science Letters* 228: 511–523.
Elliot DH and Fleming TH (2004) Occurrence and dispersal of magmas in the Jurassic Ferrar Large igneous province, Antarctica. *Gondwana Research* 7: 223–237.
Emerick CM and Duncan RA (1982) Age progressive volcanism in the Comores Archipelago, western Indian Ocean and implications for Somali plate tectonics. *Earth and Planetary Science Letters* 60: 415–428.
Encarnacion J, Fleming TH, Elliot DH, and Eales HV (1996) Synchronous emplacement of Ferrar and Karoo dolerites and the early breakup of Gondwana. *Geology* 24: 535–538.
Ernst RE and Baragar WRA (1992) Evidence from magnetic fabric for the flow pattern of magma in the mackenzie giant radiating dyke swarm. *Nature* 356: 511–513.
Ernst RE and Buchan KL (eds.) (2001) *Mantle Plumes: Their Identification Through Time*. Boulder, CO: Geological Society of America.

Ernst RE and Buchan KL (2003) Recognizing mantle plumes in the geological record. *Annual Review of Earth and Planetary Sciences* 31: 469–523.

Ewart A, Marsh JS, Milner SC, *et al.* (2004) Petrology and geochemistry of Early Cretaceous bimodal continental flood volcanism of the NW Etendeka, Namibia; part 1, introduction, mafic lavas and re-evaluation of mantle source components. *Journal of Petrology* 45: 59–105.

Farnetani CG (1997) Excess temperature of mantle plumes: The role of chemical stratification of D″. *Geophysical Research Letters* 24: 1583–1586.

Farnetani CG and Richards MA (1995) Thermal entrainment and melting in mantle plumes. *Earth and Planetary Science Letters* 133: 251–267.

Farnetani CG and Samuel H (2005) Beyond the thermal plume hypothesis. *Geophysical Research Letters* 32: L07311 (doi:10.1029/2005GL022360).

Fee D and Dueker K (2004) Mantle transition zone topography and structure beneath the Yellowstone hotspot. *Geophysical Research Letters* 31: L18603 (doi:10.1029/2004GL020636).

Feigenson MD, Carr MJ, Maharaj SV, Juliano S, and Bolge LL (2004) Lead isotope composition of Central American volcanoes; influence of the Galapagos plume. *Geochemistry, Geophysics and Geosystems* 5: Q06001 (doi:10.1029/2003GC000621).

Feighner MA and Richards MA (1995) The fluid dynamics of plume-ridge and plume-plate interactions: An experimental investigation. *Earth and Planetary Science Letters* 129: 171–182.

Ferrachat S and Ricard Y (2001) Mixing properties in the Earth's mantle: Effects of viscosity stratification and of oceanic crust segregation. *Geochemistry, Geophysics and Geosystems* 2 (doi:10.1029/2000GC000092).

Fitton JG and Godard M (2004) Origin and evolution of magmas on the Ontong Java Plateau. In: Fitton JG, Mahoney JJ, Wallace PJ, and Saunders AD (eds.) *Origin and Evolution of the Ontong Java Plateau*, pp. 151–178. London: Geological Society.

Fitton JG, Mahoney JJ, Wallace PJ, and Saunders AD (eds.) (2004) *Origin and Evolution of the Ontong Java Plateau*. London: Geological Society.

Fodor RV and Hanan BB (2000) Geochemical evidence for the Trindade hotspot trace; Columbia Seamount ankaramite. *Lithos* 51: 293–304.

Fontaine FR, Hooft EEE, Burkett PG, Toomey DR, Solomon SC, and Silver PG (2005) Shear-wave splitting beneath the Galapagos archipelago. *Geophysical Research Letters* 32: 121308.

Foulger GR, Natland JH, and Anderson DL (2005) A source for Icelandic magmas in remelted Iapetus crust. *Journal of Volcanology and Geothermal Research* 141: 23–44.

Foulger GR, Pritchard MJ, Julian BR, *et al.* (2001) Seismic tomography shows that upwelling beneath Iceland is confined to the upper mantle. *Geophysical Journal International* 146: 504–530.

Frey FA, Coffin MF, Wallace PJ, *et al.* (2000) Origin and evolution of a submarine large igneous province; the Kerguelen Plateau and Broken Ridge, southern Indian Ocean. *Earth and Planetary Science Letters* 176: 73–89.

Frey FA, Weis D, Borisova AY, and XU G (2002) Involvement of continental crust in the formation of the Cretaceous Kerguelen Plateau: New perspectives from ODP Leg 120 sites. *Journal Of Petrology* 43: 1207–1239.

Fukao Y, Koyama T, Obayashi M, and Utada H (2004) Trans-Pacific temperature field in the mantle transition region derived from seismic and electromagnetic tomography. *Earth and Planetary Science Letters* 217: 425–434.

Gans KD, Wilson DS, and Macdonald KC (2003) Pacific Plate gravity lineaments: Diffuse extension or thermal contraction? *Geochemistry, Geophysics and Geosystems* 4: 1074 (doi:10.1029/2002GC000465).

Gashawbeza EM, Klemperer SL, Nyblade AA, Walker KT, and Keranen KM (2004) Shear-wave splitting in Ethiopia: Precambrian mantle anisotropy locally modified by Neogene rifting. *Geophysical Research Letters* 31: L18602 (doi:10.1029/2004GL020471).

Geldmacher J, Hoernle K, van Der Bogaard P, Duggen S, and Werner R (2005) New Ar-40/Ar-39 age and geochemical data from seamounts in the Canary and Madeira volcanic provinces: Support for the mantle plume hypothesis. *Earth and Planetary Science Letters* 237: 85–101.

Gente P, Dyment J, Maia M, and Goslin J (2003) Interaction between the Mid-Atlantic Ridge and the Azores hot spot during the last 85 Myr: Emplacement and rifting of the hot spot-derived plateaus. *Geochemistry Geophysics Geosystems* 4: 8514 (doi:10.1029/2003GC000527).

Georgen JE, Lin J, and Dick HJB (2001) Evidence from gravity anomalies for interactions of the Marion and Bouvet hotspots with the Southwest Indian Ridge: Effects of transform offsets. *Earth and Planetary Science Letters* 187: 283–300.

Gibson SA, Thompson RN, Weska R, Dickin AP, and Leonardos OH (1997) Late Cretaceous rift-related upwelling and melting of the Trindade starting mantle plume head beneath western Brazil. *Contributions to Mineralogy and Petrology* 126: 303–314.

GILL RCO, Holm PM, and Nielsen TFD (1995) Was a short-lived Baffin Bay plume active prior to initiation of the present Icelandic plume? Clues from the high-Mg picrites of West Greenland. *Lithos* 34: 27–39.

Gill RCO, Pedersen AK, and Larsen JG (1992) Tertiary picrites from West Greenland: Melting at the periphery of a plume? In: Storey BC, Alabaster T, and Pankhurst RJ (eds.) *Magmatism and the Causes of Continental Break-Up*, pp. 335–348. London: Geological Society.

Gladczenko TP, Coffin MF, and Eldholm O (1997) Crustal structure of the Ontong Java Plateau: Modeling of new gravity and existing seismic data. *Journal of Geophysical Research* 102: 22711–22729.

Goes S, Spakman W, and Bijwaard H (1999) A lower mantle source for central European volcanism. *Science* 286: 1928–1931.

Gomer BM and Okal EA (2003) Multiple ScS probing of the Ontong Java Plateau. *Physics of the Earth and Planetary Interiors* 138: 317–331.

Gonnermann HM, Jellinek AM, Richards MA, and Manga M (2004) Modulation of mantle plumes and heat flow at the core mantle boundary by plate-scale flow: Results from laboratory experiments. *Earth and Planetary Science Letters* 226: 53–67.

Graham DW, Johnson KTM, Priebe LD, and Lupton JE (1999) Hotspot-ridge interaction along the Southeast Indian Ridge near Amsterdam and St. Paul islands; helium isotope evidence. *Earth and Planetary Science Letters* 167: 297–310.

Grand SP (1994) Mantle shear structure beneath the Americas and surrounding oceans. *Journal of Geophysical Research* 99: 11591–11621.

Grand SP (2002) Mantle shear-wave tomography and the fate of subducted slabs. *Philosophical Transactions of the Royal Society of London Series A, Mathematical Physical and Engineering Sciences* 360: 2475–2491.

Grand SP, van Der Hilst RD, and Widiyantoro S (1997) Global seismic tomography: A snapshot of convection in the mantle. *GSA Today* 7: 1–7.

Green DH, Falloon TJ, Eggins SM, and Yaxley GM (2001) Primary magmas and mantle temperatures. *European Journal of Mineralogy* 13: 437–451.

Griffiths RW and Campbell IH (1990) Stirring and structure in mantle starting plumes. *Earth and Planetary Science Letters* 99: 66–78.

Gripp AE and Gordon RG (2002) Young tracks of hotspots and current plate velocities. *Geophysical Journal International* 150: 321–361.

Guillou H, Carrecedo JC, Paris R, and Torrado FJP (2004) Implications for the early shield-stage evolution of Tenerife from K/Ar ages and magnetic stratigraphy. *Earth and Planetary Science Letters* 222: 599–614.

Hager BH and Clayton RW (1989) Constraints on the structure of mantle convection using seismic observations, flow models, and the geoid. In: Peltier WR (ed.) *Mantle Convection*, pp. 98–201. New York: Gordon and Breach.

Hales TC, Abt DL, Humphreys ED, and Roering JU (2005) A lithospheric instability origin for Columbia River flood basalts and Wallowa Mountains uplift in northeast Oregon. *Nature* 438: 842–845.

Hames WE, Renne PR, and Ruppel C (2000) New evidence for geologically instantaneous emplacement of earliest Jurassic Central Atlantic magmatic province basalts on the North American margin. *Geology* 28: 859–862.

Hanan BB and Graham DW (1996) Lead and helium isotope evidence from oceanic basalts for a common deep source of mantle plumes. *Science* 272: 991–995.

Harada Y and Hamano Y (2000) Recent progress on the plate motion relative to hotspots. In: Richards MA, Gordon RG, and Vanderhilst RD (eds.) *AGU Geophysics Monograph Series: The History and Dynamics of Global Plate Motions*, pp. 327–338. Washington, DC: AGU.

Harmon N, Forsyth D, and Scheirer D (2007) Analysis of gravity and topography in the GLIMPSE study region: Isostatic compensation and uplift of the Sojourn and Hotu Matua ridge systems. *Journal of Geophysical Research* 111: B11406, doi: 10.1029/2005JB004071.

Harris RN and Mcnutt MK (2007) Heat flow on hotspot swells: Evidence for fluid flow. *Journal of Geophysical Research* 112(B3): B03407, doi: 10.1029/2006JB004299.

Hart SR, Hauri EH, Oschmann LA, and Whitehead JA (1992) Mantle plumes and entrainment: Isotopic evidence. *Science* 256: 517–520.

Hart SR, Schilling J-G, and Powell JL (1973) Basalts from Iceland and along the Reykjanes Ridge: Sr isotope geochemistry. *Nature* 246: 104–107.

Hauri E (1996) Major-element variability in the Hawaiian mantle plume. *Nature* 382: 415–419.

Hawkesworth C, Kelley S, Turner S, Le Roex A, and Storey B (1999) Mantle processes during Gondwana break-up and dispersal. *Journal of African Earth Sciences* 28: 239–261.

Haxby WF and Weissel JK (1986) Evidence for small-scale mantle convection from Seasat altimeter data. *Journal of Geophysical Research* 91: 3507–3520.

He B, Xu YG, Chung SL, Xiao L, and Wang Y (2003) Sedimentary evidence for a rapid, kilometer-scale crustal doming prior to the eruption of the Emeishan flood basalts. *Earth and Planetary Science Letters* 213: 391–405.

Heintz M, Debayle E, and Vauchez A (2005) Upper mantle structure of the South American continent and neighboring oceans from surface wave tomography. *Tectonophysics* 406: 115–139.

Hekinian R, Stoffers P, and Cheminee J-L (eds.) (2004) *Oceanic Hotspots*. New York: Springer.

Helffrich G (2000) Topography of the transition zone seismic discontinuities. *Reviews of Geophysics* 38: 141–158.

Helffrich G (2002) Thermal variations in the mantle inferred from 660 km discontinuity topography and tomographic wave speed variations. *Geophysical Journal International* 151: 935–943.

Helmberger DV, Wen L, and Ding X (1998) Seismic evidence that the source of the Iceland hotspot lies at the core–mantle boundary. *Nature* 396: 248–251.

Hendrie DB, Kusznir NJ, Morley CK, and Ebinger CJ (1994) Cenozoic extension in Northern Kenya – A quantitative model of rift basin development in the Turkana Region. *Tectonophysics* 236: 409–438.

Herzberg C (2004a) Geodynamic information in peridotite petrology. *Journal of Petrology* 45: 2507–2530.

Herzberg C (2004b) Partial melting below the Ontong Java Plateau. In: Fitton JG, Mahoney JJ, Wallace PJ, and Saunders AD (eds.) *Origin and Evolution of the Ontong Java Plateau*, pp. 179–184. London: Geological Society.

Herzberg C, Asimow P, Arndt P, et al. (in press) Temperatures in ambient mantle and plumes: Constraints from basalts, picrites and komatiites. *Geochemistry, Geophysics and Geosystems* 8: Q02006, doi: 10.1029/2006GC001390.

Herzberg C and O'hara MJ (2002) Plume-associated ultramafic magmas of Phanerozoic age. *Journal of Petrology* 43: 1857–1883.

Hieronymus CF and Bercovici D (1999) Discrete alternating hotspot islands formed by interaction of magma transport and lithospheric flexure. *Nature* 397: 604–607.

Hieronymus CF and Bercovici D (2000) Non-hotspot formation of volcanic chains; control of tectonic and flexural stresses on magma transport. *Earth and Planetary Science Letters* 181: 539–554.

Hirose K and Fei Y (2002) Subsolidus and melting phase relations of basaltic composition in the uppermost lower mantle. *Geochimica etCosmochimica Acta* 66: 2099–2108.

Hirose K, Fei Y, Ma Y, and Ho-Kwang M (1999) The fate of subducted basaltic crust in the Earth's lower mantle. *Nature* 387: 53–56.

Hirschmann MM, Asimow PD, Ghiorso MS, and Stolper EM (1999) Calculation of peridotite partial melting from thermodynamic models of minerals and melts. III. Controls on isobaric melt production and the effect of water on melt production. *Journal of Petrology* 40: 831–851.

Hirth G and Kohlstedt DL (1996) Water in the oceanic upper mantle: Implications for rheology, melt extraction, and the evolution of the lithosphere. *Earth and Planetary Science Letters* 144: 93–108.

Hoernle K, Hauff F, and van Den Bogaard P (2004) 70 my. history (139-69 Ma) for the Caribbean large igneous province. *Geology* 32: 697–700.

Hoernle K, van Den Bogaard P, Werner R, Lissina BHF, Alvarado G, and Garbe-Schönberg D (2002) Missing history (16-71 Ma) of the Galápagos hotspot: Implications for the tectonic and biological evolution of the Americas. *Geology* 30: 795–798.

Hofmann AW (1997) Mantle geochemistry: The message from oceanic volcanism. *Nature* 385: 219–229.

Hofmann AW and White WM (1982) Mantle plumes from ancient oceanic crust. *Earth and Planetary Science Letters* 57: 421–436.

Hofmann C, Courtillot V, Feraud G, *et al.* (1997) Timing of the Ethiopian flood basalt event and implications for plume birth and global change. *Nature* 389: 838–841.

Hofmann C, Feraud G, and Courtillot V (2000) Ar-40/Ar-39 dating of mineral separates and whole rocks from the Western Ghats lava pile: Further constraints on duration and age of the Deccan traps. *Earth and Planetary Science Letters* 180: 13–27.

Holbrook WS and Kelemen PB (1993) Large igneous province on the US Atlantic margin and implications for magmatism during continental breakup. *Nature* 364: 433–436.

Holm PM, Gill RCO, Pedersen AK, *et al.* (1993) The Tertiary picrites of West Greenland; contributions from 'Icelandic' and other sources. *Earth and Planetary Science Letters* 115: 227–244.

Hooft EEE, Brandsdóttir B, Mjelde R, Shimamura H, and Murai Y (2006) Asymmetric plume-ridge interaction around Iceland: The Kolbeinsey Ridge Iceland Seismic Experiment. *Geophysics Geochemistry and Geosystems* 7: Q05015 (doi:10.1029/2005GC001123).

Hooft EEE, Toomey DR, and Solomon SC (2003) Anomalously thin transition zone beneath the Galapagos hotspot. *Earth and Planetary Science Letters* 216: 55–64.

Hooper PR (1997) The Columbia River flood basalt province: Current status. In: Mahoney JJ and Coffin MF (eds.) *Large Igneous Provinces: Continental, Oceanic, and Planetary Flood Volcanism*, pp. 1–27. Washington, DC: AGU.

Hooper PR, Binger GB, and Lees KR (2002) Ages of the Steens and Columbia River flood basalts and their relationship to extension-related calc-alkalic volcanism in eastern Oregon. *Geological Society of America Bulletin* 114: 43–50.

Hopper JR, Dahl-Jensen T, Holbrook WS, *et al.* (2003) Structure of the SE Greenland margin from seismic reflection and refraction data: Implications for nascent spreading center subsidence and asymmetric crustal accretion during North Atlantic opening. *Journal of Geophysical Research* 108: 2269.

Huang J, Zhong S, and van Hunen J (2003) Controls on sublithospheric small-scale convection. *Journal of Geophysical Research* 108: (doi:10.1029/2003JB002456).

Hung SH, Shen Y, and Chiao LY (2004) Imaging seismic velocity structure beneath the Iceland hot spot: A finite frequency approach. *Journal of Geophysical Research* 109: B08305 (doi:10.1029/2003JB002889).

Ingle S and Coffin MF (2004) Impact origin for the greater Ontong Java Plateau? *Earth and Planetary Science Letters* 218: 123–134.

Irifune T, Sekine T, Ringwood AE, and Hibberson WO (1986) The eclogite–garnetite transformations at high pressure and some geophysical implications. *Earth and Planetary Science Letters* 77: 245–256.

Ito E and Takahashi E (1989) Postspinel transformations in the system Mg_2SiO_4–Fe_2SiO_4 and some geophysical implications. *Journal of Geophysical Research* 94: 10637–10646.

Ito G (2001) Reykjanes 'V'-shaped ridges originating from a pulsing and dehydrating mantle plume. *Nature* 411: 681–684.

Ito G and Clift P (1998) Subsidence and growth of Pacific Cretaceous plateaus. *Earth and Planetary Science Letters* 161: 85–100.

Ito G and Lin J (1995) Oceanic spreading center-hotspot interactions: Constraints from along-isochron bathymetric and gravity anomalies. *Geology* 23: 657–660.

Ito G, Lin J, and Gable C (1997) Interaction of mantle plumes and migrating mid-ocean ridges: Implications for the Galápagos plume-ridge system. *Journal of Geophysical Research* 102: 15403–15417.

Ito G, Lin J, and Gable CW (1996) Dynamics of mantle flow and melting at a ridge-centered hotspot: Iceland and the Mid-Atlantic Ridge. *Earth and Planetary Science Letters* 144: 53–74.

Ito G, Lin J, and Graham D (2003) Observational and theoretical studies of the dynamics of mantle plume–mid-ocean ridge interaction. *Review of Geophysics* 41: 1017 (doi:10.1029/2002RG000117).

Ito G and Mahoney J (2006) Melting a high $^3He/^4He$ source in a heterogeneous mantle. *Geochemistry, Geophysics and Geosystems* 7: Q05010 (doi:10.1029/2005GC001158).

Ito G and Mahoney JJ (2005) Flow and melting of a heterogeneous mantle: 1. Method and importance to the geochemistry of ocean island and mid-ocean ridge basalts. *Earth And Planetary Science Letters* 230: 29–46.

Ito G, Mcnutt M, and Gibson RL (1995) Crustal structure of the Tuamotu Plateau, 15°S, and implications for its origin. *Journal of Geophysical Research* 100: 8097–8114.

Ito G, Shen Y, Hirth G, and Wolfe CJ (1999) Mantle flow, melting, and dehydration of the Iceland mantle plume. *Earth and Planetary Science Letters* 165: 81–96.

Ivanov BA and Melosh HJ (2003) Impacts do not initiate volcanic eruptions: Eruptions close to the crater. *Geology* 31: 869–872.

Jackson I (*ed.*) (1998) *The Earth's Mantle, Composition, Structure, and Evolution*. Cambridge: Cambridge University Press.

Janney PE, Macdougall JD, Natland JH, and Lynch MA (2000) Geochemical evidence from the Pukapuka volcanic ridge system for a shallow enriched mantle domain beneath the South Pacific Superswell. *Earth and Planetary Science Letters* 181: 47–60.

Jellinek AM and Manga M (2002) The influence of the chemical boundary layer on the fixity, spacing and lifetime of mantle plumes. *Nature* 418: 760–763.

Jellinek AM and Manga M (2004) Links between long-lived hot spots, mantle plumes, D″, and plate tectonics. *Reviews of Geophyiscs* 42: RG3002 (doi:10.1029/2003RG000144).

Jha K, Parmentier EM, and Morgan JP (1994) The role of mantle depletion and melt-retention buoyancy in spreading-center segmentation. *Earth and Planetary Science Letters* 125: 221–234.

Jones AP, Price GD, Price NJ, Decarli PS, and Clegg RA (2002a) Impact induced melting and the development of large igneous provinces. *Earth and Planetary Science Letters* 202: 551–561.

Jones SM, White N, and Maclennan J (2002b) V-shaped ridges around Iceland: Implications for spatial and temporal patterns of mantle convection. *Geochemistry, Geophysics and Geosystems* 3: 1059 (doi:10.1029/2002GC000361).

Jordan TH (1979) Mineralogies, densities and seismic velocities of garnet lherzolites and their geophysical implications. In: Boyd FR and Meyer HOA (eds.) *Mantle Sample: Inclusions in Kimberlites and Other Volcanics*, pp. 1–14. Washington, DC: American Geophysical Union.

Jourdan F, Feraud G, Bertrand H, *et al.* (2004) The Karoo triple junction questioned: Evidence from Jurassic and Proterozoic Ar-40/Ar-39 ages and geochemistry of the giant Okavango dyke swarm (Botswana). *Earth and Planetary Science Letters* 222: 989–1006.

Jourdan F, Feraud G, Bertrand H, *et al.* (2005) Karoo large igneous province: Brevity, origin, and relation to mass extinction questioned by new Ar-40/Ar-39 age data. *Geology* 33: 745–748.

Jourdan F, Feraud G, Bertrand H, Watkeys MK, Kampunzu AB, and Le Gall B (2006) Basement control on dyke distribution in Large Igneous Provinces: Case study of the Karoo triple junction. *Earth and Planetary Science Letters* 241: 307–322.

Kaminski E and Jaupart C (2003) Laminar starting plumes in high-Prandtl-number fluids. *Journal of Fluid Mechanics* 478: 287–298.

Katzman R, Zhao L, and Jordan TH (1998) High-resolution, two-dimensional vertical tomography of the central Pacific mantle using ScS reverberations and frequency-dependent travel times. *Journal of Geophysical Research* 103: 17933–17971.

Kellogg LH and King SD (1997) The effect of temperature dependent viscosity on the structure of new plumes in the mantle; results of a finite element model in a spherical, axisymmetric shell. *Earth and Planetary Science Letters* 148: 13–26.

Kelly A and Bercovici D (1997) The clustering of rising diapirs and plume heads. *Geophysical Research Letters* 24: 201–204.

Kendall JM, Stuart GW, Ebinger CJ, Bastow ID, and Keir D (2005) Magma-assisted rifting in Ethiopia. *Nature* 433: 146–148.

Kennett BLN and Engdahl ER (1991) Traveltimes for global earthquake location and phase identification. *Geophysical Journal International* 105: 429–465.

Kennett BLN and Widiyantoro S (1999) A low seismic wavespeed anomaly beneath northwestern India; a seismic signature of the Deccan Plume? *Earth and Planetary Science Letters* 165: 145–155.

Kent AJR, Stolper EM, Francis D, Woodhead J, Frei R, and Eiler J (2004) Mantle heterogeneity during the formation of the North Atlantic Igneous Province: Constraints from trace element and Sr-Nd-Os-O isotope systematics of Baffin Island picrites. *Geochemistry, Geophysics and Geosystems* 5: Q11004 (doi:10.1029/2004GC000743).

Kent RW, Pringle MS, Müller RD, Sauders AD, and Ghose NC (2002) $^{40}Ar/^{39}Ar$ geochronology of the Rajmahal basalts, India, and their relationship to the Kerguelen Plateau. *Journal of Petrology* 43: 1141–1153.

Kent W, Saunders AD, Kempton PD, and Ghose NC (1997) Rajmahal Basalts, Eastern India: Mantle sources and melt distribution at a volcanic rifted margin. In: Mahoney JJ and Coffin MF (eds.) *Large Igneous Provinces: Continental, Oceanic and Planetary Flood Volcanism*, pp. 183–216. Washington, DC: American Geophysical Union.

Kerr RC and Meriaux C (2004) Structure and dynamics of sheared mantle plumes. *Geochemistry, Geophysics and Geosystems* 5: Q12009 (doi:10.1029/2004GC000749).

Keyser M, Ritter JRR, and Jordan M (2002) 3D shear-wave velocity structure of the Eifel Plume, Germany. *Earth and Planetary Science Letters* 203: 59–82.

Kieffer B, Arndt N, Lapierre H, *et al.* (2004) Flood and shield basalts from Ethiopia: Magmas from the African superswell. *Journal of Petrology* 45: 793–834.

King S and Anderson DL (1998) Edge-driven convection. *Earth and Planetary Science Letters* 160: 289–296.

King SD and Anderson DL (1995) An alternative mechanism of flood basalt formation. *Earth and Planetary Science Letters* 136: 269–279.

Klein EM and Langmuir CH (1987) Global correlations of ocean ridge basalt chemistry with axial depth and crustal thickness. *Journal of Geophysical Research* 92: 8089–8115.

Klosko ER, Russo RM, Okal EA, and Richardson WP (2001) Evidence for a rheologically strong chemical mantle root beneath the Ontong-Java Plateau. *Earth and Planetary Science Letters* 186: 347–361.

Kogiso T, Hirschmann MM, and Reiners PW (2004) Length scales of mantle heterogeneities and their relationship to ocean island basalt geochemistry. *Geochemica et Cosmochimica Acta* 68: 345–360.

Koppers AA, Staudigel H, Pringle MS, and Wijbrans JR (2003) Short-lived and discontinuous intraplate volcanism in the South Pacific: Hot spots or extensional volcanism. *Geochemistry, Geophysics and Geosystems* 4: 1089 (doi:10.1029/2003GC000533).

Koppers AAP, Duncan RA, and Steinberger B (2004) Implications of a nonlinear$^{40}Ar/^{39}Ar$ age progression along the Louisville seamount trail for models of fixed and moving hot spots. *Geochemistry, Geophysics and Geosystems* 5: Q06L02 (doi:10.1029/2003GC000671).

Koppers AAP, Phipps Morgan J, Morgan JW, and Staudigel H (2001) Testing the fixed hotspot hypothesis using (super 40) Ar/ (super 39) Ar age progressions along seamount trails. *Earth and Planetary Science Letters* 185: 237–252.

Koppers AAP and Staudigel H (2005) Asynchroneous bends in Pacific seamounts trails: A case for extensional volcanism? *Science* 307: 904–907.

Koppers AAP, Staudigel H, Wijbrans JR, and Pringle MS (1998) The Magellan Seamount Trail; implications for Cretaceous hotspot volcanism and absolute Pacific Plate motion. *Earth and Planetary Science Letters* 163: 53–68.

Korenaga J (2004) Mantle mixing and continental breakup magmatism. *Earth and Planetary Science Letters* 218: 463–473.

Korenaga J (2005a) Firm mantle plumes and the nature of the core–mantle boundary region. *Earth And Planetary Science Letters* 232: 29–37.

Korenaga J (2005b) Why did not the Ontong Java Plateau form subaerially? *Earth and Planetary Science Letters* 234: 385–399.

Korenaga J and Jordan TH (2003) Physics of multiscale convection in Earth's mantle: Onset of sublithospheric convection. *Journal of Geophysical Research* 108(B7): (doi:10.1029/2002JB001760).

Korenaga J and Kelemen PB (2000) Major element heterogeneity in the mantle source of the North Atlantic igneous province. *Earth and Planetary Science Letters* 184: 251–268.

Kumar AR and Mohan G (2005) Mantle discontinuities beneath the Deccan volcanic province. *Earth and Planetary Science Letters* 237: 252–263.

Labrosse S (2002) Hotspots, mantle plumes and core heat loss. *Earth and Planetary Science Letters* 199: 147–156.

Langmuir CH, Klein EM, and Plank T (1992) Petrological systematics of mid-ocean ridge basalts: Constraints on melt generation beneath ocean ridges. In: Phipps Morgan J, Blackman DK, and Sinton JM (eds.) *Mantle Flow and Melt Generation at Mid-Ocean Ridges*, pp. 1–66. Washington, DC: American Geophysical Union.

Lanyon R, Varne R, and Crawford AJ (1993) Tasmanian Tertiary basalts, the Balleny plume, and opening of the Tasman Sea (Southwest Pacific Ocean). *Geology* 21: 555–558.

Larsen TB and Yuen DA (1997) Ultrafast upwelling bursting through the upper mantle. *Earth and Planetary Science Letters* 146: 393–399.

Larsen TB, Yuen DA, and Storey M (1999) Ultrafast mantle plumes and implications for flood basalt volcanism in the Northern Atlantic region. *Tectonophysics* 311: 31–43.

Laske G and Masters G (1997) A Global digital map of sediment thickness. *EOS, Transactions American Geophysical Union, Fall Meeting Supplement* 78: F483.

Laske G, Morgan JP, and Orcutt JA (1999) First results from the Hawaiian SWELL pilot experiment. *Geophysical Research Letters* 26: 3397–3400.

Lawver LA and Mueller RD (1994) Iceland hotspot track. *Geology* 22: 311–314.

Lecheminant AN and Heaman LM (1989) Mackenzie igneous events, Canada – Middle Proterozoic hotspot magmatism associated with ocean opening. *Earth and Planetary Science Letters* 96: 38–48.

Lei JS and Zhao DP (2006) A new insight into the Hawaiian plume. *Earth And Planetary Science Letters* 241: 438–453.

Leitch AM, Steinbach V, and Yuen DA (1996) Centerline temperature of mantle plumes in various geometries: Incompressible flow. *Journal of Geophysical Research* 101: 21829–21846.

Li A and Detrick RS (2003) Azimuthal anisotropy and phase velocity beneath Iceland: Implication for plume–ridge interaction. *Earth and Planetary Science Letters* 214: 153–165.

Li A and Detrick RS (2006) Seismic structure of Iceland from Rayleigh wave inversions and geodynamic implications. *Earth and Planetary Science Letters* 241: 901–912.

Li X, Kind R, Priestley K, Sobolev SV, Tilmann F, Yuan X, and Weber M (2000) Mapping the Hawaiian plume conduit with converted seismic waves. *Nature* 405: 938–941.

Li X, Kind R, Yuan X, *et al.* (2003a) Seismic observation of narrow plumes in the oceanic upper mantle. *Geophysical Research Letters* 30: 1334 (doi:10.1029/2002GL015411).

Li X, Kind R, Yuan X, Woelbern I, and Hanka W (2004) Rejuvenation of the lithosphere by the Hawaiian Plume. *Nature* 427: 827–829.

Li XD and Romanowicz B (1996) Global mantle shear velocity model developed using nonlinear asymptotic coupling theory. *Journal of Geophysical Research* 101: 22245–22272.

Li XQ, Kind R, and Yuan XH (2003b) Seismic study of upper mantle and transition zone beneath hotspots. *Physics of the Earth and Planetary Interiors* 136: 79–92.

Lin S-C and Van Keken PE (2006a) Dynamics of thermochemical plumes: 1. Plume formation and entrainment of a dense layer. *Geochemistry, Geophysics and Geosystems* 7: Q02006 (doi:10.1029/2005GC001071).

Lin SC and Van Keken PE (2005) Multiple volcanic episodes of flood basalts caused by thermochemical mantle plumes. *Nature* 436: 250–252.

Lin SC and Van Keken PE (2006b) Dynamics of thermochemical plumes: 2. Complexity of plume structures and its implications for mapping mantle plumes. *Geochemistry, Geophysics and Geosystems* 7: Q03003 (doi:10.1029/2005GC001072).

Lithgow-Bertelloni C and Richards MA (1998) The dynamics of Cenozoic and Mesozoic plate motions. *Reviews of Geophysics* 36: 27–78.

Lithgow-Bertelloni C, Richards MA, Conrad CP, and Griffiths RW (2001) Plume generation in natural thermal convection at high Rayleigh and Prandtl numbers. *Journal of Fluid Mechanics* 434: 1–21.

Lodge A and Helffrich G (2006) Depleted swell root beneath the Cape Verde Islands. *Geology* 34: 449–452.

Mackay LM, Turner J, Jones SM, and White NJ (2005) Cenozoic vertical motions in the Moray Firth Basin associated with initiation of the Iceland Plume. *Tectonics* 24: TC5004.

Maclennan J, Mckenzie D, and Gronvold K (2001) Plume-driven upwelling under central Iceland. *Earth and Planetary Science Letters* 194: 67–82.

Macnab R, Verhoef J, Roest W, and Arkani-Hamed J (1995) New database documents the magnetic character of the Arctic and North Atlantic. *EOS Transactions of American Geophysical Union* 76(45): 449.

Mahoney JJ and Coffin MF (eds.) (1997) *Large Igneous Provinces: Continental, Oceanic and Planetary Flood Volcanism*. Washington, DC: American Geophysical Union.

Mahoney JJ, Duncan RA, Tejada MLG, Sager WW, and Bralower TJ (2005) Jurassic–Cretaceous boundary age and mid-oceanic-ridge-type mantle source for Shatsky Rise. *Geology* 33: 185–188.

Mahoney JJ, Fitton JG, Wallace PJ, *et al.* (2001) *Proceedings of the Ocean Drilling Program, Initial Reports, 192* (online).

Mahoney JJ, Jones WB, Frey FA, Salters VJ, Pyle DG, and Davies HL (1995) Geochemical characteristics of lavas from Broken Ridge, the Naturaliste Plateau and southernmost Kerguelen plateau: Cretaceous plateau volcanism in the SE Indian Ocean. *Chemical Geology* 120: 315–345.

Mahoney JJ, Storey M, Duncan RA, Spencer KJ, and Pringle M (1993) Geochemistry and age of the Ontong Java Plateau. In: Pringle M, Sager W, Sliter W, and Stein S (eds.) *Geophysical Monograph Series: The Mesozoic Pacific: Geology, Tectonics, and Volcanism*, pp. 233–261. Washington, DC: AGU.

Maia M, Ackermand D, Dehghani GA, *et al.* (2000) The Pacific–Antarctic ridge-foundation hotspot interaction; a case study of a ridge approaching a hotspot. *Marine Geology* 167: 61–84.

Malamud BD and Turcotte DL (1999) How many plumes are there?. *Earth and Planetary Science Letters* 174: 113–124.

Manga M (1997) Interactions between mantle diapirs. *Geophysical Research Letters* 24: 1871–1874.

Manga M, Weeraratne D, and Morris SJS (2001) Boundary-layer thickness and instabilities in Bénard convection of a liquid with a temperature-dependent viscosity. *Physics of Fluids* 13: 802–805.

Marzoli A, Piccirillo EM, Renne PR, *et al.* (2000) The Cameroon volcanic line revisited; petrogenesis of continental basaltic magmas from lithospheric and asthenospheric mantle sources. *Journal of Petrology* 41: 87–109.

Marzoli A, Renne PR, Piccirillo EM, Ernesto M, Bellieni G, and de Min A (1999) Extensive 200-million-year-old continental flood basalts of the Central Atlantic magmatic province. *Science* 284: 616–618.

Matyska C, Moser J, and Yuen DA (1994) The potential influence of radiative heat transfer on the formation of megaplumes in the lower mantle. *Earth and Planetary Science Letters* 125: 255–266.

Matyska C and Yuen DA (2005) The importance of radiative heat transfer on superplumes in the lower mantle with the new post-perovskite phase change. *Earth and Planetary Science Letters* 234: 71–81.

Matyska C and Yuen DA (2006a) Lower mantle dynamics with the post-perovskite phase change, radiative thermal conductivity, temperature- and depth-dependent viscosity. *Physics of the Earth and Planetary Interiors* 154: 196–207.

Matyska C and Yuen DA (2006b) Upper-mantle versus lower-mantle plumes: Are they the same? In: Foulger GR and Jurdy DM (eds.) *The Origins of Melting Anomalies: Plates, Plumes, and Planetary Processes*. Vancouver, BC: GSA.

Mayborn KR and Lesher CE (2004) Paleoproterozoic mafic dike swarms of northeast Laurentia: Products of plumes or ambient mantle? *Earth and Planetary Science Letters* 225: 305–317.

Mcdougall I and Duncan RA (1988) Age progressive volcanism in the Tasmantid Seamounts. *Earth and Planetary Science Letters* 89: 207–220.

Mcdougall I, Verwoerd W, and Chevallier L (2001) K–Ar geochronology of Marion Island, Southern Ocean. *Geological Magazine* 138: 1–17.

Mckenzie D (1984) The generation and compaction of partially molten rock. *Journal of Petrology* 25: 713–765.

Mckenzie D and Bickle MJ (1988) The volume and composition of melt generated by extension of the lithosphere. *Journal of Petrology* 29: 625–679.

Mcnamara AK, Van Keken PE, and Karato SI (2002) Development of anisotropic structure in the Earth's lower mantle by solid-state convection. *Nature* 416: 310–314.

Mcnamara AK and Zhong SJ (2005) Thermochemical structures beneath Africa and the Pacific Ocean. *Nature* 437: 1136–1139.

Mcnutt M (1988) Thermal and mechanical properties of the Cape Verde Rise. *Journal of Geophysical Research* 93: 2784–2794.

Mcnutt MK (1998) Superswells. *Reviews of Geophysics* 36: 211–244.

Mcnutt MK (2002) Heat flow variations over Hawaiian swell controlled by near-surface processes, not plume properties. In: Takahashi E (ed.) *Hawaiian Volcanoes: Deep Underwater Presepectives, Geophysics Monograph 128*. Washington, DC: American Geophysical Union.

Mcnutt MK, Caress DW, Reynolds J, Jordahl KA, and Duncan RA (1997) Failure of plume theory to explain midplate volcanism in the southern Austral Island. *Nature* 389: 479–482.

Mcnutt MK and Fischer KM (1987) The South Pacific superswell. In: Keating GH, Fryer P, Batiza R, and Boehlert GW (eds.) *Seamounts, Islands, and Atolls*, pp. 25–34. Washington, DC: AGU.

Mcnutt MK, Winterer EL, Sager WW, Natland JH, and Ito G (1990) The Darwin Rise: A Cretacous superswell? *Geophysical Research Letters* 17: 1101–1104.

Mege D and Korme T (2004) Dyke swarm emplacement in the Ethiopian large igneous province: Not only a matter of stress. *Journal of Volcanology and Geothermal Research* 132: 283–310.

Meibom A, Sleep NH, Zahnle K, and Anderson DL (2005) Models for nobel gasses in mantle geochemistry: Some observations and alternatives. *Plumes*, *Plates*, *and Paradigms*: *Geological Society of America Special Paper* 388. GSA.

Menzies M, Baker J, Chazot G, and Al'kadasi M (1997) Evolution of the Red Sea volcanic margin, Western Yemen. In: Mahoney JJ and Coffin MF (eds.) *Large Igneous Provinces: Continental, Oceanic, and Planetary Flood Volcanism*. Washington, DC: American Geophysical Union.

Minor DR and Mukasa SB (1997) Zircon U-Pb and hornblende Ar-40-Ar-39 ages for the Dufek layered mafic intrusion, Antarctica: Implications for the age of the Ferrar large igneous province. *Geochimica et Cosmochimica Acta* 61: 2497–2504.

Mitrovica JX and Forte AM (1997) Radial profile of mantle viscosity: Results from the joint inversion of convection and postglacial rebound observables. *Journal of Geophysical Research* 102: 2751–2769.

Mittelstaedt E and Tackley PJ (2006) Plume heat flow is much lower than CMB heat flow. *Earth and Planetary Science Letters* 241: 202–210.

Mittelstaedt EL and Ito G (2005) Plume–ridge interaction, lithospheric stresses, and origin of near-ridge volcanic linements. *Geochemistry, Geophysics and Geosystems* 6: Q06002 (doi:10.1029/2004GC000860).

Molnar P and Stock J (1987) Relative motions of hotspots in the Pacif, Atlantic and Indian Oceans since late Cretaceous time. *Nature* 327: 587–591.

Montague NL and Kellogg LH (2000) Numerical models for a dense layer at the base of the mantle and implications for the geodynamics of D″. *Journal of Geophysical Research* 105: 11101–11114.

Montelli R, Nolet G, Dahlen FA, Masters G, Engdahl ER, and Hung SH (2004) Finite-frequency tomography reveals a variety of plumes in the mantle. *Science* 303: 338–343.

Morgan WJ (1971) Convection plumes in the lower mantle. *Nature* 230: 42–43.

Morgan WJ (1972) Plate motions and deep mantle convection. *The Geological Society of America Memoir* 132: 7–22.

Morgan WJ (1983) Hotspot tracks and the early rifting of the Atlantic. *Tectonophysics* 94: 123–139.

Morley CK, Wescott WA, Stone DM, Harper RM, Wigger ST, and Karanja FM (1992) Tectonic evolution of the Northern Kenyan Rift. *Journal of the Geological Society* 149: 333–348.

Muller JR, Ito G, and Martel SJ (2001) Effects of volcano loading on dike propagation in an elastic half-space. *Journal of Geophysical Research* 106: 11101–11113.

Müller RD, Roest WR, Royer J-Y, Gahagan LM, and Sclater JG (1993a) A digital age map of the ocean floor. 93-30 ed., Scripps Institution of Oceanography Reference Series.

Müller RD, Royer J-Y, and Lawver LA (1993b) Revised plate motions relative to the hotspots from combined Atlantic and Indian Ocean hotspot tracks. *Geology* 21: 275–278.

Nadin PA, Kusznir NJ, and Cheadle MJ (1997) Early Tertiary plume uplift of the North Sea and Faeroe-Shetland basins. *Earth and Planetary Science Letters* 148: 109–127.

Nakakuki T, Yuen DA, and Honda S (1997) The interaction of plumes with the transition zone under continents and oceans. *Earth and Planetary Science Letters* 146: 379–391.

Nakanishi M, Sager WW, and Klaus A (1999) Magnetic lineations within Shatsky Rise, northwest Pacific Ocean: Implications for hot spot-triple junction interaction and oceanic plateau formation. *Journal of Geophysical Research* 104: 7539–7556.

Nataf HC (2000) Seismic imaging of mantle plumes. *Annual Review of Earth and Planetary Sciences* 28: 391–417.

Nataf HC and Vandecar J (1993) Seismological detection of a mantle plume? *Nature* 364: 115–120.

Natland JH and Winterer EL (2005) Fissure control on volcanic action in the Pacific. In: Foulger GR, Natland JH, Presnall DC, and Anderson DL (eds.) *Plumes, Plates, and Paradigms*, pp. 687–710. Vancouver: Geological Society of America.

Neal CR, Mahoney JJ, and Chazey WJ (2002) Mantle sources and the highly variable role of continental lithosphere in basalt petrogenesis of the Kerguelen Plateau and Broken Ridge LIP: Results from ODP Leg 183. *Journal of Petrology* 43: 1177–1205.

Neal CR, Mahoney JJ, Kroenke LW, Duncan RA, and Petterson MG (1997) The Ontong Java Plateau. In: Mahoney JJ and Coffin MF (eds.) *Large Igneous Provinces: Continental, Oceanic, and Planetary Flood Volcanism*, pp. 183–216. Washington, DC: American Geophysical Union.

Ni SD, Helmberger DV, and Tromp J (2005) Three-dimensional structure of the African superplume from waveform modelling. *Geophysical Journal International* 161: 283–294.

Ni SD, Tan E, Gurnis M, and Helmberger D (2002) Sharp sides to the African superplume. *Science* 296: 1850–1852.

Nicolaysen K, Frey FA, Hodges KV, Weis D, and Giret A (2000) $^{40}Ar/^{39}Ar$ geochronology of flood basalts from the Kerguelen Archipelago, southern Indian Ocean; implications for Cenozoic eruption rates of the Kerguelen plume. *Earth and Planetary Science Letters* 174: 313–328.

Nielsen TK, Larsen HC, and Hopper JR (2002) Contrasting rifted margin styles south of Greenland; implications for mantle plume dynamics. *Earth and Planetary Science Letters* 200: 271–286.

Niu F, Solomon SC, Silver PG, Suetsugu D, and Inoue H (2002) Mantle transition-zone structure beneath the South Pacific Superswell and evidence for a mantle plume underlying the Society Hotspot. *Earth and Planetary Science Letters* 198: 371–380.

Niu Y, Waggoner G, Sinton JM, and Mahoney JJ (1996) Mantle source heterogeneity and melting processes beneath seafloor spreading centers: The East Pacific Rise 18°–19° S. *Journal of Geophysical Research* 101: 27711–27733.

Norton IO (2000) Global hotspot reference frames and plate motion. In: Richards MA, Gordon RG, and Vanderhilst RD (eds.) *The History and Dynamics of Global Plate Motions*. Washington, DC: AGU.

Nyblade AA, Owens TJ, Gurrola H, Ritsema J, and Langston CA (2000) Seismic evidence for a deep upper mantle thermal anomaly beneath East Africa. *Geology* 28: 599–602.

Nyblade AA and Robinson SW (1994) The African superswell. *Geophysical Research Letters* 21: 765–768.

O'connor JM and Duncan RA (1990) Evolution of the Walvis Ridge-Rio Grande Rise hot spot system: Implications for African and South American plate motions over plumes. *Journal of Geophysical Research* 95: 17475–17502.

O'connor JM and Roex APL (1992) South Atlantic hot spot-plume systems: 1. Distribution of volcanism in time and space. *Earth and Planetary Science Letters* 113: 343–364.

O'connor JM, Stoffers P, van Den Bogaard P, and Mcwilliams M (1999) First seamount age evidence for significantly slower African Plate motion since 19 to 30 Ma. *Earth and Planetary Science Letters* 171: 575–589.

O'connor JM, Stoffers P, and Wijbrans JR (2002) Pulsing of a focused mantle plume; evidence from the distribution of foundation chain hotspot volcanism. *Geophysical Research Letters* 29(9): 4.

O'connor JM, Stoffers P, and Wijbrans JR (2004) The foundation chain; inferring hotspot–plate interaction from a weak seamount trail. In: Hekinian R, Stoffers P, and Cheminee J-L (eds.) *Oceanic Hotspots*, pp. 349–372. Berlin: Springer.

O'neill C, Mueller D, and Steinberger B (2003) Geodynamic implications of moving Indian Ocean hotspots. *Earth and Planetary Science Letters* 215: 151–168.

O'neill C, Müller D, and Steinberger B (2005) On the uncertainties in hot spot reconstructions and the significance of moving hot spot reference frames. *Geochemistry, Geophysics and Geosystems* 6: Q04003 (doi:10.1029/2004GC000784).

Olson P (1990) Hot spots, swells and mantle plumes. In: Ryan MP (ed.) *Magma Transport and Storage*, pp. 33–51. New York: John Wiley and Sons.

Olson P, Schubert G, and Anderson C (1987) Plume formation in the D″-layer and the roughness of the core–mantle boundary. *Nature* 327: 409–413.

Olson P, Schubert G, Anderson C, and Goldman P (1988) Plume formation and lithosphere erosion: A comparison of laboratory and numerical experiments. *Journal of Geophysical Research* 93: 15065–15084.

Ono S, Ito E, and Katsura T (2001) Mineralogy of subduction basaltic crust (MORB) for 27 to 37 GPa and the chemical heterogeneity of the lower mantle. *Earth and Planetary Science Letters* 190: 57–63.

Operto S and Charvis P (1996) Deep structure of the southern Kerguelen Plateau (southern Indian Ocean) from ocean bottom seismometer wide-angle seismic data. *Journal of Geophysical Research* 101: 25077–25103.

Owens TJ, Nyblade AA, Gurrola H, and Langston CA (2000) Mantle transition zone structure beneath Tanzania, East Africa. *Geophysical Research Letters* 27: 827–830.

Oxburgh ER and Parmentier EM (1977) Compositional and density stratification in oceanic lithosphere – Causes and consequences. *Geological Society of London* 133: 343–355.

Ozawa A, Tagami T, and Garcia MO (2005) Unspiked K–Ar dating of the Honolulu rejuvenated and Koolau shield volcanism on O'ahu, Hawaii. *Earth and Planetary Science Letters* 232: 1–11.

Pankhurst RJ, Leat PT, Sruoga P, *et al.* (1998) The Chon Aike province of Patagonia and related rocks in West Antarctica: A silicic large igneous province. *Journal of Volcanology and Geothermal Research* 81: 113–136.

Pankhurst RJ, Riley TR, Fanning CM, and Kelley SP (2000) Episodic silicic volcanism in Patagonia and the Antarctic Peninsula: Chronology of magmatism associated with the break-up of Gondwana. *Journal of Petrology* 41: 605–625.

Pares JM and Moore TC (2005) New evidence for the Hawaiian hotspot plume motion since the Eocene. *Earth and Planetary Science Letters* 237: 951–959.

Parkinson IJ, Shaefer BF, and Arculus RJ (2002) A lower mantle origin for the world's biggest LIP? A high precision Os isotope isochron from Ontong Java Plateau basalts drilled on ODP Leg 192. *Geochimica et Cosmochimica Acta* 66: A580.

Parman SW, Kurz MD, Hart SR, and Grove TL (2005) Helium solubility in olivine and implications for high $^{3}He/^{4}He$ in ocean island basalts. *Nature* 437: 1140–1143 (doi:10.1038/nature04215).

Passier ML and Snieder RK (1996) Correlation between shear wave upper mantle structure and tectonic surface expressions: Application to central and southern Germany. *Journal of Geophysical Research* 101: 25293–25304.

Peate DW (1997) The Paraná–Etendeka provinces. In: Mahoney JJ and Coffin MF (eds.) *Large Igneous Provinces: Continental, Oceanic, and Planetary Flood Volcanism*, pp. 145–182. Washington, DC: American Geophysical Union.

Pertermann M and Hirschmann MM (2003) Partial melting experiments on a MORB-like pyroxenite between 2 and 3 GPa: Constraints on the presence of pyroxenite in basalt source regions from solidus locations and melting rate. *Journal of Geophysical Research* 108(B2): (doi:10.1029/2000JB000118).

Petterson MG (2004) The geology of north and central Malaita, Solomon Islands: The thickest and most accessible part of the world's largest (Ontong Java) oceanic plateau. In: Fitton JG, Mahoney JJ, Wallace PJ, and Saunders AD (eds.) *Origin and Evolution of the Ontong Java Plateau*, pp. 63–81. London: Geological Society.

Phipps Morgan J (1999) Isotope topology of individual hotspot basalt arrays: Mixing curves or melt extraction trajectories. *Geochemistry, Geophysics and Geosystems* 1: (doi:10.1029/1999GC000004).

Phipps Morgan J (2001) Thermodynamics of pressure release melting of a veined plum pudding mantle. *Geochemistry, Geophysics and Geosystems* 2: (doi:10.1029/2000GC000049).

Pik R, Deniel C, Coulon C, Yirgu G, Hofmann C, and Ayalew D (1998) The northwestern Ethiopian Plateau flood basalts. Classification and spatial distribution of magma types. *Journal of Volcanology and Geothermal Research* 81: 91–111.

Pilidou S, Priestley K, Debayle E, and Gudmundsson O (2005) Rayleigh wave tomography in the North Atlantic: High resolution images of the Iceland, Azores and Eifel mantle plumes. *Lithos* 79: 453–474.

Pilidou S, Priestley K, Gudnmundsson O, and Debayle E (2004) Upper mantle S-wave speed heterogeneity and anisotropy beneath the North Atlantic from regional surface wave tomography: The Iceland and Azores plumes. *Geophysical Journal International* 159: 1057–1076.

Pollack HN, Hurter SJ, and Johnson JR (1993) Heat-flow from the earths interior - analysis of the global data set. *Reviews of Geophysics* 31: 267–280.

Presnall DC, Gudfinnsson GH, and Walter MJ (2002) Generation of mid-ocean ridge basalts at pressures from 1 to 7 GPa. *Geochimica et Cosmochimica Acta* 66: 2073–2090.

Putirka KD (2005) Mantle potential temperatures at Hawaii, Iceland, and the mid-ocean ridge system, as inferred from olivine phenocrysts: Evidence for thermally driven mantle plumes. *Geochemistry, Geophysics and Geosystems* 6: Q05L08 (doi:10.1029/2005GC000915).

Raddick MJ, Parmentier EM, and Scheirer DS (2002) Buoyant decompression melting: A possible mechanisms for intra plate volcanism. *Journal of Geophysical Research* 107: 2228 (doi: 1029/2001JB000617).

Raymond C, Stock JM, and Cande SC (2000) Fast Paleogene motion of the Pacific hotspots from revised global plate circuit constraints. *The History and Dynamics of Global Plate Motions, AGU Geophysical Monographs* 121: 359–375.

Reichow MK, Saunders AD, White RV, Al'mukhamedov AL, and Medvedev AY (2005) Geochemistry and petrogenesis of basalts from the West Siberian basin: An extension of the Permo-Triassic Siberian Traps, Russia. *Lithos* 79: 425–452.

Reiners PW (2002) Temporal-compositional trends in intraplate basalt eruptions: Implications for mantle heterogeneity and melting processes. *Geochemistry, Geophysics and Geosystems* 3: 1011 (doi:10.1029/2002GC000250).

Renne PR, Deckart K, Ernesto M, Feraud G, and Piccirillo EM (1996) Age of the Ponta Grossa dike swarm (Brazil), and implications to Parana flood volcanism. *Earth and Planetary Science Letters* 144: 199–211.

Ribe N (1996) The dynamics of plume–ridge interaction 2. Off-ridge plumes. *Journal of Geophysical Research* 101: 16195–16204.

Ribe N, Christensen UR, and Theissing J (1995) The dynamics of plume–ridge interaction, 1: Ridge-centered plumes. *Earth and Planetary Science Letters* 134: 155–168.

Ribe NM and Christensen UR (1994) Three-dimensional modelling of plume–lithosphere interaction. *Journal of Geophysical Research* 99: 669–682.

Ribe NM and Christensen UR (1999) The dynamical origin of Hawaiian volcanism. *Earth and Planetary Science Letters* 171: 517–531.

Ribe NM, Davaille A, and Christensen UR (2007) Fluid dynamics of mantle plumes. In: Ritter J and Christensen U (eds.) *Mantle Plumes – A Multidisciplinary Approach.* Springer.

Ribe NM and de Valpine DP (1994) The global hotspot distribution and instability of D″. *Geophysical Research Letters* 21: 1507–1510.

Richards MA, Duncan RA, and Courtillot VE (1989) Flood basalts and hotspot tracks: Plume heads and tails. *Science* 246: 103–107.

Richards MA and Hager BH (1984) Geoid anomalies in a dynamic Earth. *Journal of Geophysical Research* 89: 5987–6002.

Richards MA and Lithgow-Bertelloni C (1996) Plate motion changes, the Hawaiian-Emperor bend, and the apprent success and failure of geodynamic models. *Earth and Planetary Science Letters* 137: 19–27.

Richardson WP, Okal EA, and van der Lee S (2000) Rayleigh-wave tomography of the Ontong-Java Plateau. *Physics of the Earth and Planetary Interiors* 118: 29–61.

Richter FM (1973) Convection and the large-scale circulation of the mantle. *Journal of Geophysical Research* 78: 8735–8745.

Richter FM and Mckenzie DP (1981) On some consequences and possible causes of layered mantle convection. *Journal of Geophysical Research* 86: 6133–6142.

Ringwood AE and Irifune T (1988) Nature of the 650-km seismic discontinuity: Implications for mantle dynamics and differentiation. *Nature* 331: 131–136.

Ritsema J and Allen RM (2003) The elusive mantle plume. *Earth and Planetary Science Letters* 207: 1–12.

Ritsema J, Nyblade AA, Owens TJ, Langston CA, and Vandecar JC (1998) Upper mantle seismic velocity structure beneath Tanzania, east Africa: Implications for the stability of cratonic lithosphere. *Journal of Geophysical Research* 103: 21201–21213.

Ritsema J, van Heijst HJ, and Woodhouse JH (1999) Complex shear velocity structure beneath Africa and Island. *Science* 286: 1925–1928.

Ritter JRR, Jordan M, Christensen UR, and Achauer U (2001) A mantle plume below the Eifel volcanic fields, Germany. *Earth and Planetary Science Letters* 186: 7–14.

Roberge J, Wallace PJ, White RV, and Coffin MF (2005) Anomalous uplift and subsidence of the Ontong Java Plateau inferred from CO_2 contents of submarine basaltic glasses. *Geology* 33: 501–504.

Roberge J, White RV, and Wallace PJ (2004) Volatiles in submarine basaltic glasses from the Ontong Java Plateau (ODP Leg 192): Implications for magmatic processes and source region compositions. In: Fitton JG, Mahoney JJ, Wallace PJ, and Saunders AD (eds.) *Origin and Evolution of the Ontong Java Plateau*, pp. 339–342. London: Geological Society.

Rogers GC (1982) Oceanic plateaus as meteorite impact signatures. *Nature* 299: 341–342.

Rost S and Williams Q (2003) Seismic detection of sublithospheric plume head residue beneath the Pitcairn hot-spot chain. *Earth and Planetary Science Letters* 209: 71–83.

Roy AB (2003) Geological and geophysical manifestations of the Reunion Plume–Indian lithosphere interactions; evidence from northwest India. *Gondwana Research* 6: 487–500.

Russo RM and Okal EA (1998) Shear wave splitting and upper mantle deformation in French Polynesia; evidence from small-scale heterogeneity related to the Society Hotspot. *Journal of Geophysical Research, B, Solid Earth and Planets* 103: 15089–15107.

Saal AE, Hart SR, Shimizu N, Hauri EH, and Layne GD (1998) Pb isotopic variability in melt inclusions from oceanic island basalt, Polynesia. *Science* 282: 1481–1484.

Saffman PG and Taylor GI (1958) The penetration of a fluid into a porous medium of Hele-Shaw cell containing a more viscous liquid. *Proceedings of the Royal Society of London A* 245: 312–329.

Sager WW (2005) What built Shatsky Rise, a mantle plume or ridge tectonics? In: Foulger G, Natland JH, Presnall DC, and Anderson DL (eds.) *Plumes, Plates, and Paradigms*, pp. 721–733. Boulder, CO: Geological Society of America.

Sager WW, Lamarch AJ, and Kopp C (2005) Paleomagnetic modeling of seamounts near the Hawaiian-Emperor bend. *Tectonophysics* 405: 121–140.

Sallares V, Charvis P, Flueh ER, and Bialas J (2005) Seismic structure of the Carnegie ridge and the nature of the Galapagos hotspot. *Geophysical Journal International* 161: 763–788.

Salters VJM and Dick HJB (2002) Mineralogy of the mid-ocean-ridge basalt source from neodymium and isotopic composition of abyssal peridotites. *Nature* 418: 68–72.

Saltzer RL and Humphreys ED (1997) Upper mantle P wave velocity structure of the eastern Snake River Plain and its relationship to geodynamic models of the region. *Journal of Geophysical Research* 102: 11829–11841.

Samuel H and Bercovici D (2006) Oscillating and stagnating plumes in the Earth's lower mantle. *Earth and Planetary Science Letters* 248: 90–105.

Sandwell D and Fialko Y (2004) Warping and cracking of the Pacific plate by thermal contraction. *Journal of Geophysical Research* 109: B10411 (doi:10.1029/2004JB0003091).

Sandwell DT, Winterer EL, Mammerickx J, *et al.* (1995) Evidence for diffuse extension of the Pacific plate from Pukapuka ridges and cross-grain gravity lineations. *Journal of Geophysical Research* 100: 15087–15099.

Saunders AD, England RW, Relchow MK, and White RV (2005) A mantle plume origin for the Siberian traps: Uplift and extension in the West Siberian Basin, Russia. *Lithos* 79: 407–424.

Saunders AD, Fitton JG, Kerr AC, Norry MJ, and Kent RW (1997) The North Atlantic igneous province. In: Mahoney JJ and Coffin MF (eds.) *Large Igneous Provinces: Continental, Oceanic, and Planetary Flood Volcanism*, pp. 45–93. Washington, DC: American Geophysical Union.

Schilling J-G (1973) Iceland mantle plume: Geochemical study of Reykjanes Ridge. *Nature* 242: 565–571.

Schimmel M, Assumpcao M, and Vandecar JC (2003) Seismic velocity anomalies beneath SE Brazil from P and S wave travel time inversions. *Journal of Geophysical Research* 108: 2191 (doi:10.1029/2001JB000187).

Schlanger SO and Al E (1984) Geology and geochronology of the Line Islands. *Journal of Geophysical Research* 89: 11261–11272.

Schubert G, Turcotte DL, and Olson P (2001) *Mantle Convection in the Earth and Planets*. Cambridge: Cambridge University Press.

Schutt DL and Humphreys ED (2004) P and S wave velocity and V-P/V-S in the wake of the Yellowstone hot spot. *Journal of Geophysical Research, Solid Earth* 109: B01305.

Scott DR and Stevenson DJ (1989) A self-consistent model for melting, magma migration and buoyancy-driven circulation beneath mid-ocean ridges. *Journal of Geophysical Research* 94: 2973–2988.

Sebai A, Stutzmann E, Montaner J-P, Sicilia D, and Beucler E (2006) Anisotropic structure of the African upper mantle from Rayleigh and Love wave tomography. *Physics of the Earth and Planetary Interiors* 155: 48–62.

Sharma M (1997) Siberian Traps. In: Mahoney JJ and Coffin MF (eds.) *Large Igneous Provinces: Continental, Oceanic, and Planetary Flood volcanism*. Washington, DC: American Geophysical Union.

Sharpe WD and Clague DA (2006) 50-Ma initiation of Hawaiian-Emperor bend records major change in Pacific plate motion. *Science* 313: 1281–1284.

Shen Y and Forsyth DW (1995) Geochemical constraints on initial and final depths of melting beneath mid-ocean ridges. *Journal of Geophysical Research* 100: 2211–2237.

Shen Y, Solomon SC, Bjarnason IT, and Wolfe C (1998) Seismic evidence for a lower mantle origin of the Iceland plume. *Nature* 395: 62–65.

Sheth HC (2005) From Deccan to Réunion: No trace of a mantle plume. In: Foulger G, Natland JH, Presnall DC, and Anderson DL (eds.) *Plumes, Plates, and Paradigms*, pp. 477–501. Vancouver: Geological Society of America.

Shirey SB and Walker RJ (1998) The Re-Os isotope system in cosmochemistry and high-temperature geochemistry. *Annual Reviews of the Earth and Planetary Sciences* 26: 423–500.

Sinton CW, Christie DM, and Duncan RA (1996) Geochronology of the Galápagos seamounts. *Journal of Geophysical Research* 101: 13689–13700.

Sinton CW, Duncan RA, and Denyer P (1997) Nicoya Peninsula, Costa Rica: A single suite of Caribbean oceanic plateau magmas. *Journal of Geophysical Research* 102: 15507–15520.

Sleep NH (1987) Lithospheric heating by mantle plumes. *Geophysical Journal of the Royal Astronomical Society* 91: 1–11.

Sleep NH (1988) Gradual entrainment of a chemical layer at the base of the mantle by overlying convection. *Geophysical Journal International* 95: 437–447.

Sleep NH (1990) Hotspots and mantle plumes: Some phenomenology. *Journal of Geophysical Research* 95: 6715–6736.

Smallwood JR and White RS (2002) Ridge-plume interaction in the North Atlantic and its influence on continental breakup and seafloor spreading. *Geological Society Special Publications* 197: 15–37.

Smith RB and Braile LW (1994) The yellowstone hotspot. *Journal of Volcanology and Geothermal Research* 61: 121–187.

Smith WHF and Sandwell DT (1997) Global seafloor topography from satellite altimetry and ship depth soundings. *Science* 277: 1957–1962.

Sparks DW, Parmentier EM, and Morgan JP (1993) Three-dimensional mantle convection beneath a segmented spreading center: Implications for along-axis variations in crustal thickness and gravity. *Journal of Geophysical Research* 98: 21977–21995.

Sparrow EM, Husar RB, and Goldstein RJ (1970) Observations and other characteristics of thermals. *Journal of Fluid Mechanics* 41: 793–800.

Stein CA and Stein S (1992) A model for the global variation in oceanic depth and heat flow with lithospheric age. *Nature* 359: 123–129.

Stein CA and Stein S (1993) Constraints on Pacific midplate swells from global depth-age and heat flow-age models. In: Pringle M, Sager W, Sliter W, and Stein S (eds.) *Geophysical Monograph 76: The Mesozoic Pacific*, pp. 53–76. Washington, DC: American Geophysical Union.

Stein CA and Stein S (2003) Mantle plumes: Heat-flow near Iceland. *Astronomy and Geophysics* 44: 8–10.

Steinberger B (2000) Plumes in a convecting mantle: Models and observations for individual hotspots. *Journal of Geophysical Research* 105: 11127–11152.

Steinberger B (2002) Motion of the Easter Hot Spot relative to Hawaii and Louisville hot spots. *Geochemistry, Geophysics and Geosystems* 3: 8503 (doi:10.1029/2002GC000334).

Steinberger B and O'connell RJ (1998) Advection of plumes in mantle flow; implications for hot spot motion, mantle viscosity and plume distribution. *Geophysical Journal International* 132: 412–434.

Steinberger B and O'connell RJ (2000) Effects of mantle flow on hotspot motion. *Geophysical Monograph* 121: 377–398.

Steinberger B, Sutherland R, and O'connell RJ (2004) Prediction of Emperor-Hawaii seamount locations from a revised model of global plate motion and mantle flow. *Nature* 430: 167–173.

Stewart K, Turner S, Kelley S, Hawkesworth C, Kirstein L, and Mantovani M (1996) 3-D, (super 40) Ar- (super 39) Ar geochronology in the Parana continental flood basalt province. *Earth and Planetary Science Letters* 143: 95–109.

Storey M, Mahoney JJ, and Saunders AD (1997) Cretaceous basalts in Madagascar and the transition between plume and continental lithosphere mantle sources. In: Mahoney JJ and Coffin MF (eds.) *Large Igneous Provinces: Continental, Oceanic, and Planetary Flood Volcanism*, pp. 95–122. Washington, DC: American Geophysical Union.

Stracke A, Zindler A, Salters VJM, *et al.* (2003) Theistareykir revisited. *Geochemistry, Geophysics and Geosystems* 4: 8507 (doi:10.1029/2001GC000201).

Stuart FM, Lass-Evans S, Fitton JG, and Ellam RM (2003) High $^{3}He/^{4}He$ ratios in pictritic basalts from Baffin Island and the role of a mixed reservoir in mantle plumes. *Nature* 424: 57–59.

Su W-J, Woodward RL, and Dziewonski AM (1994) Degree 12 model of shear velocity heterogeneity in the mantle. *Journal of Geophysical Research* 99: 6945–6980.

Tackley PJ (2002) Strong heterogeneity caused by deep mantle layering. *Geochemistry, Geophysics and Geosystems* 3 (doi:10.1029/2001GC000167).

Tackley PJ and Stevenson DJ (1993) A mechanism for spontaneous self-perpetuating volcanism on terrestrial planets. In: Stone DB and Runcorn SK (eds.) *Flow and Creep in the Solar System: Observations, Modeling and Theory*, pp. 307–322. Norwell, MA: Kluwer.

Takahashi E (2002) The Hawaiian plume and magma genesis. *Geophysical Monograph* 128: 347–348.

Takahashi E, Nakajima K, and Wright TL (1998) Origin of the Columbia Rivers basalts: Melting model of a heterogeneous plume head. *Earth and Planetary Science Letters* 162: 63–80.

Tan E and Gurnis M (2005) Metastable superplumes and mantle compressibility. *Geophysical Research Letters* 32: L20307 (doi:10.1029/2005GL024190).

Tarduno JA, Duncan RA, Scholl DW, *et al.* (2003) The Emperor Seamounts; southward motion of the Hawaiian Hotspot plume in Earth's mantle. *Science* 301: 1064–1069.

Tarduno JA and Gee J (1995) Large-scale motion between Pacific and Atlantic hotspots. *Nature* 378: 477–480.

Tarduno JA, Sliter WV, Kroenke LW, *et al.* (1991) Rapid formation of Ontong Java Plateau by Aptian mantle plume volcanism. *Science* 254: 399–403.

Taylor B (2006) The single largest oceanic plateau: Ontong Java-Manihiki-Hikurangi. *Earth and Planetary Science Letters* 241: 372–380.

Tejada MLG, Mahoney JJ, Castillo PR, Ingle SP, Sheth HC, and Weis D (2004) Pin-pricking the elephant: Evidence on the origin of the Ontong Java Plateau from Pb-Sr-Hf-Nd isotopic characteristics of ODP Leg 192. In: Fitton JG, Mahoney JJ, Wallace PJ, and Saunders AD (eds.) *Origin and Evolution of the Ontong Java Plateau*, pp. 133–150. London: Geological Society.

Tejada MLG, Mahoney JJ, Duncan RA, and Hawkins MP (1996) Age and geochemistry of basement and alkalic rocks of Malaita and Santa Isabel, Solomon Islands, southern margin of Ontong Java Plateau. *Journal of Petrology* 37: 361–394.

Tejada MLG, Mahoney JJ, Neal CR, Duncan RA, and Petterson MG (2002) Basement geochemistry and geochronology of central Malaita and Santa Isabel, Solomon Islands, with implications for the origin and evolution of the Ontong Java Plateau. *Journal of Petrology* 37: 449–484.

Thompson RN and Gibson SA (1991) Subcontinental mantle plumes, hotspots and preexisting thinspots. *Journal of the Geological Society* 148: 973–977.

To A, Romanowicz B, Capdeville Y, and Takeuchi N (2005) 3D effects of sharp boundaries at the borders of the African and Pacific Superplumes: Observation and modeling. *Earth and Planetary Science Letters* 233: 137–153.

Toomey DR, Hooft EEE, Solomon SC, James DE, and Hall ML (2001) Upper mantle structure beneath the Galapagos Archipelago from body wave data. *EOS Transactions of the American Geophysical Union, Fall Meeting Supplement* 82: F1205.

Torsvik TH, van der Voo R, and Redfield TF (2002) Relative hotspot motions versus true polar wander. *Earth and Planetary Science Letters* 202: 185–200.

Trampert J, Deschamps F, Resovsky J, and Yuen D (2004) Probabilistic tomography maps chemical heterogeneities throughout the lower mantle. *Science* 306: 853–856.

Trumbull RB, Vietor T, Hahne K, Wackerle R, and Ledru P (2004) Aeromagnetic mapping and reconnaissance geochemistry of the Early Cretaceous Henties Bay-Outjo dike swarm, Etendeka Igneous Province, Namibia. *Journal of African Earth Sciences* 40: 17–29.

Turner DL, Jarrard RD, and Forbes RB (1980) Geochronology and origin of the Pratt-Welker seamount chain, Gulf of Alaska: A new pole of rotation for the Pacific plate. *Journal of Geophysical Research* 85: 6547–6556.

Turner S and Al E (1994) Magmatism and continental bread-up in the South Atlantic: High precision ^{40}Ar–^{39}Ar geochronology. *Earth and Planetary Science Letters* 121: 333–348.

Van Den Berg AP, Rainey ESG, and Yuen DA (2005) The combined influences of variable thermal conductivity, temperature- and pressure-dependent viscosity and core–mantle coupling on thermal evolution. *Physics of the Earth and Planetary Interiors* 149: 259–278.

Van Der Hilst RD and De Hoop MV (2005) Banana-doughnut kernels and mantle tomography. *Geophysical Journal International* 163: 956–961.

Van Der Hilst RD and Karason H (1999) Compositional heterogeneity in the bottom 1000 kilometers of Earth's mantle: Toward a hybrid convection model. *Science* 283: 1885–1888.

van Hunen J and Zhong S (2003) New insight in the Hawaiian plume swell dynamics from scaling laws. *Geophysical Research Letters* 30: 1785 (doi:10.1029/2003GL017646).

van Keken PE (1997) Evolution of starting mantle plumes: A comparison between numerical and laboratory models. *Earth and Planetary Science Letters* 148: 1–11.

van Keken PE and Ballentine CJ (1998) Whole-mantle versus layered mantle convection and the role of a high-viscosity lower mantle in terrestrial volatile evolution. *Earth And Planetary Science Letters* 156: 19–32.

van Keken PE and Ballentine CJ (1999) Dynamical models of mantle volatile evolution and the role of phase transitions and temperature-dependent rheology. *Journal of Geophysical Research* 104: 7137–7151.

van Keken PE and Gable CW (1995) The interaction of a plume with a rheological boundary: A comparision between two- and three-dimensional models. *Journal of Geophysical Research* 100: 20291–20302.

van Keken PE, Yuen DA, and Vandenberg AP (1992) Pulsating diapiric flows: Consequences of vertical variations in mantle creep laws. *Earth and Planetary Science Letters* 112: 179–194.

van Keken PE, Yuen DA, and Vandenberg AP (1993) The effects of shallow rheological boundaries in the upper mantle on inducing shorter time scales of diapiric flows. *Geophysical Research Letters* 20: 1927–1930.

Van Wijk JW, Huismans RS, ter Voorde M, and Cloetingh S (2001) Melt generation at volcanic continental margins: No need for a mantle plume? *Geophysical Research Letters* 28: 3995–3998.

Vandamme D, Courtillot V, Besse J, and Montinny R (1991) Paleomagnetism and age determinations of the Deccan Traps (India): Results of a Nagpur–Bombay traverse and review of earlier work. *Reviews of Geophysics* 29: 159–190.

Vandecar JC, James DE, and Assumpcao M (1995) Seismic evidence for a fossil mantle plume beneath South America and implications for plate driving forces. *Nature* 378: 25–31.

Vdovin O, Rial JA, Levshin AL, and Ritzwoller MH (1999) Group-velocity tomography of South America and the surrounding oceans. *Geophysical Journal International* 136: 324–340.

Vogt PR (1971) Asthenosphere motion recorded by the ocean floor south of Iceland. *Earth and Planetary Science Letters* 13: 153–160.

Waite GP, Schutt DL, and Smith RB (2005) Models of lithosphere and asthenosphere anisotropic structure of the Yellowstone hot spot from shear wave splitting. *Journal of Geophysical Research* 110: B11304.

Waite GP, Smith RB, and Allen RM (2006) V-P and V-S structure of the Yellowstone hot spot from teleseismic tomography: Evidence for an upper mantle plume. *Journal of Geophysical Research* 111: B04303.

Walker KT, Bokelmann GHR, Klemperer SL, and Bock G (2005) Shear-wave splitting around the Eifel hotspot: Evidence for a mantle upwelling. *Geophysical Journal International* 163: 962–980.

Walker KT, Nyblade AA, Klemperer SL, Bokelmann GHR, and Owens TJ (2004) On the relationship between extension and anisotropy: Constraints from shear wave splitting across the East African Plateau. *Journal of Geophysical Research* 109.

Wang S and Wang R (2001) Current plate velocities relative to hotspots; implications for hotspot motion, mantle viscosity and global reference frame. *Earth and Planetary Science Letters* 189: 133–140.

Watson S and Mckenzie D (1991) Melt generation by plumes – A study of Hawaiian volcanism. *Journal of Petrology* 32: 501–537.

Watts AB, Weissel JK, Duncan RA, and Larson RL (1988) Origin of the Louisville ridge and its relationship to the Eltanin fracture zone system. *Journal of Geophysical Research* 93: 3051–3077.

Weeraratne DS, Forsyth DW, and Yang Y (in press) Rayleigh wave tomography of the oceanic mantle beneath intraplate seamount chains in the South Pacific. *Journal of Geophysical Research*.

Weeraratne DS, Parmentier EM, and Forsyth DW (2003) Viscous fingering of miscible fluids in laboratory experiments and the oceanic mantle asthenosphere. *AGU Fall Meeting Supplement*, abstract V21B-03.

Werner R, Hoernle K, van den Bogaard P, Ranero C, von Huene R, and Korich D (1999) Drowned 14-my.-old Galapagos Archipelago off the coast of Costa Rica; implications for tectonic and evolutionary models. *Geology* 27: 499–502.

Wessel P, Harada Y, and Kroenke LW (2006) Toward a self-consistent, high resolution absolute plate motion model for the Pacific. *Geochemistry, Geophysics and Geosystems* 7: Q03L12.

Wessel P and Kroenke LW (1997) A geometric technique for relocating hotspots and refining absolute plate motions. *Nature* 387: 365–369.
Wessel P and Smith WHF (1995) New version of the generic mapping tools released. *EOS Transactions of American Geophysical Union* 76: 329.
White RS (1988) A hot-spot model for early Tertiary volcanism in the N Atlantic. *Geological Society Special Publications* 39: 3–13.
White RS (1997) Rift–plume interaction in the North Atlantic. *Philosophical Transactions of the Royal Society of London Series A* 355: 319–339.
White RS, Bown JW, and Smallwood JR (1995) The temperature of the Iceland plume and origin of outward propagating V-shaped ridges. *Journal of the Geological Society of London* 152: 1039–1045.
White RS, Mckenzie D, and O'nions RK (1992) Oceanic crustal thickness from seismic measurements and rare earth element inversions. *Journal of Geophysical Research* 97: 19683–19715.
Whitehead JA and Luther DS (1975) Dynamics of laboratory diapir and plume models. *Journal of Geophysical Research* 80: 705–717.
Wilson JT (1963) A possible origin of the Hawaiin Islands. *Canadian Journal of Physics* 41: 863–870.
Wilson JT (1973) Mantle plumes and plate motions. *Tectonophysics* 19: 149–164.
Wolfe CJ, Bjarnason IT, Vandecar JC, and Solomon SC (1997) Seismic structure of the Iceland mantle plume. *Nature* 385: 245–247.
Wolfe CJ, Solomon SC, Silver PG, Vandecar JC, and Russo RM (2002) Inversion of body-wave delay times for mantle structure beneath the Hawaiian Islands; results from the PELENET experiment. *Earth and Planetary Science Letters* 198: 129–145.
Xie S and Tackley PJ (2004) Evolution of helium and argon isotopes in a convecting mantle. *Earth and Planetary Science Letters* 146: 417–439.
Xu Y, Chung S-L, Jahn B-M, and WU G (2001) Petrologic and geochemical constraints on the petrogenesis of Permian-Triassic Emeishan flood basalts in southwestern China. *Lithos* 58: 145–168.
Xu Y, He B, Chung S-L, Menzies MA, and Frey FA (2004) Geologic, geochemical, and geophysical consequences of plume involvement in the Emeishan flood-basalt province. *Geology* 32: 917–920.
Xue M and Allen RM (2005) Asthenospheric channeling of the Icelandic upwelling: Evidence from seismic anisotropy. *Earth and Planetary Science Letters* 235: 167–182.
Yang T and Shen Y (2005) P-wave velocity structure of the crust and uppermost mantle beneath Iceland from local earthquake tomography. *Earth and Planetary Science Letters* 235: 597–609.
Yoshida Y and Suetsugu D (2004) Lithospheric thickness beneath the Pitcairn hot spot trail as inferred from Rayleigh wave dispersion. *Physics of the Earth and Planetary Interiors* 146: 75–85.
Yuan HY and Dueker K (2005) Teleseismic P-wave tomogram of the Yellowstone plume. *Geophysical Research Letters* 32: L07304 (doi:10.1029/2004GL022056).
Zhang ZC, Mahoney JJ, Mao JW, and Wang FH (2006) Geochemistry of picritic and associated basalt flows of the western Emeishan flood basalt province, China. *Journal of Petrology* 47: 1997–2019.
Zhao D (2001) Seismic structure and origin of hotspots and mantle plumes. *Earth and Planetary Science Letters* 192: 251–265.
Zhong SJ (2006) Constraints on thermochemical convection of the mantle from plume heat flux, plume excess temperature, and upper mantle temperature. *Journal of Geophysical Research* 111: B04409 (doi:10.1029/2005JB003972).
Zhong SJ and Hager BH (2003) Entrainment of a dense layer by thermal plumes. *Geophysical Journal International* 154: 666–676.
Zhong SJ and Watts AB (2002) Constraints on the dynamics of mantle plumes from uplift of the Hawaiian Islands. *Earth and Planetary Science Letters* 203: 105–116.
Zhou Z, Malpas J, Song XY, *et al.* (2002) A temporal link between the Emeishan large igneous province (SW China) and the end-Guadalupian mass extinction. *Earth and Planetary Science Letters* 196: 113–122.
Zindler A and Hart S (1986) Chemical geodynamics. *Annual Reviews of Earth and Planetary Sciences* 14: 493–571.

Relevant Websites

http://www.mantleplumes.org – Discussing the Origin of 'Hot Spot' Volcanism.
http://www.georoc.mpch-mainz.gwdg.de – Geochemistry of the Rocks of the Oceans and Continents.
http://www.petdb.org – Petrological Database of the Ocean Floor.